UNIVERSITÀ DEGLI STUDI DI PALERMO

Corso di Dottorato in Ingegneria Elettrica, Elettronica e delle Telecomunicazioni, Matematica e Automatica – Indirizzo in **Ingegneria Elettronica e delle Telecomunicazioni**

DIPARTIMENTO DI ENERGIA, INGEGNERIA DELL'INFORMAZIONE
E MODELLI MATEMATICI

Settore Scientifico Disciplinare: ING-INF/03

Opportunistic traffic Offloadings Mechanisms for Mobile/4G Networks

IL DOTTORE
Ing. Antonino Masaracchia

IL COORDINATORE
Prof. Ing. Alessandro Busacca

IL TUTOR
Ing. Stefano Mangione

CO TUTOR
Ing. Andrea Passarella

Ing. Raffaele Bruno

CICLO XXVI
ANNO CONSEGUIMENTO TITOLO 2016

Abstract

In the last few years, it has been observed a drastic surge of data traffic demand from mobile personal devices (smartphones and tablets) over cellular networks [1]. Even though a significant improvement in cellular bandwidth provisioning is expected with LTE-Advanced systems, the overall situation is not expected to change significantly. In fact, the diffusion of M2M and IoT devices is expected to increase at an exponential pace (the share of M2M devices is predicted to increase 5x by 2018 [1]) while the capacity of the cellular network is expected to increase linearly [1]. In order to meet such a high demand and to increase the capacity of the channel, multiple offloading techniques are currently under investigation, from modifications inside the cellular network architecture, to integration of multiple wireless broadband infrastructures, to exploiting direct communications between mobile devices. All these approaches can be diveded in two main classes:

- To develop more sophisticated physical layer technologies (e.g. massive MIMO, higher-order modulation schemes, cooperative multi-period transmission/reception)
- To offload part of the traffic from the cellular to another complementary network.

From this perspective the thesis contributes on both areas. On the one hand we discuss our investigations about the performance of the LTE channel capacity through the development of a unified modelling framework of the MAC-level downlink throughput of a sigle LTE cell, which caters for wideband CQI feedback schemes, AMC and HARQ protocols as defined in the LTE standard. Furthemore we also propose a solution, based on reinforcement learning, to improve the LTE Adaptive Modulation and coding Scheme (MCS).
On the other hand we have proposed and validated offloading mechanisms which are minimally invasive for users' mobile devices, as they use only minimally their resources. Furthemore, as opposed to most of the literature, we consider the case where requests for content are non-synchronised, i.e. users request content at random points in time.

Acknowledgements

This work was partly funded by the EC under the EINS (FP7- FIRE 288021),MOTO (FP7 317959), and EIT Digital MOSES (Business Plan 2014-15) projects in wich the National Resarch Council of Pisa is a Partner.
I really thank all my supervisors, Ing. Stefano Mangione from University of Palermo, which has given me many advices and technical support, Ing. Andrea Passarella and Ing. Raffaele Bruno from the CNR of Pisa , which have given me insights in the opportunistic Network context.

Contents

List of Figures

List of Tables

Chapter 1

Introduction

In the last few years, we have observed a drastic surge of data traffic demand from mobile personal devices (smartphones and tablets) over cellular networks [1]. This has already generated famous collapses of 3G networks in the recent past, (e.g. [2]), showing that standard cellular technologies may not be enough to cope with this data demand. Even though significant improvement in cellular bandwidth provisioning are expected through LTE-Advanced systems, the overall situation is not expected to change significantly [3]. Besides personal mobile devices, the diffusion of M2M and IoT devices is expected to increase at an exponential pace (the share of M2M devices is predicted to increase 5x by 2018 [1]), which is likely to generate a corresponding increase in the demand for mobile traffic (11-fold increase by 2018 [1]). Considerable progress is constantly made at the physical layer to increase raw bitrates, and clearly LTE and LTE-Advanced will help in this direction, but this is neither sufficient nor cost-efficient to accomodate all the increase in data service demand. This is because the trend of traffic demand is exponentilally increasing [1], while the improvements at the physical layer are bounded by the famous Shannon theorem and by the fact that the licensed spectrum is a limited and scarse resource. As a result, it is expected that the amount of traffic generated by 4G users may cause also the collapses of the new cellular technologies such as LTE and LTE-Advanced. The operator will need to decide to either drastically reduce the quality of service (QoS) for all the users, or block a significant fraction of the users to provide acceptable QoS to a few. Both alternatives are largely sub-optimal and generate user dissatisfaction. As mobile data traffic continues to rise, maintaining an adequate quality of service is becoming more challenging. This is not just due to the sheer rise in

traffic, but also because today's traffic is drastically different from the one a few years ago. The type of data traffic has transitioned from basic data services (such as email or SMS) to QoS-sensitive and bandwidth-hungry applications such as video. On the network management side of the "capacity crunch" challenge, operators have a number of choices to deal with the consequences of rising data traffic and, like Russian dolls, there are yet more choices nested within each strategy. For example, they can choose to expand network capacity through upgrades; but they must then select how to do this – such as adding more cell sites, upgrading cell sites, rolling out Ethernet in the backhaul and so on. Furthermore, these choices are also dependent on commercial, regulatory, operational, and customer-related factors such as the availability of the wireless spectrum, how much money they have for upgrades, whether they can easily build or share more towers. In simple terms, operators have three options: add, optimise, and avoid. Resolving the "capacity gap" in order to maintain network quality is only one facet of the problem. The real "killer" issue is commercial: revenues are not rising in line with traffic. This creates what Telesperience terms "the revenue gap". It adds to the challenges because operators are facing rising costs without receiving compensating revenue rises. This, in turn, constrains their ability to tackle the capacity crunch. To resolve this challenge, operators need to find new revenue streams and optimise revenues from existing services.

This problematic context has been the starting point of my PhD studies. In fact my studies has been focused on possible solutions to alleviate the emerging overloadig problem of the LTE cellular network. In particular the contribution of this thesis is two-fold. On the one hand I have investigated the performance of the LTE channel capacity. This study has been necessary to understand the LTE standard technology and how the protocols layers interact with each other, but at the same time to characterise the limits of the standard itself. Through this preliminary study I have developed a complete mathematical model of the LTE channel throughput at the MAC and PHY layers, which take into account all the main mechanism of the LTE standard such as the Channel Quality Indicator (CQI) feedack schemes, as well as the Adaptive Modulation and Coding (AMC) schemes and Hybrid-ARQ (HARQ) protocols. Furthemore I have proposed a new flexible AMC framework based on reinforcement learning, which has been able to significantly increase the channel capacity. In particular I have exploited a Reinforcement Learning algorithm in the selection of the best Modulation and Coding Scheme (MCS) by taking into account the outcomes of the previous AMC decisions.

On the other hand, I have focused my attention on the data traffic offloading of the LTE network, over a complementary network, in particular over an opportunistic network. In fact the data traffic offloading is considered one of the most promising approaches to cope with the overloading problem of cellular networks [1]. In this part I have preliminary analyzed the performance of several protocols for traffic offloading and then proposed and evaluated new offloading protocols. In particular I have studied the efficiency in the case when the requests from the users are not synchronised and thus the multicast operation is not possible. Through the obtained results, I have shown the efficiency of the offloading tecnique in reducing the network congestion by achieving a reduction of the traffic carried by the cellular network up to 90%, without introducing any additional delay of message loss for end users [4].

1.1 Thesis contributions in the area of LTE throughput modelling and improvement

The Long Term Evolution (LTE) is an acronym that refers to a series of cellular standards developed by 3GPP to meet the requirements of 4G systems. In particular, LTE has been designed to provide high data rates, low latency, and an improved spectral efficiency compared to previous cellular systems. To achieve these goals LTE adopts advanced physical layer technologies, such as OFDMA and multi-antenna techniques, and it supports new Radio Resource Management (RRM) functions for link adaptation. In particular, to achieve high throughput performance, in addition to an advanced physical layer design, LTE exploits a combination of sophisticated radio resource management functionalities, such as Channel Quality Indicator (CQI) reporting, link rate adaptation through Adaptive Modulation and Coding (AMC), and Hybrid Automatic Retransmission Request (HARQ) [5].

Adaptive Modulation and Coding (AMC) in LTE networks is commonly employed to improve system throughput by ensuring more reliable transmissions. Most of existing AMC methods select the modulation and coding scheme (MCS) using pre-computed mappings between MCS indexes and channel quality indicator (CQI) feedbacks that are periodically sent by the receivers. However, the effectiveness of this approach heavily depends on the assumed channel model. In addition CQI feedback delays may cause throughput losses. Regarding the HARQ protocol, LTE employs two types of HARQ

schemes. In HARQ type-I, each encoded data frame is retransmitted until the frame passes the CRC test or the maximum number of retransmissions is reached. Erroneous frames are simply discarded. In contrast, in HARQ type-II, each transmission contains incremental redundancy (IR) about the data frame. Thus, consecutive transmissions can be combined at the receiver to improve error correction.

1.1.1 LTE Channel Modelling

As mantioned above, a contribution of this thesis is the development of an analytical tool to accurately assess and optimise the user perceived throughput under realistic channel assumptions. In particular the main contribution presented in this thesis is a unified modelling framework of the MAC-level downlink throughput that is valid for homogeneous cells [6] and Rayleigh-distributed fading. Our model simultaneously caters for CQI feedback schemes that use spectral efficiency to generate CQI, as well as AMC and HARQ protocols. Furthermore, we include in the analysis an accurate link layer abstraction model that uses the Mean Mutual Information per coded Bit (MMIB) metric to derive the physical error probability [7].
The contribution of this part of study was two-fold. On the one hand it represents an innovation because, from literature, most studies have limited the analysis only to the radio link throughput or consider single MAC functions in isolation [8]. On the other hand this study contribute to the development of a tool which can help the cellular network operators to estimate its network congestion, in order to decide when to start the offloading process. In fact, the throughput estimates of our model are accurate, as validated using the ns-3 simulator extended with the LENA module for LTE. Furthermore, our results confirm that the IR-HARQ mechanism is very effective in improving error correction. However, the effectiveness of the IR-HARQ scheme depends on the appropriate selection of the modulation and coding scheme of the first transmission attempt.
A more detailed description of the model will be discussed in Chapter 4.

1.1.2 Reinforcement Learning in LTE-AMC scheme

Despite all the above mentioned innovations of LTE technology, some challenges have to be addressed. For instance , with respect to the AMC mechanism, the SINR values of

multiple subcarriers are aggregated and translated into a one-dimensional link quality metric (LQM), since the same MCS must be assigned to all subcarriers assigned to each UE. Once the LQM is found, AMC schemes typically exploit *static mappings* between these link quality metrics and the BLER performance of each MCS to select the best MCS (in terms of link throughput). In other words, for each MCS a range of LQM values is associated via a look-up table, over which that MCS maximises link throughput. Either link-level simulations or mathematical models can be used to generate such static BLER curves under a specific channel model. Unfortunately, past research has shown that it is difficult to derive accurate link performance predictors under realistic channel assumptions [7, 9–11]. Furthermore, a simulation-based approach to derive the mapping between LQM values and BLER performance is not scalable since it is not feasible to exhaustively analyse all possible channel types or several possible sets of parameters [12]. The second main problem with table-based AMC solutions is that a delay of several transmission time intervals (TTIs) may exist between the time when a CQI report is generated and the time when that CQI feedback is used for channel adaptation. This mismatch between the current channel state and its CQI representation, known as *CQI ageing*, can negatively affect the efficiency of AMC decisions [13, 14]. In order to address these iusses, in this thesis we have proposed a new AMC scheme that exploits a reinforcement learning algorithm to adjust at run-time the MCS selection rules based on the knowledge of the effect of previous AMC decisions.

The salient features of our proposed solution are: i) the low-dimensional space that the learner has to explore, and ii) the use of direct link throughput measurements to guide the decision process. As explained in Chapter 5 simulation results demonstrate the robustness of our AMC scheme that is capable of discovering the best MCS even if the CQI feedback provides a poor prediction of the channel performance.

1.2 Thesis contribution in the area of Mobile Data Offloading

In a near future, finding new, alternative communication possibilities to help alleviate overloaded infrastructures may become a need in operated networks handling mobile data. *Offloading* part of the traffic from the cellular to another, complementary, network, is currently considered one of the most promising approaches to cope with this

problem, with offloaded traffic being foreseen to account for at least 50% of the overall traffic in the coming years [1].

Besides the obvious benefit of relieving the infrastructure network load, shifting data to a complementary wireless technology leads to a number of other improvements, including: the increase of the overall throughput, the reduction of content delivery time, the extension of network coverage, the increase of network availability, and better energy efficiency. These improvements hit both cellular operators and users; therefore, offloading is often described in the literature as a $win - win$ strategy [15]. Unfortunately, this does not come for free, and a number of challenges need to be addressed, mainly related to infrastructure coordination, mobility of users, service continuity, pricing, business models, and lack of standards. Diverting traffc through fixed WiFi Access Points (AP), represents a conventional solution to reduce traffic on cellular networks. End-users located inside a hot-spot coverage area (typically much smaller than the one of a cellular macrocell) might use it as a worthwhile alternative to the cellular network when they need to exchange data. However, coverage is limited and mobility is in general constrained within the cell. Since the monetary cost of deploying an array of fixed APs is far lower than deploying a single cellular base station, the major worldwide cellular providers such have started integrating an increasing number of wireless APs in their cellular networks to encourage data offloading [16].

Furthermore, the increasing popularity of smart mobile devices proposing several alternative communication options makes it possible to deploy a device-to-device (D2D) network that relies on direct communication between mobile users, without any need for an infrastructure backbone. This innovative approach has intrinsic properties that can be employed to offload traffic. Benefiting from shared interests among co-located users, a cellular provider may decide to send popular content only to a small subset of users via the cellular network, and let these users spread the information through D2D communications and opportunistic contacts. In fact, typically content popularity follows Zipf-like distributions, i.e., a small subset of content items is extremely popular and is accessed by a very large number of users. In such scenarios, the same content item will be requested by a significant fraction of the users, and the total request in terms of bandwidth will peak.

Beyond the distinction between AP-based and D2D approaches, another aspect plays a major role in the categorization. In particular the requirements of the applications generating the traffic in terms of delivery guarantees. This translates into two additional

categories: (i) non-delayed offoading and (ii) delayed offoading.

In non-delayed offoading, each packet presents a hard delivery delay constraint defined by the application, which in general is independent of the network. No extra delay is added to data reception in order to preserve QoS requirements (other than the delay due to packet processing, physical transmission, and radio access). For instance, interactive audio and video streams cannot sustain any additional delay in order to preserve their real-time requirements. Non-delayed offoading in most cases may be difficult to implement if one considers that users are mobile and able to switch between various access technologies. If operators want to allow users to be truly mobile and not only nomadic inside the coverage area, they should focus on issues such as transparent handover and interoperability between the alternative access technologies and the existing cellular infrastructure.

In delayed offoading, content reception may be intentionally deferred up to a certain point in time, in order to reach more favorable delivery conditions. The following types of traffic are included in this category: (i) traffic with loose QoS guarantees on a per-content basis (meaning that individual packets can be delayed, but the entire content must reach the user within a given deadline) and (ii) truly delay-tolerant traffic (possibly without any delay guarantees). If data transfer does not end by the expected deadline, the cellular channel is employed as a fall-back means to complete the transfer, guaranteeing a minimal QoS. Despite the loss of the real-time support due to the added transmission delay, note that many mobile applications generate content intrinsically delay-tolerant just think about smartphone-based applications that synchronize emails or podcasts in background. Enabling an alternate distribution method for this content during peaktimes (when the cellular network is overloaded or even in outage) becomes an interesting extension and represents a fundamental challenge for offloading solutions.

1.2.1 Mobile Opportunisitc Traffic Offloading

Among the various forms of offloading that are currently investigated, in this thesis we consider offloading through opportunistic networks. Opportunistic networks [17] exploit physical proximity between mobile nodes to enable direct communication between them. They typically exploit ad hoc enabling technologies like WiFi-direct or Bluetooth, and support dissemination of messages through multi-hop space-time paths , i.e., multi-hop paths that develop both over space - as in conventional ad hoc multi-hop networks -

and over time - by exploiting contact opportunities between nodes that become available over time due to their mobility. The most common scenario where opportunistic offloading is used is content dissemination to a set of interested users. In most cases, it is assumed that the set of users interested in receiving a piece of content is known when the content is generated (or, alternatively, the content is implicitly requested by all interested users immediately when it is generated) and do not change over time. In addition, content is "seeded" through the cellular network on a subset of interested users, and then a dissemination process starts in the opportunistic network in order to reach the rest of the users [18]. Typically, epidemic dissemination is assumed [19]. In addition, as mentioned above in other cases (e.g. [20, 21]) is considered that content must be delivered to users within a given deadline. To meet this deadline, content can be sent through the cellular network to additional seeds during the dissemination process, and is finally sent to users that are still missing it when the deadline is about to expire ("panic zone"). To know which users have received the content, a lightweight control channel is implemented through the cellular network, whereby users send an ACK to a central controller that tracks the status of the dissemination process, and determines when to seed additional copies of the content, and when to directly deliver content to the users in the panic zone.

With respect to this body of work, this thesis differs in two main aspects. On the one hand, we release the assumption that users interested in a content request it simultaneously. In our scenarios content requests occur over time dynamically. On the other hand, we do not assume epidemic dissemination of content, but consider that content is exchanged in the opportunistic network only between users that have requested it, when they encounter directly. Therefore, our scenario covers more general cases with respect to strictly synchronised requests, and, in addition, provides a worst-case analysis of the potential of offloading, as we use the least possible aggressive form of dissemination in the opportunistic network.

As performance metrics we have used the offloading efficiency, defined as the fraction of nodes receiving content through the opportunistic network. As show in Chapter 6, we have characterised efficiency as a function of key parameters such as the number of users, the deadline of content requests, the time after which users drop the content after having received it, the popularity of the content. Also in this Chapter is possible to see that, even with an unfavourable opportunistic dissemination scheme, we find that

offloading can be very efficient, as it is possible to offload up to more than 90% of the traffic.

Chapter 2

State of the Art

In this Chapter I present a brief discussion about the work related of my thesis. In particular, Section 2.1 discusses related works on the AMC scheme based on Reinforcement Learning, and on the state of art of the LTE channel Modelling. Finally the Section 2.2 is dedicated to the related works on the opportunistic offloading.

2.1 LTE Related Works

With respect to the LTE Channel Modelling, several analytical and simulation models, as well as experimental studies, have been proposed for characterising the throughput performance of LTE systems. It is out of the scope of this section to provide an extensive overview of all these studies and we only focus on reviewing analytical models that are most related to this work. Several works are reported in the literature that focuses on analysing the bit error probability (BER) for OFDM systems under various channel configurations and in the presence of channel estimation errors. For instance, in [22] closed-form expressions for the BER performance of equalized OFDM signals in Rayleigh fading are derived for various signal constellations. The analytical results of [22] are extended in [23] to calculate the BER of an OFDM system in the presence of channel estimation errors. In [24] the BER performance of uncoded OFDM systems are analysed for Rayleigh and Rice frequency-selective fading channels in the presence of transmitter nonlinearities. Significant research efforts have been also dedicated to generalise the BER performance analysis to multiple-input multiple-output (MIMO) channels [25–27].

Most related to our work are the studies that focus on analysing the capacity of LTE systems with scheduling, rate adaptation and limited channel-state feedback. In [28] an upper bound is derived for the achievable throughput in LTE systems using the so-called "best-M" CQI reduction scheme and max-SNR user scheduling. Closed-form expressions for the throughput achieved in LTE systems under different schedulers (proportional fair, greedy, and round robin), multiple-antenna diversity modes and CQI feedback schemes are derived in [29, 30]. Specifically, the model in [29] applies to LTE systems that use EESM to generate CQI reports (an explanation of the EESM method is provided in Section 4.2), while the model in [30] applies to LTE systems that generate CQI reports by simply taking an arithmetic average of the SNRs of the subcarriers. A SNR quantisation feedback scheme is also analysed in [31]. However, most of these works assume a simplified model for the channel outage, which does not take into account HARQ procedures as specified in the LTE standard. The performance of HARQ with rate adaption for the LTE downlink is studied in [8], but only through simulations.
Regarding the AMC scheme in LTE, it is important to point out that other studies [32–35] have proposed to use machine learning techniques to improve AMC in wireless systems. The main weakness of most of these solutions is to rely on machine learning algorithms (e.g., pattern classification [33] or SVM [32, 34]) that require large sets of training samples to build a model of the wireless channel dynamics. Similar to our work, the AMC scheme proposed in [35] exploits Q-learning algorithms to avoid the use of model-training phases. However, the MCS selection problem in [35] is defined over a continuous state space (i.e., received SINR), and even after discretisation a large number of states must be handled by the learning algorithm.

2.2 Opportunistic Offloading Related Works

Offloading can take several forms. In some cases, traffic is offloaded by using modifications inside the cellular architecture (e.g. LIPA/SIPTO [36] or small cells [37]), or other wireless access infrastructures, primarily WiFi [38, 39]. In our work we have consider offloading that exploits direct communications between mobile devices. Also in this case there are several approaches. In the 3GPP area, the device-to-device (D2D) [40] architectural modification to LTE has been defined, that devotes part of the cellular resources to direct communication between devices under strict control of a common

eNB. Instead, we focus on using opportunistic networks together with cellular networks, as previously proposed, e.g. in [18, 20, 21, 41]. In this case, offloading exploits technologies (such as WiFi direct or Bluetooth) that do not interfere with cellular transmissions, and therefore no coordination is required with the eNB. In addition, mobile devices run self-organising networking algorithm to disseminate offloaded content without strict control of the eNBs or any other central controller. The most common scenario where opportunistic offloading is used is content dissemination to a set of interested users. In most cases, it is assumed that the set of users interested in receiving a piece of content is known when the content is generated (or, alternatively, the content is implicitly requested by all interested users immediately when it is generated) and do not change over time. In addition, content is "seeded" through the cellular network on a subset of interested users, and then a dissemination process starts in the opportunistic network in order to reach the rest of the users [18]. Typically, epidemic dissemination is assumed [19]. In addition, in other cases (e.g. [20, 21]) is assumed that content must be delivered to users within a given deadline. To meet this deadline, content can be sent through the cellular network to additional seeds during the dissemination process, and is finally sent to users that are still missing it when the deadline is about to expire ("panic zone"). To know which users have received the content, a lightweight control channel is implemented through the cellular network, whereby users send an ACK to a central controller that tracks the status of the dissemination process, and determines when to seed additional copies of the content, and when to directly deliver content to the users in the panic zone. With respect to this body of work, this work differs in two main aspects. On the one hand, we release the assumption that users interested in a content request it simultaneously. In our scenarios content requests occur over time dynamically. On the other hand, we do not assume epidemic dissemination of content, but consider that content is exchanged in the opportunistic network only between users that have requested it, when they encounter directly. Therefore, our scenario covers more general cases with respect to strictly synchronised requests, and, in addition, provides a worst-case analysis of the potential of offloading, as we use the least possible aggressive form of dissemination in the opportunistic network. To the best of our knowledge, the only other work where content requests are not synchronised is [42]. In this work is assumed that users become interested in the content after a random amount of time after its generation, and the goal of the proposed system is to maximise the probability that the user have already the content by then. This is very different from our scheme,

which works reactively, *after* users generate requests. Finally, offloading has been also proposed specifically in vehicular environments. In this case offloading schemes often assume the presence of RoadSide Units (RSU) [43] to support the dissemination process (e.g., by pre-fetching popular contents), which we do not assume here, to obtain a solution requiring no additional infrastructure development. Last but not least, offloading is proposed also for aggregating and uploading traffic generated by cars, e.g., in the context of Floating Car Data (FCD) [44].

Chapter 3

3GPP LTE Standard

3.1 Introduction

The term "Long Term Evolution" (LTE) stands for the process to gerate a novel air interface by the 3rd Generation Partnership Project (3GPP), and for the specified technology. LTE was initiated as a study item and its technical requirements were agreed in June 2005 [45]. The target of LTE included reduced latency, higher userdata rates, improved system capacity and coverage and reduced cost of operations. Lte was required to become a stand-alone system with packet-switched networking. The study item was reported the first time in the technical report [46], where it was decided that LTE is based on a new air interface, different from the WCDMA/HSPA enhancements. The salient characteristics of LTE are as follows:

- A flat architecture ture based on distributed servers, LTE base stations having transport connections to the core network without intermediate RAN network nodes (such as radio network controllers)
- Simplified and efficient radio protocols, where channel state information is available at the radio protocol peers to optimize the access and to minimize the overhead.
- A physical layer design favouring frequency domain processing for efficiency, enabling high data rate transmissions e.g. by multiantenna transmission methods, and alleviating interference conditions by intracell orthogonality.

- Radio resource management enabling scalability of transmission bandwidth (BW), and a high degree of multiuser diversity e.g. by time–frequency domain scheduling. Efficient operation in power saving modes as a designed fundamental property of the User Equipment (UE).

The evolution of the LTE system, its architecture, protocols and performance are described widely e.g. in [47–50]. This chapter contains a brief overview of the overall architecture of an LTE radio-access network and the associated core network. In particular a depth description about the Physical and MAC layer is given in order to make you able to understand the mathematical model of the channel present in Capter 3.

3.2 System Architecture

In parallel to the work on the LTE radio-access technology in 3GPP, the overall system architecture of both the Radio-Access Network (RAN) and the Core Network (CN) was revisited, including the split of functionality between the two network parts. This work was known as the System Architecture Evolution (SAE) and resulted in a flat RAN architecture, as well as a new core network architecture referred to as the Evolved Packet Core (EPC). Together, the LTE RAN and the EPC can be referred to as the Evolved Packet System (EPS). The RAN is responsible for all radio-related functionality of the overall network including, for example, scheduling, radio-resource handling, retransmission protocols, coding and various multiantenna schemes. The EPC is responsible for functions not related to the radio interface but needed for providing a complete mobile-broadband network. This includes, for example, authentication, charging functionality, and setup of end-to-end connections.

3.2.1 Core Network

The EPC is a radical evolution from the GSM/GPRS core network used for GSM and WCDMA/ HSPA. EPC supports access to the packet-switched domain only, with no access to the circuitswitched domain. As show in Figure 3.1, it consists of several different types of nodes, in particular:

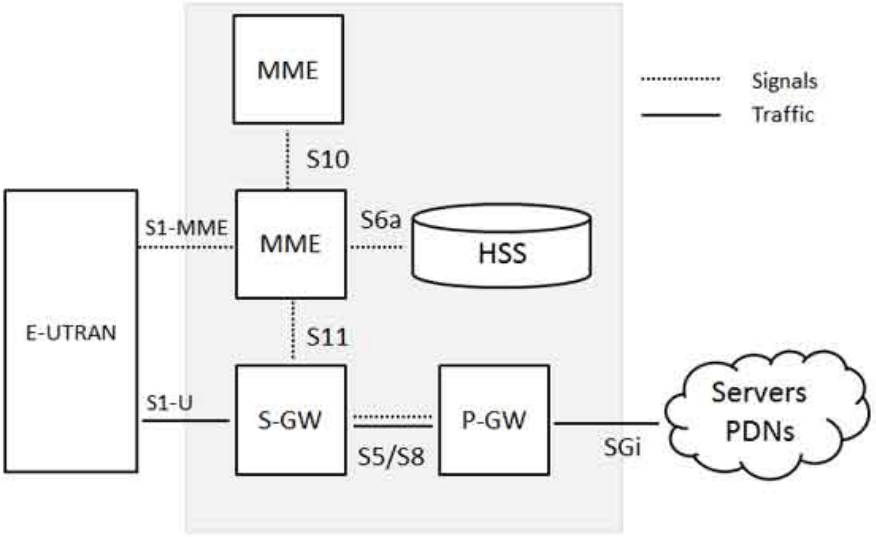

FIGURE 3.1: Core-network (EPC) architecture.

- The Mobility Management Entity (MME) is the control-plane node of the EPC. Its responsibilities include connection/release of bearers to a terminal, handling of IDLE to ACTIVE transitions, and handling of security keys. The functionality operating between the EPC and the terminal is sometimes referred to as the Non-Access Stratum (NAS), to separate it from the Access Stratum (AS) which handles functionality operating between the terminal and the radio-access network.

- The Serving Gateway (S-GW) is the user-plane node connecting the EPC to the LTE RAN. The S-GW acts as a mobility anchor when terminals move between eNodeBs, as well as a mobility anchor for other 3GPP technologies (GSM/GPRS and HSPA). Collection of information and statistics necessary for charging is also handled by the S-GW.

- The Packet Data Network Gateway (PDN Gateway, P-GW) connects the EPC to the internet. Allocation of the IP address for a specific terminal is handled by the P-GW, as well as quality of service enforcement according to the policy controlled by the PCRF (see below). The P-GW is also the mobility anchor for non-3GPP radio-access technologies, such as CDMA2000, connected to the EPC.

In addition, the EPC also contains other types of nodes such as Policy and Charging Rules Function (PCRF) responsible for quality-of-service (QoS) handling and charging, and the Home Subscriber Service (HSS) node, a database containing subscriber information. There are also some additional nodes present as regards network support of

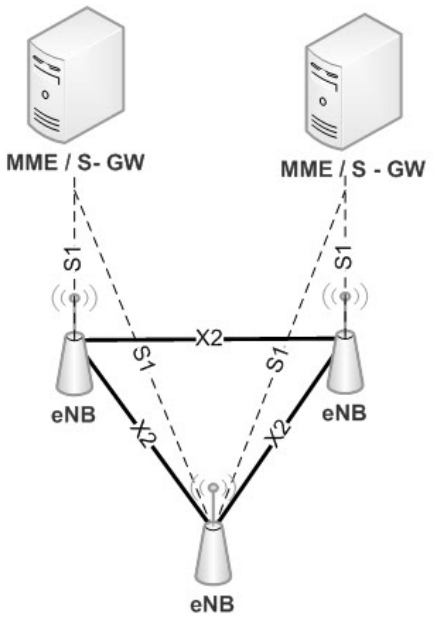

FIGURE 3.2: Radio-access-network interfaces.

Multimedia Broadcast Multicast Services (MBMS). It should be noted that the nodes discussed above are logical nodes. In an actual physical implementation, several of them may very well be combined. For example, the MME, P-GW, and S-GW could very well be combined into a single physical node.

3.2.2 Radio-Access Network

The LTE radio-access network uses a flat architecture with a single type of node: the eNodeB. The eNodeB is responsible for all radio-related functions in one or several cells. It is important to note that an eNodeB is a logical node and not a physical implementation. One common implementation of an eNodeB is a three-sector site, where a base station is handling transmissions in three cells, although other implementations can be found as well, such as one baseband processing unit to which a number of remote radio heads are connected. As can be seen in Figure 3.2, the eNodeB is connected to the EPC by means of the S1 interface, more specifically to the S-GW by means of the S1 user-plane part, S1-u, and to the MME by means of the S1 control-plane part, S1-c. One eNodeB can be connected to multiple MMEs/S-GWs for the purpose of load sharing and redundancy. The X2 interface, connecting eNodeBs to each other, is mainly used to support active-mode mobility. This interface may also be used for multi-cell Radio Resource Management (RRM) functions such as Inter-Cell Interference Coordination

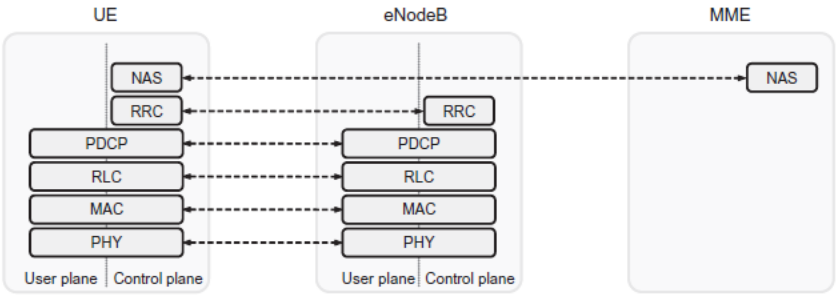

FIGURE 3.3: Overall RAN protocol architecture.

(ICIC). It is also used to support lossless mobility between neighboring cells by means of packet forwarding.

3.3 Radio Protocol Architecture

Figure 3.3 illustrates the RAN protocol architecture. The LTE radio-access network provides one or more Radio Bearers to which IP packets are mapped according to their Quality-of-Service requirements. The different protocol entities of the radio-access network are summarized as follow:

- Packet Data Convergence Protocol (PDCP) performs IP header compression to reduce the number of bits to transmit over the radio interface. The header-compression mechanism is based on Robust Header Compression (ROHC), a standardized header-compression algorithm also used for several mobile-communication technologies. PDCP is also responsible for ciphering and, for the control plane, integrity protection of the transmitted data, as well as in-sequence delivery and duplicate removal for handover. At the receiver side, the PDCP protocol performs the corresponding deciphering and decompression operations. There is one PDCP entity per radio bearer configured for a terminal.

- Radio-Link Control (RLC) is responsible for segmentation/concatenation, retransmission handling, duplicate detection, and in-sequence delivery to higher layers. The RLC provides services to the PDCP in the form of radio bearers. There is one RLC entity per radio bearer configured for a terminal.

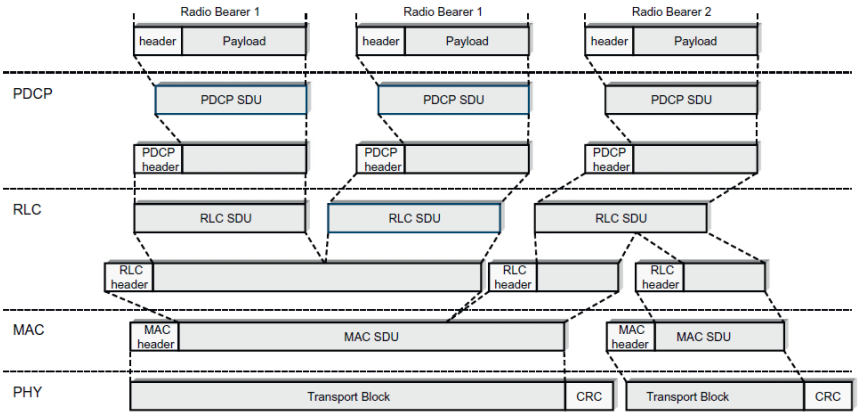

FIGURE 3.4: LTE data flow.

- Medium-Access Control (MAC) handles multiplexing of logical channels, hybrid-ARQ retransmissions, and uplink and downlink scheduling. The scheduling functionality is located in the eNodeB for both uplink and downlink. The hybrid-ARQ protocol part is present in both the transmitting and receiving ends of the MAC protocol. The MAC provides services to the RLC in the form of logical channels.

- Physical Layer (PHY) handles coding/decoding, modulation/demodulation, multi-antenna mapping, and other typical physical-layer functions. The physical layer offers services to the MAC layer in the form of transport channels.

To summarize the flow of downlink data through all the protocol layers, an example illustration for a case with three IP packets, two on one radio bearer and one on another radio bearer, is given in Figure 3.4. The data flow in the case of uplink transmission is similar. The PDCP performs (optional) IP-header compression, followed by ciphering. A PDCP header is added, carrying information required for deciphering in the terminal. The output from the PDCP is forwarded to the RLC. The RLC protocol performs concatenation and/or segmentation of the PDCP SDUs and adds an RLC header. The header is used for in-sequence delivery (per logical channel) in the terminal and for identification of RLC PDUs in the case of retransmissions. The RLC PDUs are forwarded to the MAC layer, which multiplexes a number of RLC PDUs and attaches a MAC header to form a transport block. The transport-block size depends on the instantaneous data rate selected by the linkadaptation mechanism. Thus, the link adaptation affects both the MAC and RLC processing. Finally, the physical layer attaches a CRC to

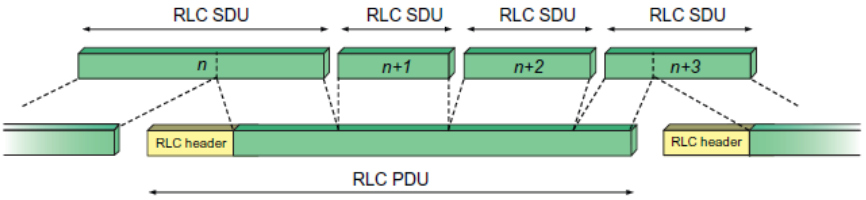

FIGURE 3.5: RLC Segmentation.

the transport block for error-detection purposes, performs coding and modulation, and transmits the resulting signal, possibly using multiple transmit antennas.

3.3.1 Radio-Link Control

The RLC protocol is responsible for segmentation/concatenation of (header-compressed) IP packets, also known as RLC SDUs, from the PDCP into suitably sized RLC PDUs. It also handles retransmission of erroneously received PDUs, as well as removal of duplicated PDUs. Finally, the RLC ensures in-sequence delivery of SDUs to upper layers. Depending on the type of service, the RLC can be configured in different modes to perform some or all of these functions. Segmentation and concatenation, one of the main RLC functions, is illustrated in Figure 3.5. Depending on the scheduler decision, a certain amount of data is selected for transmission from the RLC SDU buffer and the SDUs are segmented/concatenated to create the RLC PDU. Thus, for LTE the RLC PDU size varies dynamically. For high data rates, a large PDU size results in a smaller relative overhead, while for low data rates, a small PDU size is required as the payload would otherwise be too large. Hence, as the LTE data rates may range from a few kbit/s up to 3 Gbit/s, dynamic PDU sizes are motivated for LTE in contrast to earlier mobile-communication technologies, which typically use a fixed PDU size. Since the RLC, scheduler, and rate adaptation mechanisms are all located in the eNodeB, dynamic PDU sizes are easily supported for LTE. In each RLC PDU, a header is included, containing, among other things, a sequence number used for in-sequence delivery and by the retransmission mechanism. The RLC retransmission mechanism is also responsible for providing error-free delivery of data to higher layers. To accomplish this, a retransmission protocol operates between the RLC entities in the receiver and transmitter. By monitoring the sequence numbers of the incoming PDUs, the receiving RLC can identify missing PDUs. Status reports are then fed back to the transmitting RLC

entity, requesting retransmission of missing PDUs. Based on the received status report, the RLC entity at the transmitter can take the appropriate action and retransmit the missing PDUs if needed. Although the RLC is capable of handling transmission errors due to noise, unpredictable channel variations, etc., error-free delivery is in most cases handled by the MAC-based hybrid-ARQ protocol.

3.3.2 Medium-Access Control

The MAC layer handles logical-channel multiplexing, hybrid-ARQ retransmissions, and uplink and downlink scheduling. It is also responsible for multiplexing/demultiplexing data across multiple component carriers when carrier aggregation is used.

3.3.3 Logical Channels and Transport Channels

The MAC provides services to the RLC in the form of logical channels. A logical channel is defined by the type of information it carries and is generally classified as a control channel, used for transmission of control and configuration information necessary for operating an LTE system, or as a traffic channel, used for the user data. The set of logical-channel types specified for LTE includes:

- The Broadcast Control Channel **(BCCH)**, used for transmission of system information from the network to all terminals in a cell. Prior to accessing the system, a terminal needs to acquire the system information to find out how the system is configured and, in general, how to behave properly within a cell.
- The Paging Control Channel **(PCCH)**, used for paging of terminals whose location on a cell level is not known to the network. The paging message therefore needs to be transmitted in multiple cells.
- The Common Control Channel **(CCCH)**, used for transmission of control information in conjunction with random access.
- The Dedicated Control Channel **(DCCH)**, used for transmission of control information to/from a terminal. This channel is used for individual configuration of terminals such as different handover messages.

- The Multicast Control Channel **(MCCH)**, used for transmission of control information required for reception of the MTCH.
- The Dedicated Traffic Channel **(DTCH)**, used for transmission of user data to/from a terminal. This is the logical channel type used for transmission of all uplink and non-MBSFN downlink user data.
- The Multicast Traffic Channel **(MTCH)**.

From the physical layer, the MAC layer uses services in the form of transport channels. A transport channel is defined by how and with what characteristics the information is transmitted over the radio interface. Data on a transport channel is organized into transport blocks. In each Transmission Time Interval (TTI), at most one transport block of dynamic size is transmitted over the radio interface to/from a terminal in the absence of spatial multiplexing. In the case of spatial multiplexing (MIMO), there can be up to two transport blocks per TTI. Associated with each transport block is a Transport Format (TF), specifying how the transport block is to be transmitted over the radio interface. The transport format includes information about the transport-block size, the modulation-and-coding scheme, and the antenna mapping. By varying the transport format, the MAC layer can thus realize different data rates. Rate control is therefore also known as transport-format selection. The following transport-channel types are defined for LTE:

- The Broadcast Channel **(BCH)** has a fixed transport format, provided by the specifications. It is used for transmission of parts of the BCCH system information, more specifically the so-called Master Information Block (MIB).
- The Paging Channel **(PCH)** is used for transmission of paging information from the PCCH logical channel. The PCH supports discontinuous reception (DRX) to allow the terminal to save battery power by waking up to receive the PCH only at predefined time instants.
- The Downlink Shared Channel **(DL-SCH)** is the main transport channel used for transmission of downlink data in LTE. It supports key LTE features such as dynamic rate adaptation and channeldependent scheduling in the time and frequency domains, hybrid ARQ with soft combining, and spatial multiplexing. It

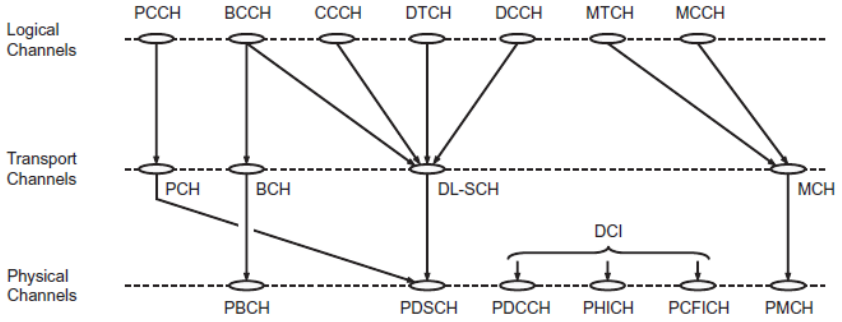

FIGURE 3.6: Downlink channel mapping.

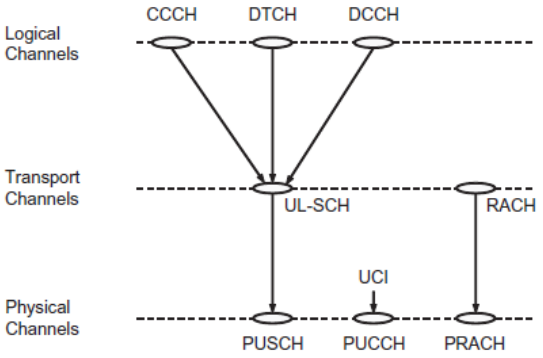

FIGURE 3.7: Uplink channel mapping.

also supports DRX to reduce terminal power consumption while still providing an always-on experience. The DL-SCH is also used for transmission of the parts of the BCCH system information not mapped to the BCH. There can be multiple DL-SCHs in a cell, one per terminal scheduled in this TTI, and, in some subframes, one DL-SCH carrying system information.

- The Multicast Channel **(MCH)**.
- The Uplink Shared Channel **(UL-SCH)** is the uplink counterpart to the DL-SCH that is, the uplink transport channel used for transmission of uplink data.

Part of the MAC functionality is multiplexing of different logical channels and mapping of the logical channels to the appropriate transport channels. The supported mappings between logical-channel types and transport-channel types are given in Figure 3.6 for the downlink and Figure 3.7 for the uplink.

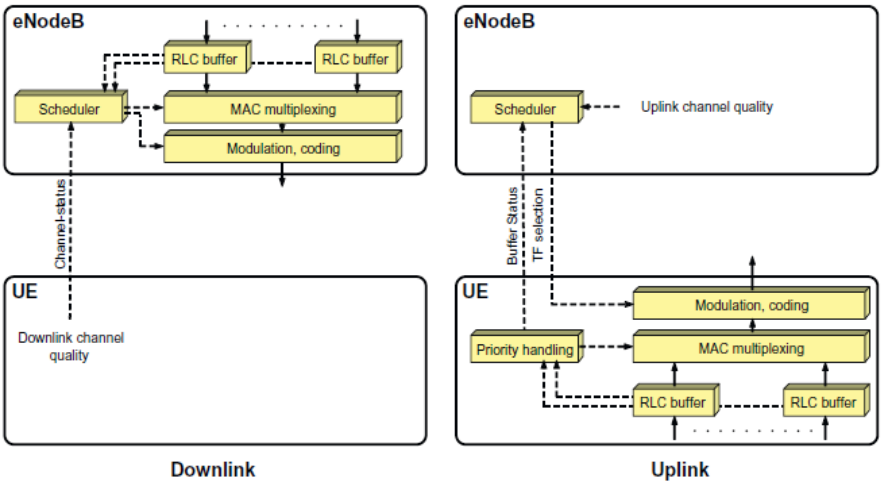

FIGURE 3.8: Transport-format selection in downlink and uplink.

3.4 Scheduling

The purpose of the scheduler is to determine to/from which terminal(s) to transmit data and on which set of resource blocks. The scheduler is a key element and to a large degree determines the overall behavior of the system. The basic operation is so-called dynamic scheduling, where the eNodeB in each 1 ms TTI transmits scheduling information to the selected set of terminals, controlling the uplink and downlink transmission activity. The scheduling decisions are transmitted on the PDCCHs. To reduce the control signaling overhead, there is also the possibility of semi-persistent scheduling. Semipersistent scheduling is only supported on the primary component carriers, motivated by the fact that the main usage is for small payloads not requiring multiple component carriers. The downlink scheduler is responsible for dynamically controlling the terminal(s) to transmit to and, for each of these terminals, the set of resource blocks upon which the terminal's DL-SCH (or DL-SCHs in the case of carrier aggregation) is transmitted. Transport-format selection (selection of transport-bock size, modulation-and-coding scheme, resource-block allocation, and antenna mapping) for each component carrier and logical channel multiplexing for downlink transmissions are controlled by the eNodeB, as illustrated in the left part of Figure 3.8. The uplink scheduler serves a similar purpose, namely to dynamically control which terminals are to transmit on their UL-SCH (or UL-SCHs in the case of carrier aggregation) and on which uplink resources. The uplink scheduler is in complete control of the transport format the terminal will use, whereas the logical-channel multiplexing is controlled by the terminal according to

a set of rules. Thus, uplink scheduling is per terminal and not per radio bearer. This is illustrated in the right part of Figure 3.8, where the scheduler controls the transport format and the terminal controls the logical-channel multiplexing.

3.4.1 Downlink Scheduling

The task of the downlink scheduler is to dynamically determine the terminal(s) to transmit to and, for each of these terminals, the set of resource blocks upon which the terminal's DL-SCH should be transmitted. In most cases, a single terminal cannot use the full capacity of the cell, for example due to lack of data. Also, as the channel properties may vary in the frequency domain, it is useful to be able to transmit to different terminals on different parts of the spectrum. Therefore, multiple terminals can be scheduled in parallel in a subframe, in which case there is one DL-SCH per scheduled terminal and component carrier, each dynamically mapped to a (unique) set of frequency resources. The scheduler is in control of the instantaneous data rate used, and the RLC segmentation and MAC multiplexing will therefore be affected by the scheduling decision. Although formally part of the MAC layer but to some extent better viewed as a separate entity, the scheduler is thus controlling most of the functions in the eNodeB associated with downlink data transmission:

- RLC. Segmentation/concatenation of RLC SDUs is directly related to the instantaneous data rate. For low data rates, it may only be possible to deliver a part of an RLC SDU in a TTI, in which case segmentation is needed. Similarly, for high data rates, multiple RLC SDUs may need to be concatenated to form a sufficiently large transport block.

- MAC. Multiplexing of logical channels depends on the priorities between different streams. For example, radio resource control signaling, such as handover commands, typically has a higher priority than streaming data, which in turn has higher priority than a background file transfer. Thus, depending on the data rate and the amount of traffic of different priorities, the multiplexing of different logical channels is affected. Hybrid-ARQ retransmissions also need to be accounted for.

- L1. Coding, modulation and, if applicable, the number of transmission layers and the associated precoding matrix are obviously affected by the scheduling decision.

The choices of these parameters are mainly determined by the radio conditions and the selected data rate – that is, the transport block size.

The scheduling decision is communicated to each of the scheduled terminals through the downlink L1/L2 control signaling using one PDCCH per downlink assignment. Each terminal monitors a set of PDCCHs for downlink scheduling assignments. A scheduling assignment is transmitted in the same subframe as the data. If a valid assignment matching the identity of the terminal is found, then the terminal receives and processes the transmitted signal as indicated in the assignment. Once the transport block is successfully decoded, the terminal will demultiplex the received data into the appropriate logical channels. The scheduling strategy is implementation specific and not part of the 3GPP specifications. However, the overall goal of most schedulers is to take advantage of the channel variations between terminals and preferably to schedule transmissions to a terminal when the channel conditions are advantageous. Most scheduling strategies therefore need information about:

- channel conditions at the terminal;
- buffer status and priorities of the different data flows;
- the interference situation in neighboring cells (if some form of interference coordination is implemented).

Information about the channel conditions at the terminal can be obtained in several ways. In principle, the eNodeB can use any information available, but typically the channel-state reports from the terminal are used. However, additional sources of channel knowledge, for example exploiting channel reciprocity to estimate the downlink quality from uplink channel estimates in the case of TDD, can also be exploited by a particular scheduler implementation.

3.4.2 Uplink Scheduling

The basic function of the uplink scheduler is similar to its downlink counterpart, namely to dynamically determine, for each 1 ms interval, which terminals are to transmit and on which uplink resources. As discussed before, the LTE uplink is primarily based

on maintaining orthogonality between different uplink transmissions and the shared resource controlled by the eNodeB scheduler is time–frequency resource units. In addition to assigning the time–frequency resources to the terminal, the eNodeB scheduler is also responsible for controlling the transport format the terminal will use for each of the uplink component carriers. As the scheduler knows the transport format the terminal will use when it is transmitting, there is no need for outband control signaling from the terminal to the eNodeB. This is beneficial from a coverage perspective, taking into account that the cost per bit of transmitting outband control information can be significantly higher than the cost of data transmission, as the control signaling needs to be received with higher reliability. It also allows the scheduler to tightly control the uplink activity to maximize the resource usage compared to schemes where the terminal autonomously selects the data rate, as autonomous schemes typically require some margin in the scheduling decisions. A consequence of the scheduler being responsible for selection of the transport format is that accurate and detailed knowledge about the terminal situation with respect to buffer status and power availability is more accentuated in LTE compared to systems where the terminal autonomously controls the transmission parameters. The basis for uplink scheduling is scheduling grants, containing the scheduling decision and providing the terminal information about the resources and the associated transport format to use for transmission of the UL-SCH on one component carrier. Only if the terminal has a valid grant is it allowed to transmit on the corresponding UL-SCH; autonomous transmissions are not possible without a corresponding grant. Dynamic grants are valid for one subframe – that is, for each subframe in which the terminal is to transmit on the UL-SCH, the scheduler issues a new grant. Uplink component carriers are scheduled independently; if the terminal is to transmit simultaneously on multiple component carriers, multiple scheduling grants are needed. The terminal monitors a set of PDCCHs for uplink scheduling grants. Upon detection of a valid uplink grant, the terminal will transmit its UL-SCH according to the information in the grant. Obviously, the grant cannot relate to the same subframe it was received in as the uplink subframe has already started when the terminal has decoded the grant. The terminal also needs some time to prepare the data to transmit. Therefore, a grant received in subframe n affects the uplink transmission in a later subframe. Similarly to the downlink case, the uplink scheduler can exploit information about channel conditions, buffer status, and priorities of the different data flows, and, if some form of interference coordination is

employed, the interference situation in neighboring cells. Channel-dependent scheduling, which typically is used for the downlink, can be used for the uplink as well.

3.4.3 Channel-State Reporting

As mentioned several times, the possibility for downlink channel-dependent scheduling – that is, selecting the downlink transmission configuration and related parameters depending on the instantaneous downlink channel conditions – is a key feature of LTE. An important part of the support for downlink channel-dependent scheduling is channel-state reports provided by terminals to the network, reports on which the latter can base its scheduling decisions. The channel-state reports consist of one or several pieces of information:

- Rank indication (RI), providing a recommendation on the transmission rank to use or, expressed differently, the number of layers that should preferably be used for downlink transmission to the terminal. RI only needs to be reported by terminals that are configured to be in one of the spatial multiplexing transmission modes. There is at most one RI reported, valid across the full bandwidth- that is, the RI is frequency non-selective. Frequency-dependent transmission rank would be impossible to utilize since all layers are transmitted on the same set of resource blocks in LTE.

- Precoder matrix indication (PMI), indicating which of the precoder matrices should preferably be used for the downlink transmission. The reported precoder matrix is determined assuming the number of layers indicated by the RI. The precoder recommendation may be frequency selective, implying that the terminal may recommend different precoders for different parts of the downlink spectrum. Furthermore, the network can restrict the set of matrices from which the terminal should select the recommended precoder, so-called codebook subset restriction, to avoid reporting precoders that are not useful in the antenna setup used.

- Channel-quality indication (CQI), representing the highest modulation-and-coding scheme that, if used, would mean PDSCCH transmissions (using the recommended RI and PMI) were received with a block-error rate of at most 10%. The reason to use CQI as a feedback quantity instead of, for example, the signal-to-noise ratio,

is to account for different receiver implementation in the terminal. Also, basing the feedback reports on CQI instead of signal-to-noise ratio also simplifies the testing of terminals; a terminal delivering data with more than 10% block-error probability when using the modulation-and-coding scheme indicated by the CQI would fail the test. As will be discussed further below, multiple CQI reports, each representing the channel quality in a certain part of the downlink spectrum, can be part of a channel-state report.

Together, a combination of the RI, PMI, and CQI forms a channel-state report.

3.5 HYBRID ARQ WITH SOFT COMBINING

The hybrid-ARQ functionality spans both the physical layer and the MAC layer; generation of different redundancy versions at the transmitter as well as the soft combining at the receiver are handled by the physical layer, while the hybrid-ARQ protocol is part of the MAC layer. In the presence of carrier aggregation, there is, as already stated, one independent hybrid-ARQ entity per component carrier and terminal. Unless otherwise noted, the description below holds for one component carrier – that is, the description is on a per-component carrier basis. The basis for the LTE hybrid-ARQ mechanism is a structure with multiple stop-and-wait protocols, each operating on a single transport block. In a stop-and-wait protocol, the transmitter stops and waits for an acknowledgement after each transmitted transport block. This is a simple scheme; the only feedback required is a single bit indicating positive or negative acknowledgement of the transport block. However, since the transmitter stops after each transmission, the throughput is also low. LTE, as illustated in Figure 3.9 , therefore applies multiple stop-and-wait processes operating in parallel such that, while waiting for acknowledgement from one process, the transmitter can transmit data to another hybrid-ARQ process. Upon receiving a transport block for a certain hybrid-ARQ process, the receiver makes an attempt to decode the transport block and informs the transmitter about the outcome through a hybrid-ARQ acknowledgement, indicating whether the transport block was correctly decoded or not. The time from reception of data until transmission of the hybrid-ARQ acknowledgement is fixed, hence the transmitter knows from the timing relation which hybrid-ARQ process a received acknowledgement relates to. This is beneficial from an

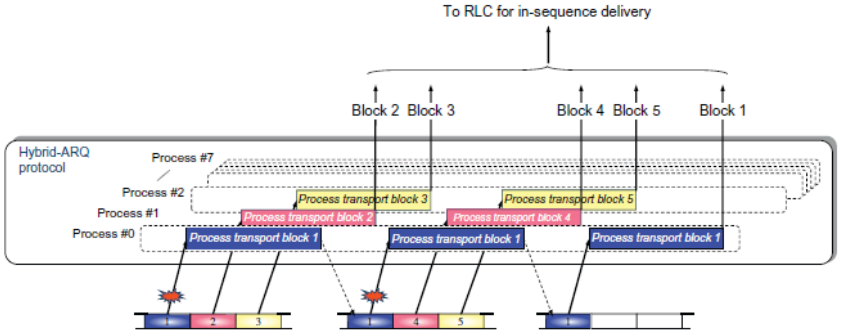

FIGURE 3.9: Multiple parallel hybrid-ARQ processes forming one hybrid-ARQ entity.

overhead perspective as there is no need to signal the process number along with the acknowledgement. An important part of the hybrid-ARQ mechanism is the use of soft combining, which implies that the receiver combines the received signal from multiple transmission attempts.

3.6 Physical Layer Organizzation

OFDM is the basic transmission scheme for both the downlink and uplink transmission directions in LTE although, for the uplink. The LTE OFDM subcarrier spacing equals 15 kHz for both downlink and uplink. The selection of the subcarrier spacing in an OFDM-based system needs to carefully balance overhead from the cyclic prefix against sensitivity to Doppler spread/shift and other types of frequency errors and inaccuracies. The choice of 15 kHz for the LTE subcarrier spacing was found to offer a good balance between these two constraints. Assuming an FFT-based transmitter/receiver implementation, 15 kHz subcarrier spacing corresponds to a sampling rate $f_s = 15000 * NFFT$, where NFFT is the FFT size. It is important to understand though that the LTE specifications do not in any way mandate the use of FFT-based transmitter/ receiver implementations and even less so a particular FFT size or sampling rate. Nevertheless, FFT-based implementations of OFDM are common practice and an FFT size of 2048, with a corresponding sampling rate of 30.72 MHz, is suitable for the wider LTE carrier bandwidths, such as bandwidths of the order of 15 MHz and above. However, for smaller carrier bandwidths, a smaller FFT size and a correspondingly lower sampling rate can very well be used. The sampling rate above illustrates another factor influencing the choice of the LTE subcarrier spacing, namely a desire to simplify implementation of

dual-mode LTE/HSPA terminals. Assuming a power-of-two FFT size and a subcarrier spacing of 15 kHz, the sampling rate $\Delta f * NFFT$ will be a multiple or sub-multiple of the HSPA chip rate of 3.84 Mchip/s. In the time domain, LTE transmissions are organized into (radio) frames of length 10 ms, each of which is divided into ten equally sized subframes of length 1 ms, as illustrated in Figure 3.10. Each subframe consists of two equally sized slots of length $T_{slot} = 0.5\ ms$, with each slot consisting of a number of OFDM symbols including cyclic prefix. On a higher level, each frame is identified by a System Frame Number (SFN). The SFN is used to control different transmission cycles that may have a period longer than one frame, such as paging sleep-mode cycles and periods for channel-status reporting. The SFN period equals 1024, thus the SFN repeats itself after 1024 frames or roughly 10 seconds. LTE defines two cyclic-prefix lengths, the normal cyclic prefix and an extended cyclic prefix, corresponding to seven and six OFDM symbols per slot respectively. In particular a longer cyclic prefix, although less efficient from a cyclic-prefix-overhead point of view, may be beneficial in specific environments with extensive delay spread, for example in very large cells. It is important to have in mind, though, that a longer cyclic prefix is not necessarily beneficial in the case of large cells, even if the delay spread is very extensive in such cases. If, in large cells, link performance is limited by noise rather than by signal corruption due to residual time dispersion not covered by the cyclic prefix, the additional robustness to radio-channel time dispersion, due to the use of a longer cyclic prefix, may not justify the corresponding additional energy overhead of a longer cyclic prefix. The overall Time organizzation is illustrated in Figure 3.10. A resource element, consisting of one subcarrier during one OFDM symbol, is the smallest physical resource in LTE. Furthermore, as illustrated in Figure 3.11, resource elements are grouped into resource blocks, where each resource block consists of 12 consecutive subcarriers in the frequency domain and one 0.5 ms slot in the time domain. Each resource block thus consists of $7 * 12 = 84$ resource elements in the case of a normal cyclic prefix and $6 * 12 = 72$ resource elements in the case of an extended cyclic prefix. Although resource blocks are defined over one slot, the basic time-domain unit for dynamic scheduling in LTE is one subframe, consisting of two consecutive slots. The minimum scheduling unit, consisting of two time-consecutive resource blocks within one subframe (one resource block per slot), can be referred to as a resource-block pair. The LTE physical-layer specification allows for a carrier to consist of any number of resource blocks in the frequency domain, ranging from a minimum of six resource blocks up to a maximum of 110 resource blocks. This corresponds to an

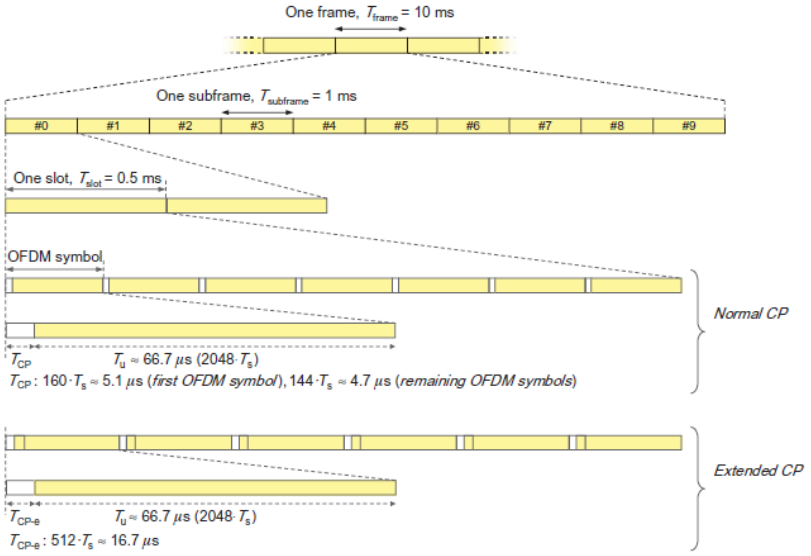

FIGURE 3.10: LTE time-domain structure.

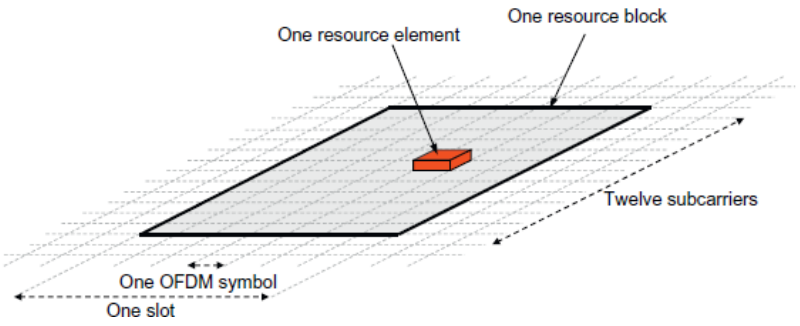

FIGURE 3.11: The LTE physical time–frequency resource.

overall transmission bandwidth ranging from roughly 1 MHz up to in the order of 20 MHz with very fine granularity and thus allows for a very high degree of LTE bandwidth flexibility, at least from a physical-layer-specification point of view. The resource-block definition above applies to both the downlink and uplink transmission directions. However, there is a minor difference between the downlink and uplink in terms of where the carrier center frequency is located in relation to the subcarriers.

Chapter 4

Analysis of MAC-level Throughput in LTE Systems

4.1 Introduction

As mentioned in Chapter 3 3GPP-LTE is the emerging standard for future 4G cellular systems. To achieve high throughput performance, in addition to an advanced physical layer design, LTE exploits a combination of sophisticated radio resource management functionalities, such as Channel Quality Indicator (CQI) reporting, link rate adaptation through Adaptive Modulation and Coding (AMC), and Hybrid Automatic Retransmission Request (HARQ) [5]. Specifically, a base station (eNB) can simultaneously serve multiple users on orthogonal subcarriers that are grouped into frequency resource blocks (RBs). Then, each user (UE) periodically measures channel state information that is fed back to the eNB in terms of CQI reports. Typically, only aggregate CQI values are reported to reduce channel feedback information. CQI measurements are used by eNBs for scheduling and link rate adaptation on the downlink [51]. For instance, the modulation and coding scheme (MCS) is typically selected in order to maximise the data rate to the scheduled UE subject to a constraint on the error probability. Errors at the physical layer are also mitigated by exploiting automatic retransmission protocols with channel coding (HARQ). More precisely, HARQ procedures use the classical stop-and-wait algorithm, in which the eNB decides to perform a retransmission based on the exchange of ACK/NACK messages with the UE. Then, UEs try to decode the packet by combining

the retransmitted copies. Since user, cell and radio link throughputs are among the most important performance indicators that the operators adopt to assess the QoS in an LTE system [52], an extensive literature exists that investigates LTE throughput performance based on analytical models [28, 29, 31], simulation tools [51] or field tests [53, 54]. However, it is evident that a complex interplay exists among the various mechanisms that operate at the MAC layer to improve communication reliability and to increase data rates. This makes accurate LTE throughput analysis notably difficult. Thus, most studies limit the analysis only to the radio link throughput or consider single MAC functions in isolation [8]. Furthermore, simplified error models are typically considered that only allow deriving upper bounds for the LTE throughput [28]. This Chapter illustrates a unified modelling framework of the MAC-level downlink throughput [55] that is valid for homogeneous cells [6] and Rayleigh-distributed fading. This model simultaneously caters for CQI feedback schemes that use spectral efficiency to generate CQI, as well as AMC and HARQ protocols. Furthermore, we include in the analysis an accurate link layer abstraction model that uses the Mean Mutual Information per coded Bit (MMIB) metric to derive the physical error probability [7]. The throughput estimates of our model are accurate, as validated using the ns-3 simulator extended with the LENA module for LTE[1]. Furthermore, the results confirm that the IR-HARQ mechanism is very effective in improving error correction. However, the effectiveness of the IR-HARQ scheme depends on the appropriate selection of the modulation and coding scheme of the first transmission attempt.

4.2 LTE MAC Protocol Specification

Now a briefly describe relevant details of the LTE MAC for downlink transmissions, with special attention to frame structure, CQI feedback mechanisms and HARQ protocols. We also introduce the system model and notation, and we discuss the main assumptions that underlay our analysis. More details can be found in Chapter 3. In the downlink, LTE uses the Orthogonal Frequency Division Multiple Access (OFDMA) scheme. Specifically, in the frequency domain the system bandwidth, W, is divided into several orthogonal subcarriers. Each subcarrier has a bandwidth of 15 kHz. In the time domain, the duration of one LTE radio frame is 10 ms. One frame is divided into ten

[1] http://networks.cttc.es/mobile-networks/software-tools/lena/

transmission time intervals (TTIs) of 1 ms each. Furthermore, each TTI consists of two 0.5 ms slots. Each slot contains either six or seven OFDM symbols, depending on the Cyclic Prefix (CP) length. A set of twelve consecutive subcarriers over the duration of one slot is called a physical Resource Block (RB). Hereafter, we denote with q the total number of RBs available over the system bandwidth. Since the RB bandwidth is only 180 kHz, it is reasonable to assume that the channel response is frequency-flat across all the twelve subcarriers of the RB[2]. Then, let us denote with $\gamma_{i,k}$ the SNR of the i^{th} RB of the k^{th} UE. Clearly, the statistics of the SNR depend on the channel model and the multi-antenna diversity mode of operation. As commonly adopted in other LTE models, e.g. [29], in this study we assume that the fading from the eNB to the UEs is *Rayleigh distributed*. This implies that *the SNR of each RB is an exponential* random variable (RV) [56]. Furthermore, we also assume an *homogeneous cell model* [6], i.e. the SNR is independent for different users and RBs. This also means that the SNRs of all RBs are *uncorrelated* in frequency and space, and $\gamma_{i,k}$ can be regarded as independent and identically distributed (i.i.d.) RV. Popular methods (e.g., EESM and MIESM) that are typically used in LTE to compute CQI values rely on the concept of *effective* SNR. Basically, the UEs map the SNRs of multiple subcarriers/RBs into a single value by applying complex non-linear transformations. Then, the effective SINR is used to estimate the BLER experienced by a user and to determine the appropriate MCS, i.e. the MCS that allows the UE to decode the transport block with an error rate probability not exceeding 10%. However, the statistics of the effective SNR generated by EESM and MIESM techniques are not known in closed-form. Thus, they must be approximated or computed numerically, which makes performance analysis difficult [29, 57]. An alternative approach proposed in [58] to implement AMC capabilities is based on the *spectral efficiency*. Specifically, let us denote the with $\eta_{i,k}$ the spectral efficiency of the i^{th} RB of the k^{th} UE. Then, it holds that [59]

$$\eta_{i,k} = \log_2\left(1 + \frac{\gamma_{i,k}}{\Gamma}\right) , \tag{4.1}$$

where $\Gamma = -\ln(5\beta)/1.5$ and β is BLER upper bound. Now a static mapping can be determined between the spectral efficiency and the CQI index, as well as between the CQI index and the MCS value [58]. More formally, let us denote with $C_{i,k}$ the CQI index for the i^{th} RB of the k^{th} UE. Typically the value of CQI can range between 1

[2]This assumption will hold for highly dispersive channels with a long delay spread.

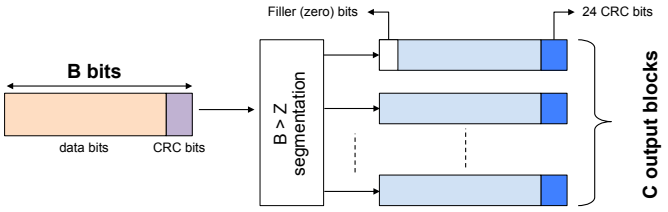

FIGURE 4.1: Transport block segmentation.

and L. Then, $C_{i,k} = j$ $(j = 0, \ldots, L)$ if $S_j \leq \eta_{i,k} \leq S_{j+1}$, with $S_0 = 0$ and $S_{L+1} = \infty$. In other words the CQI value is a quantised version of the spectral efficiency[3]. Closely related to the MCS selection is also the transport block (TB) size determination. More precisely, let n_k the number of RBs allocated to the k^{th} UE during a frame. Then, the number B of bits that can be delivered in those RBs, which is called transport block, is a function of the MCS index[4]. Furthermore, if $B > Z$ (with $Z = 6144$ bits in 3GPP-LTE) the transport block is *segmented* into a number C of *code blocks* (CBs) that are independently encoded. Note that the CB size highly impacts the actual BLER performance for a given MCS [7]. Figure 4.1 exemplifies the transport block segmentation.

Regarding the HARQ protocol, LTE employs two types of HARQ schemes. In HARQ type-I, each encoded data frame is retransmitted until the frame passes the CRC test or the maximum number of retransmissions is reached. Erroneous frames are simply discarded. In contrast, in HARQ type-II, each transmission contains incremental redundancy (IR) about the data frame. Thus, consecutive transmissions can be combined at the receiver to improve error correction. Although our model is valid for all HARQ types, in the following we only consider HARQ type-II that is the most widely used in LTE. Note that in LTE systems *retransmissions typically use the same MCS index as the initial transmission*. It is also important to point out that the transmission of HARQ feedbacks (i.e. ACK/NACK messages) is not instantaneous but each received packet experiences a processing delay. According to the LTE standard, the processing delay at the receiver is about 3 ms. Thus, assuming the same delay to process data transmissions

[3]Note that in the 3GPP-LTE standard, $L = 16$ and the S_j thresholds are specified in Table 7.2.3-1 of [60]. Furthermore, in the 3GPP-LTE standard the available MCS indexes are 32 but a 4-bit CQI allows selecting only 15 MCS (for CQI=0 no transmission will be scheduled). Thus, in practical LTE systems only a subset of available MCS is typically used.

[4]See Table 7.1.7.2.1-1 of [60] for the static mapping between TB size, MCS and number of RBs allocated to the UE.

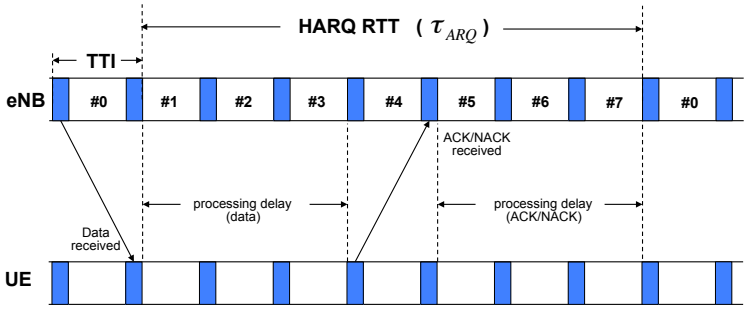

FIGURE 4.2: HARQ processes and timing in FDD-LTE DL.

and ACK/NACK messages, the HARQ round trip time, say τ_{ARQ}, is 7 TTIs, as shown in Figure 4.2. For this reason, an eNB must support up to 8 parallel HARQ processes for each UE to enable *uninterrupted* communications. In this way, an eNB can continue to transmit new TBs while the UEs are decoding already received TBs.

4.3 MAC-level Throughput Analysis

In this section we develop the mathematical model of the MAC-level downlink throughput for a single LTE cell with n randomly deployed UEs. Without loss of generality we assume asymptotic traffic conditions, i.e., infinite traffic is waiting for each user at the transmission buffer of the eNB. As discussed in Section 4.2, the packet scheduler at the eNB is responsible for both allocating RBs to UEs every TTI, and controlling up to 8 HARQ processes per UE. Intuitively, the maximum number of HARQ processes that can be concurrently activated by the scheduler during an HARQ period is bounded by the number of times the same UE is scheduled during a τ_{arq} time interval. For the sake of simplicity, in this study we consider a Round Robin (RR) scheduler, which works by dividing the total amount of available radio resources in a fair manner among the UEs. More precisely, a RR scheduler allocates to each UE a set of consecutive resource blocks, called resource block groups (RBGs), whose size P depends on the system bandwidth [60]. Consequently the number b of RBs assigned to each UE is simply given by

$$b = \max\left\{P, \left\lfloor \frac{q}{n} \right\rfloor\right\} \ . \tag{4.2}$$

Without loss of generality we consider a non-adaptive HARQ strategy, in which the scheduler maintains the same RBG and MCS configuration of the original TB when

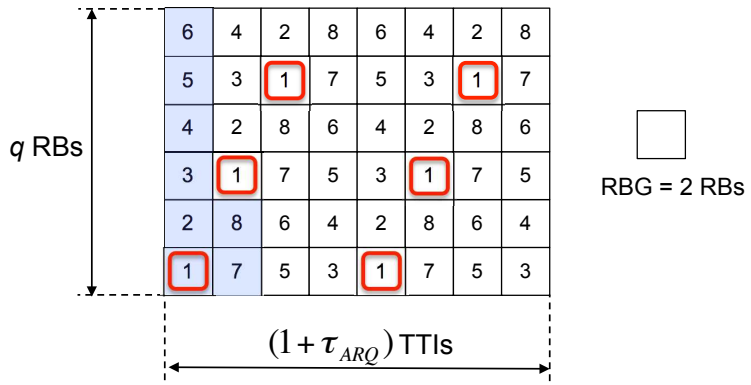

FIGURE 4.3: RR operations with $q = 12$, $P = 2$ and $n = 8$.

scheduling the retransmissions. To illustrate the dependency between the number of times a UE is scheduled during an HARQ period, the RBG size and the total number of UEs in Figure 4.3 we exemplify the scheduling decisions that are cyclically performed by the RR scheduler during an HARQ period with $q = 12$, $P = 2$ and $n = 8$. As shown in the figure, each UE is scheduled six times during an HARQ period. In general, the average number of times each UE is scheduled in $(1 + \tau_{ARQ})$ TTIs is simply given by

$$n_{RR} = \left\lfloor \frac{q(1 + \tau_{ARQ})}{n \cdot b} \right\rfloor . \tag{4.3}$$

It must be noted that not all the transmission opportunities allocated by the eNB to an UE result into a successful transmission due to signal attenuation, shadowing and fading. In the following we denote with $P_e(m, k, r)$ the TB error probability at the r retransmission for the k^{th} UE when m is the adopted MCS, with $P_s(m, k, r)$ the probability that the k^{th} UE correctly decodes a TB *after* r retransmissions when m is the adopted MCS, and with $P_d(m, k)$ the probability that the k^{th} UE discards a packet when m is the adopted MCS because it has reached the maximum number of failed retransmissions. In Section 4.3.2 we provide closed-form expressions for $P_s(m, k, r)$, $P_e(m, k, r)$ and $P_d(m, k)$. Finally, to perform the throughput analysis we observe the system at the end of each successful transmission, because all the processes that define the occupancy pattern of the channel (i.e., HARQ processing delays and retransmissions) regenerate with respect to the sequence of time instants corresponding to the completion of a successful transmission. Then, it follows that the MAC-level throughput for the k^{th}

UE is

$$\rho_k = n_{RR} \frac{E[TB|Succ]_k}{E[T_{ARQ}]_k} \ , \tag{4.4}$$

where $E[TB|Succ]_k$ is the average number of information bits that are delivered with a successful transmission of the k^{th} UE, and $E[T_{ARQ}]_k$ is the average time needed by an HARQ process to complete a successful transmission of the k^{th} UE. In equation (4.4), the multiplying factor n_{RR} is used to take into account that n_{RR} independent HARQ processes run in parallel. The following theorem provides closed-form expressions for $E[TB]_k$ and $E[T_{ARQ}]_k$. where $E[TB|Succ]_k$ is the average number of information bits that are delivered with a successful transmission of the k^{th} UE, and $E[T_{ARQ}]_k$ is the average time needed by an HARQ process to complete a successful transmission of the k^{th} UE. In equation (4.4), the multiplying factor n_{RR} is used to take into account that n_{RR} independent HARQ processes run in parallel. The following theorem provides closed-form expressions for $E[TB]_k$ and $E[T_{ARQ}]_k$.

Theorem 1. By assuming an homogenous cell with Rayleigh-distributed fading, and a RR scheduling policy

$$E[TB|Succ]_k = \sum_{j=0}^{L} TBS(m(j), b) \left[1 - P_d(m, k)\right] g_k[j] \ , \tag{4.5a}$$

$$E[T_{ARQ}]_k = \sum_{j=0}^{L} \left[\sum_{r=0}^{r_{max}} (r+1)(1+\tau_{ARQ}) P_s(m, k, r) \right] g_k[j] \ , \tag{4.5b}$$

where $TBS(m(j), b)$ is a function that computes the number of data bits transmitted in b RBs using the MCS $m(j)$[5], and $g_k[j]$ is the PMF of the CQI value reported by the k^{th} UE.

Proof. See Appendix. □

4.3.1 CQI feedback scheme and AMC strategy

The objective of this section is twofold. First, we develop the analytical tools to characterise the wideband CQI feedback scheme of LTE. Second, we analyse the performance of a link rate adaptation technique based on wideband CQI reports. Let us assume that n UEs are randomly distributed in the cell, and let d_k be the distance of the k^{th} UE

[5]For the sake of notation brevity, we indicate with $m(j)$ the MCS that the eNB uses when the CQI value reported by a UE is equal to j.

from the eNB. As discussed in Section **??** we also assume that $\gamma_{i,k} \sim Exp(\lambda_k)$, where the rate parameter λ_k of the exponential distribution depends on the UE position. Under this assumption the statistics of the spectral efficiency for each RB can be expressed in a closed-form as given by the following Theorem.

Theorem 2. If $\gamma_{i,k} \sim Exp(\lambda_k)$ then the cumulative distribution function (CDF) of the spectral efficiency $\eta_{i,k}$ in equation (4.1) is computed as:

$$F_\eta(x;i,k) = \begin{cases} 1 - e^{-\lambda_k \Gamma(2^x - 1)} & \text{if } x \geq 0 \\ 0 & \text{if } x < 0. \end{cases} . \tag{4.6}$$

Proof. See Appendix. □

LTE specifies different types of CQI reporting: *wideband* and *subband*. Specifically, the wideband CQI represents the SNR observed by the UE over the whole channel bandwidth, while the subband CQI represents the SNR observed by the UE over a collection of adjacent RBs. Note that a vector of CQI values should be transmitted to the eNB when using the latter feedback scheme. Thus, the subband-level feedback scheme ensures a finer reporting granularity but it also generates a higher overhead. In this study, we focus on the wideband feedback scheme and we assume that the CQI reported by the k^{th} UE, say $\widehat{C}_k$ is the *arithmetic mean* of the CQI values computed over all RBs[6]. Then, we use the spectral efficiency to generate the CQI values from the SNR measures of all RBs. The statistics of the wideband CQI are mathematically derived below.

Claim 1. The probability mass function (PMF) of the CQI value for the i^{th} RB assigned to the k^{th} UE is given by

$$g_{i,k}[j] = F_\eta(S_{j+1};i,k) - F_\eta(S_j;i,k) \; . \tag{4.7}$$

Proof. See Appendix. □

Claim 2. In an homogenous cell the PMF of the wideband CQI value reported by the k^{th} UE is given by

$$g_k[j] = \sum_{l=qj}^{q(j+1)-1} g_k^{(q)}[l] \; , \tag{4.8}$$

[6]Note that an alternative solution would be to report the worst CQI value over all (or a subset of) RBs as in [28].

where $g_k^{(q)}[l]$ is the q-fold convolution of $g_{i,k}[j]$.

Proof. See Appendix. □

As described in Section 4.2 a static mapping is typically established between the CQI value received at the eNB and the MCS for the downlink transmissions. Thus, $g_k[j]$ also characterizes the distribution of the MCS index $m(j)$ that is used by the eNB for the downlink transmission to the k^{th} UE when the reported wideband CQI is j.

4.3.2 Physical layer error model

We now conclude the analysis by introducing the physical layer error model. In this study we adopt the general approach initially proposed in [61] to accurately approximate the BLER curves of OFDMA-based wireless systems, and later specialised for the LTE case in [62]. Specifically, we assume that the *mutual information per coded bit* (MIB) of MCS m, as defined in [61], can be accurately approximated by a combination of Bessel functions of the SNR γ as follows

$$I_m(\gamma) \approx \sum_{h=1}^{H} \alpha_h J(\psi_h \sqrt{\gamma}) \,, \tag{4.9}$$

where H, α_h and ψ_h parameters are empirically calibrated as a function of the MCS index. Subsequently, the *mean* MIB (MMIB) value for each UE is computed by averaging the corresponding mutual information of all RBs allocated to that UE. Specifically, let $\Omega(k)$ be the set of RBs that are allocated to the k^{th} UE by the scheduler. Then, the MMIB value over the vector of SNR values for each RB assigned to the k^{th} UE when m is the adopted MCS is simply given by

$$\widehat{I}_{m,k} = \frac{1}{\omega(k)} \sum_{i \in \Omega(k)} I_m(\gamma_{i,k}) \,, \tag{4.10}$$

where $\omega(k)$ is the cardinality of the $\Omega(k)$ set. The non-linear nature of (4.9) makes an exact analysis difficult. Thus, previous studies limit the computational complexity of deriving MMIB values in multi-user scenarios by considering a quantised version of the $I_m(\gamma)$ function (4.9) in order to *discretise the MIB metric* [62]. More precisely, let us

define a set $\mathcal{V}_m = \{\mu_m[0], \mu_m[1], \ldots, \mu_m[v_m]\}$ for each MCS m such that

$$\mu_m[v] = I_m(Q_{m,v}) \ , \tag{4.11}$$

where $(Q_{m,v+1} - Q_{m,v}) = \delta\gamma$ is the quantisation step size, and $Q_{m,0}$ is the minimum usable SNR for MCS m. Now, let us denote with $H_{i,m,k}$ the discrete MIB value for the i^{th} RB scheduled to the k^{th} UE when m is the adopted MCS. Similarly to the approach adopted for CQI mapping, we assume that $H_{i,m,k} = \mu_m[v]$ $(v = 0, \ldots, V)$ if $Q_{m,v} \leq \gamma_{i,k} \leq Q_{m,v+1}$. In other words the discrete MIB value is associated to a *range* of SNRs. It is straightforward to derive the statistics of the discretised MIB metric as follows.

Claim 3. In an homogenous cell with Rayleigh-distributed fading, the PMF of $H_{i,m,k}$ is given by

$$h_{i,m,k}[v] = F_\gamma(Q_{(v+1),m}; i, k) - F_\gamma(Q_{v,m}; i, k) \ , \tag{4.12}$$

where $h_{i,m,k}[v] = Pr\{H_{i,m,k} = \mu_m[v]\}$.

Proof. See Appendix. □

Similarly, we introduce a discrete MMIB metric, say $\widehat{H}_{m,k}$, computed over the set of RBs allocated to the k^{th} UE when m is the adopted MCS. In particular, $\widehat{H}_{m,k}$ can be obtained as the mean of the $H_{i,m,k}$ values over the set $\Omega(k)$. Thus, the statistics of the discretised MMIB value are derived using the same technique of Claim 2.

Claim 4. In an homogenous cell the PMF of $\widehat{H}_{m,k}$ is given by

$$h_{m,k}[v] \approx \sum_{l \in \Phi_v} h_{i,m,k}^{(\omega(k))}[l] \ . \tag{4.13}$$

where $h_{i,m,k}^{(\omega(k))}[l]$ is the $\omega(k)$-fold convolution of $h_{i,m,k}[l]$. The definition of the Φ_v set is quite involved and is given in the proof.

Proof. See Appendix. □

Once the MMIB value is given, a direct MMIB to BLER mapping can be used to obtain the *code block error rate*, without necessarily defining an effective SINR. Following the

approach proposed in [61], the empirical BLER curve for MCS m can be approximated with a Gaussian cumulative model as follows

$$CBLER_m(y,e) = \frac{1}{2}\left[1 - erf\left(\frac{y - b_e}{c_e}\right)\right] , \tag{4.14}$$

where y is the MMIB value, while b_e and c_e are parameters used to fit the Gaussian distribution to the empirical BLER curve[7]. These parameters depend on the Effective Code Rate (ECR), i.e. the ratio between the number of downlink information bits (including CRC bits) and the number of coded bits. Intuitively, the ECR value is a result of the selected TB size, MCS, and $\Omega(k)$. Then, the overall error probability for a transport block transmitted as a combination of C code blocks, each one associated with a MMIB and ECR value, can be computed as

$$TBLER_m(y,e) = 1 - \prod_{i=1}^{C} (1 - CBLER_m(y_i, e_i)) \ . \tag{4.15}$$

However equation (4.15) does not take into account the impact of an IR-HARQ mechanism that combines retransmissions to improve error correction. To generalise equation (4.15) for a system with incremental redundancy we adopt the same approach as in [63]. In particular, we introduce an *equivalent* MMIB metric as the average of the mutual informations per HARQ block received on the total number of retransmissions. More precisely, let us assume that the original transport block has been retransmitted r times. Then, let $(\widehat{I}^{(0)}_{m,k}, \widehat{I}^{(1)}_{m,k}, \ldots, \widehat{I}^{(r)}_{m,k})$ be the vector of MMIB values for each of these transmissions. The equivalent MMIB for the r^{th} retransmission can be computed as follows

$$\widehat{I}_{m,k,r} = \frac{1}{r+1} \sum_{i=0}^{r} \widehat{I}^{(i)}_{m,k} \ , \tag{4.16}$$

Then, the PMF of the equivalent MMIB value for the r^{th} retransmission is $h^{(r)}_{m,k}[v] = Pr\{\widehat{I}_{m,k,r} = \mu_m[v]\}$. This PMF can be obtained using the same technique as in Claim 4 and it is not reported here for the sake of brevity. Similarly, we compute the effective ECR after r retransmissions, say $e^{(r)}$, by dividing the number of information bit of the original transmission with the sum of the number of coded bits of each retransmissions. Finally, by applying the law of total probability the *average* TB error probability at the

[7]Empirical BLER curves can be obtained through field measurements or detailed link-level simulations.

r retransmission for the k^{th} UE when m is the adopted MCS can be computed as

$$P_e(m,k,r) = \sum_{v=0}^{v_m} TBLER_m(\mu_m[v], e^{(r)}) \cdot h_{m,k}^{(r)}[v] \ . \tag{4.17}$$

Finally to evaluate $P_s(m,k,r)$ we can observe that the r^{th} retransmission of the k^{th} UE, when m is the adopted MCS, is a success only if the previous $(r-1)$ transmissions were TBs received erroneously and the r^{th} transmission is correctly decoded. Hence, it immediately follows that

$$P_s(m,k,r) = \left[\prod_{i=0}^{r-1} P_e(m,k,i)\right] \times \left[1 - P_e(m,k,r)\right] \ . \tag{4.18}$$

We conclude this section by noting that the probability $P_d(m,k)$ that the k^{th} UE discards a packet when m is the adopted MCS because it has reached the maximum number of failed retransmissions is simply given by:

$$P_d(m,k) = \prod_{i=0}^{r_{max}} P_e(m,k,i) \ . \tag{4.19}$$

Finally, it is straightforward to observe that the *average* probability of discarding a packet for the k^{th} UE is computed as

$$P_d(k) = \sum_{j=0}^{L} P_d(m(j),k) g_k[j] \ . \tag{4.20}$$

4.4 Model Performance Evaluation

In this section we assess the accuracy of the throughput analysis in two different scenarios. In the first one, we assume that the mapping function that is used to convert spectral efficiency into CQI feedbacks, and then into MCS indexes is sufficiently accurate. As better explained in the following, in this condition error probabilities are typically small and retransmissions may have a negligible impact on the MAC layer throughput with respect to other protocol overheads. In the second scenario we assume that a fixed CQI is fed back to the eNB by each UE. Thus, the eNB necessarily selects a fixed MCS independently of the current channel conditions. This clearly represents a worst-case scenario, which is useful to assess the robustness of our modelling framework even when the reported CQI provides a very poor prediction of channel performance.

Furthermore, it is also useful to better highlight the ability of the HARQ scheme to improve the overall system throughput without relying on per-subcarrier information.

4.4.1 Simulation setup

All the following experiments have been carried out using the ns3 packet-level simulator, which includes a detailed implementation of the LTE radio protocol stack. The main simulation parameters are summarised in Table 4.1. Specifically, we consider an *Urban Macro* scenario, in which path loss and shadowing are modelled according to the COST231-Hata model [64], which is widely accepted in the 3GPP community. The fading is Rayleigh distributed. To limit the computation complexity of the simulator pre-calculated fading traces are included in the LTE model. Given the downlink system bandwidth (see Table 4.1) a RBG comprises two RBs [60], i.e., $P = 2$. Regarding the network topology, we considered a single cell with a varying number of static UEs, chosen in the range $[1, 50]$. Note that, in our settings a maximum number of 96 (i.e., $8\lfloor q/P \rfloor$) unique UEs can be scheduled within an HARQ period. Indeed, if $n > 96$ the RR period is longer than the HARQ period. All results presented in the following graphs are averaged over multiple simulation runs with different fading traces and topology layouts. Confidence intervals are generally very tight and they are not shown in the figures if below 1%. Each simulation run lasts 300 seconds.

TABLE 4.1: Simulation parameters

Parameter	**Value**
Carrier frequency (GHz)	2.14
DL bandwidth (MHz)	5
q	25
eNB TX Power (dBm)	43
CQI processing time (TTI)	2
CQI transmission delay (TTI)	4
Antenna scheme	SISO
PDCCH & PCFICH (control ch.)	3 OFDM symbols
PDSCH (data ch.)	11 OFDM symbols
n	$[10, 50]$
r_{max}	3

In this section we validate the accuracy of our modelling approach by evaluating the throughput of an individual UE under varying channel conditions and congestion levels. Specifically, we assume that n UEs are randomly deployed in a cell and they are static.

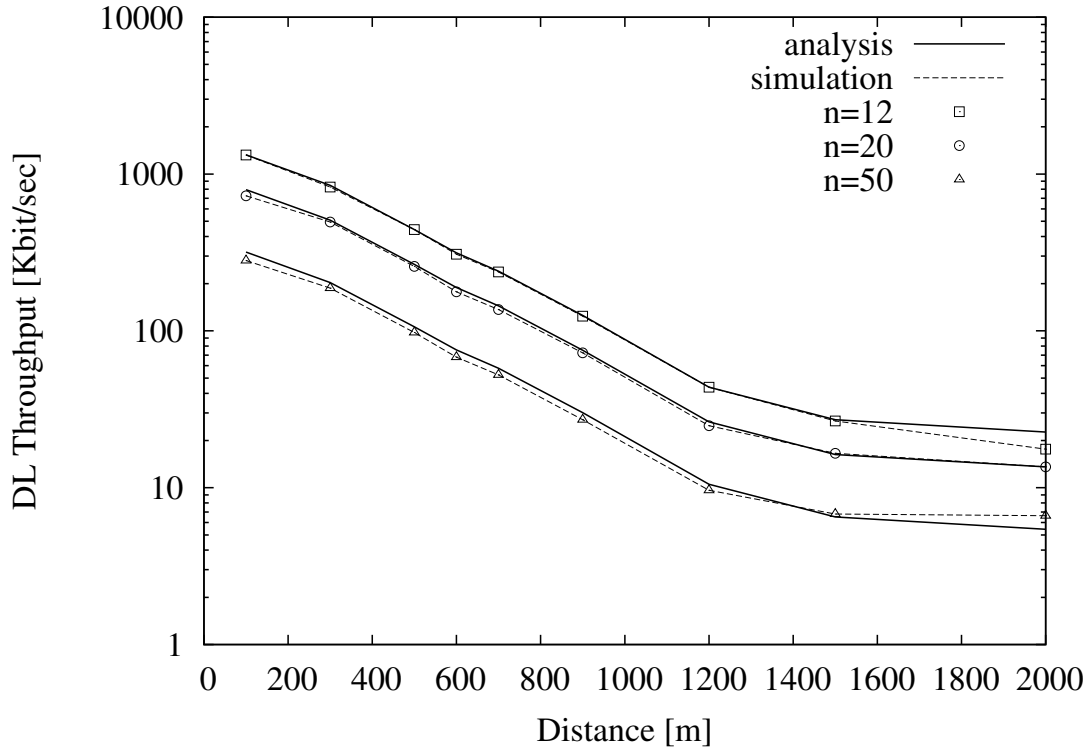

FIGURE 4.4: *Adaptive CQI*: Comparison of analytical and simulation results for the MAC-level throughput of a tagged UE versus its distance from the eNB and the total number of UEs in the cell.

Then, an additional *tagged* UE is deployed at a known distance d from the center of the cell. Figure 4.4 shows a comparison between the model predictions and the simulation results for the MAC-level downlink throughput of the tagged UE versus its distance from the eNB and for different n values. As a first important consideration, Figure 4.4 proves that our analysis provides a very accurate approximation of the MAC-level throughput independently of the fading intensity. Furthermore, the results confirm that increasing the total number of UEs in the cell has the effect of reducing in a proportional manner the throughput of the tagged UE. This is due to the fact that RR is a channel-unaware scheduler that performs fair sharing of time resources among UEs. Finally, it is also important to point out that the IR-HARQ mechanism is very effective in improving error correction. As discussed in Section 4.2 the modulation and coding scheme are selected in such a way that the error probability is well below 10%. As a matter of fact, our results (not shown here) indicate that the actual error probability for the first transmission attempt is below 5% up to a distance of 1000 meters, and the probability to perform more than one retransmission is negligible.

4.4.2 Results with fixed CQI

In this second set of simulations we consider the same network scenario as in Section **??**. However, independently of the UE position the CQI feedback is assumed constant. Figure 4.5 shows a comparison between the model predictions and the simulation results for the MAC-level downlink throughput of the tagged UE versus its distance from the eNB when $n = 12$. Note that twelve is the maximum number of UEs such that $n_{RR} = 8$. In other words, with $n = 12$ all the UEs are scheduled during one TTI and 8 HARQ process needs to be managed simultaneously. As expected a high value for the reported CQI results into the use of a very efficient MCS, which provides a high data rate at the cost of high vulnerability to channel fading. Consequently, the tagged UE obtains a high throughput when close to the eNB, but the throughput performance rapidly degrades as it gets farther from the eNB. On the contrary a low reported CQI provides a much more stable throughput performance due to the robustness of the selected MCS. However, in this case we must compromise between robustness and efficiency. To quantify this trade-off in Figure 4.6 we show the probability to discard a packet as given by formula (4.20) in the same network configurations of Figure 4.5. Interestingly, we can observe that there is a critical distance after which the $P_d(k)$ probability rapidly increases up to the value of one. Hence, after this critical distance even the IR-HARQ scheme becomes incapable of controlling the error probability. Furthermore, results in Figure 4.6(b) indicate that our model underestimates the actual $P_d(k)$ for less reliable MCSs, while results in Figure 4.6(a) indicate that our model overestimates the actual P_d for robust MCS.

4.5 Summary

In this Chapter we have developed an analytical framework to estimate the MAC-level downlink throughput in a LTE system, which carefully models practical mechanisms of the MAC layer of the LTE technology. As a matter of fact, LTE systems achieve high communication reliability by adopting a combination of link adaptation and error correction schemes. This study is a first attempt to tackle the complexity of modelling the interplay between these mechanisms and to obtain a realistic evaluation of the throughput performance at the MAC level. Our results confirm that the IR-HARQ mechanism is

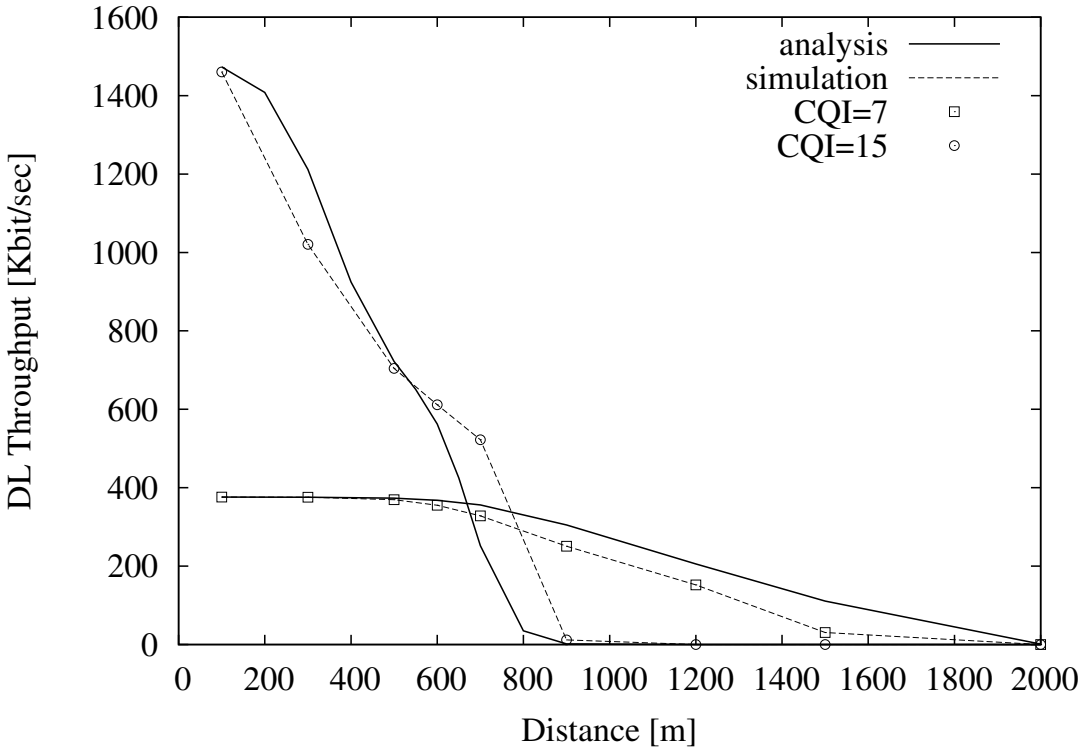

FIGURE 4.5: *Fixed CQI*: comparison of analytical and simulation results for the MAC-level throughput of a tagged UE versus its distance from the eNB for different CQI values and $n = 12$.

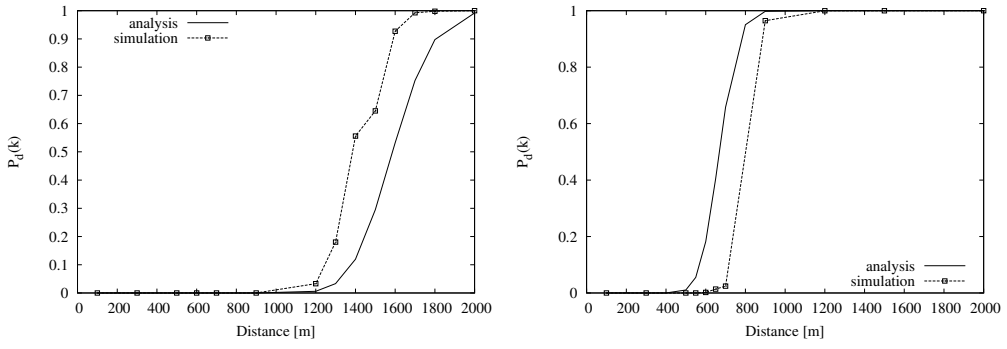

(a) CQI=7 (b) CQI=15

FIGURE 4.6: Fixed CQI: comparison of analytical and simulation results for the probability of discarding a packet for a tagged UE versus its distance from the eNB for different CQI values and $n = 12$.

very effective in improving error correction. However, the effectiveness of the IR-HARQ scheme depends on the appropriate selection of the modulation and coding scheme of the first transmission attempt. Although there is still the need for detailed system-level simulations, we believe that the proposed analytical approach will be useful to an LTE system designer for dimensioning the LTE system and configuring the optimal set of radio MAC parameters.

Chapter 5

Robust Adaptive Modulation and Coding (AMC) Selection

5.1 Introduction

Adaptive Modulation and Coding (AMC) in LTE networks is commonly employed to improve system throughput by ensuring more reliable transmissions. In particular, adaptive modulation and coding (AMC) has been proposed for LTE, as well as many other wireless communication systems, to increase channel throughput [65]. In general, AMC techniques try to optimally select the channel coding and modulation scheme (MCS), while fulfilling a certain Block Error Rate (BLER) constraint[1] by taking into account the current channel conditions and the receiver's characteristics (e.g., antenna configuration). For LTE downlink transmissions, traditional AMC schemes rely on the channel quality indicator (CQI) feedbacks that are periodically reported by the user terminals (UEs) to their base stations (eNBs) [66]. How CQI values should be computed by the UE using channel state information (e.g., SINR measurements) is implementation dependent. In practical implementations the UEs directly selects the MCS value that, if used by the eNB under the measured channel conditions, would achieve the maximum possible throughput by guaranteeing that the BLER is below 10%. This value is then mapped onto a CQI value and fed back to the eNB (that translates it back into the

[1]The BLER for a certain user is defined as the ratio between the number of erroneous resource blocks and the total number of resource blocks received by that user. In the LTE standard it is mandated that the selected MCS ensures an average BLER under the measured channel conditions lower than 10% [66].

corresponding MCS value) [11, 67]. Therefore, the key focus of AMC algorithms is to define how UEs can compute MCS values that satisfy the BLER requirements. Several technical challenges have to be addressed to design efficient AMC solutions for LTE systems. In particular, in practical LTE systems, the SINR values of multiple subcarriers are aggregated and translated into a one-dimensional link quality metric (LQM), since the same MCS must be assigned to all subcarriers assigned to each UE. Popular methods that are used in LTE to obtain a single effective SINR from a vector of physical-layer measurements related to subcarriers are the exponential effective SINR mapping (EESM) [68] or the mean mutual information per coded bit (MMIB) [69]. Once the LQM is found, AMC schemes typically exploit *static mappings* between these link quality metrics and the BLER performance of each MCS to select the best MCS (in terms of link throughput). In other words, for each MCS a range of LQM values is associated via a look-up table, over which that MCS maximises link throughput. Either link-level simulations or mathematical models can be used to generate such static BLER curves under a specific channel model. Unfortunately, past research has shown that it is difficult to derive accurate link performance predictors under realistic channel assumptions [7, 9–11]. Furthermore, a simulation-based approach to derive the mapping between LQM values and BLER performance is not scalable since it is not feasible to exhaustively analyse all possible channel types or several possible sets of parameters [12]. The second main problem with table-based AMC solutions is that a delay of several transmission time intervals (TTIs) may exist between the time when a CQI report is generated and the time when that CQI feedback is used for channel adaptation. This is due to processing times but also to the need of increasing reporting frequency to reduce signalling overheads. This mismatch between the current channel state and its CQI representation, known as *CQI ageing*, can negatively affect the efficiency of AMC decisions [13, 14]. To deal with the above issues, in this Chapter we illustate a new flexible AMC framework, called RL-AMC [70], that autonomously and at run-time decides upon the best MCS (in terms of maximum link-layer throughput) based on the knowledge of the outcomes of previous AMC decisions. To this end we exploit reinforcement learning techniques to allow each eNodeB to update its MCS selection rules taking into account past observations of achieved link-layer throughputs. Specifically, the purpose of the decision-making agent in our AMC scheme is to discover which is the correction factor that should be applied to CQI feedbacks in order to guide the transmitters in selecting more efficient MCSs. An important feature of our proposed scheme is the use of a

low-dimensional state space, which ensures a robust and efficient learning even under time-varying channel conditions and mobility. Through simulations in ns3 we show that our AMC method can improve the LTE system throughput compared to other schemes that use static mappings between SINR and MCS both under pedestrian and vehicular network scenarios. Furthermore, our AMC is capable of discovering the best MCS even if the CQI feedback provides a poor prediction of the channel performance.

5.2 AMC in LTE

For the sake of illustrative purposes, in Figure 5.1 we show a functional architecture for a practical AMC scheme for LTE systems. At the receiver's side, a first module is responsible for processing the channel state information (e.g., per-subcarrier received SINR values) to obtain a BLER estimation under the assumption of a specific channel model. Specifically, the receiver maps the channel measurements into a single link quality metric. Then, an offline look-up table is used to map this LQM to a BLER estimate for each MCS. These BLER curves are used to find the highest-rate MCS index that can satisfy a 10% BLER target. Finally, the selected MCS index is sent in the form of a CQI feedback to the transmitter. Based on such CQI feedback the transmitter performs resource scheduling and MCS selection. Most of existing research on AMC schemes for LTE is focused on the problem of CQI calculation given a link quality metric. As mentioned in Section 5.1 a popular and sufficiently accurate method for LQM calculation is EESM. For instance, the authors in [8] study the MCS performance under an AWGN channel. Accurate packet error prediction for link adaptation via a Gaussian approximation of coding and decoding performance is proposed in [71]. A novel LQM metric for link adaptation based on raw bit-error-rate, effective SINR and mutual information is investigated in [72]. In [67] the authors proposed MCS selection based on packet-level effective SINR estimates rather than block-level SINR values, and they describe different averaging schemes to map BLER onto packet error rates. On the other hand, the authors in [11, 29] develops statistical models of the EESM under different channel models and use those models to analyse the throughput of EESM-based AMC for various CQI feedback schemes. A second group paper studies channel predictors to deal with the CQI ageing. The authors in [13] derive closed-form expressions for the average throughput of an adaptive OFDMA system under the assumption of imperfect

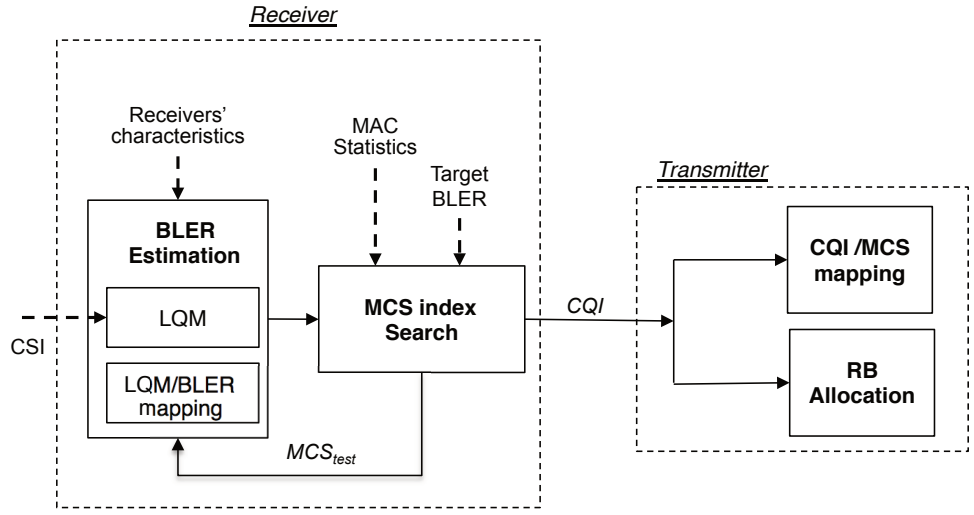

FIGURE 5.1: AMC functional architecture.

CQI knowledge. The performance of different CQI predictors, such as Kalman filtering or linear prediction with stochastic approximation, are evaluated in [14] and [73].

5.3 Background on Reinforcement Learning (RL)

Reinforcement Learning (RL) is a popular machine learning technique, which allows an agent to automatically determine the optimal behaviour to achieve a specific goal based on the positive or negative feedbacks it receives from the environment in which it operates after taking an action from a known set of admissible actions [74]. Typically, reinforcement learning problems are instances of the more general class of Markov Decision Processes (MDPs), which are formally defined through:

- a finite set $S = \{s_1, s_2, \ldots, s_n\}$ of the n possible states in which the environment can be;
- a finite set $A(t) = \{a_1(t), a_2(t), \ldots, a_m(t)\}$ of the m admissible actions that the agent may perform at time t;
- a transition matrix P over the space S. The element $P(s, a, s')$ of the matrix provides the probability of making a transition to state $s' \in S$ when taking action $a \in A$ in state $s \in S$;
- a reward function R that maps a state-action pair to a scalar value r, which represents the immediate payoff of taking action $a \in A$ in state $s \in S$.

The goal of a MDP is to find a *policy* π for the decision agent, i.e., a function that specifies the action that the agent should choose when in state $s \in S$ to maximise its expected long-term reward. More formally, if an agent follows a policy π starting from a certain state s at time t the policy value over an infinite time horizon, also called the value-state function, is simply given by

$$V^{\pi}(s) = \sum_{k=0}^{\infty} \gamma^{k} r_{t+k} \ , \tag{5.1}$$

where $\gamma \in [0, 1]$ is a *discount factor* that weights future rewards. Then an *optimal* policy π^* is, by definition, the one that maximise the value-state function. As a consequence, the policy that ensures the maximum possible expected reward, say $V^*(s)$, could be obtained by solving an optimisation problem $V^*(s) = \max_{\pi} V^{\pi}(s)$. If the transition matrix is known such optimisation problem can be expressed using a system of nonlinear equations by using techniques such as dynamic programming [74]. However, in most practical conditions it is hard, if not even impossible, to acquire such complete knowledge of the environment behaviour. In this case there are model-free learning methods that continuously update the probabilities to perform an action in a certain state by exploiting the observed rewards. Such methods adopt an alternative characterisation of policy goodness based on the state-action value function, or Q-function. Formally, the function $Q^{\pi}(s, a)$ computes the expected reward of taking an action a in a starting state s and then following the policy π hereafter. Owing to the Bellman's optimality principle, it holds that a greedy policy (i.e., a policy that at each state selects the action with the largest Q-value) is the optimal policy. In other words, it holds that $V^*(s) = \max_{a \in A} Q^*(s, a)$ with $Q^*(s, a) = \max_{\pi} Q(s, a)$. In this scheme we use a model-free solving technique for reinforcement learning problems known as *Q-learning* [75], which constructs the optimal policy by iteratively selecting the action with the highest value in each state. The core of this algorithm is an iterative value update rule that each time the agent selects an action and observes a reward makes a correction of the old Q-value for that state based on the new information. This updating rule is given by:

$$Q(s, a) = Q(s, a) + \alpha \left[r(s, a) + \gamma \max_{a'} Q(s', a') - Q(s, a) \right] \ , \tag{5.2}$$

where $\alpha \in [0, 1]$ is the learning rate. Basically, the α parameter determines the weight of the newly acquired information over state-action value information. In our AMC

framework we hev used $\alpha = 0.5$. The advantage of Q-learning is that it is guaranteed to converge to the optimal policy. On the negative side, the convergence speed may be slow if the state space is large due to the *exploration vs. exploitation dilemma* [74]. Basically, when in state s the learning agent should exploit its accumulated knowledge of the best policy to obtain high rewards, but it must also explore actions that it has not selected before to find out a better strategy. To deal with this issue, various exploration strategies have been proposed in the literature, ranging from simple greedy methods to more sophisticated stochastic techniques, which assign a probabilistic value for each action a in state s according to the current estimation of $Q(s, a)$. In Section 5.4 we discuss more in detail such exploration strategies.

5.4 An RL-based AMC Scheme (RL-AMC)

In order to apply the Q-learning approach to the MCS selection problem it is necessary to define: *i*) the state space of the problem, *ii*) the feedbacks that the decision agent receives from the LTE network, and *iii*) the admissible actions for the agent with the action selection strategy. In our RL-based AMC framework, the problem state consists of CQI feedbacks and their evolution trends. The reward is the instantaneous link throughput obtained by a user after each transmission. Finally, an action is the selection of a correction factor to be applied to each CQI feedback to identify the best MCS under the current channel conditions. In the following, we describe in details the operations of our proposed AMC algorithm. First of all, it is important to clarify that the AMC decision agent interacts with the environment (i.e., the LTE network) at discrete time instants, called epochs. At each epoch the agent receives some representation of the LTE channel state and on that basis selects an action. In the subsequent epoch the agent receives a reward, and finds itself in a new state. In our AMC framework we assume that an epoch is the time when the UE receives a segment of data, either new or retransmitted. Without loss of generality we also assume that the decision agent is provided with a mapping rule that establishes a relationship between SINR values and MCS indexes. Note that our solution is not restricted to any specific BLER models but *an initial MCS value is only needed to bootstrap the learning process* and to reduce the size of the state space. Thus, it is not necessary that this mapping is accurate nor adjusted to the unique characteristics of each communication channel. In Section 6.3 we

will investigate the robustness of our AMC scheme to inaccurate CQI representation of channel performance. Intuitively, a straightforward approach to define the state of the MCS selection problem would be to use the SINR values of received segments of data[2] as state variables, as in [35]. However, the SINR is a continuos variable and it should be discretised to be compatible with a discrete MDP formulation. The main drawback is that a fine discretisation leads to a large-dimensional state space, which increases convergence and exploration times. To avoid this problem, we directly use CQI-based metrics for the state representation. Specifically, we adopt a two-dimensional space $S = \{s_1, s_2\}$ to characterise the LTE communication channel. The first state variable represents the CQI value (called CQI^m) that the UE should select using the internal look-up table that associates BLER and MCS and received SINR. The second state variable represents the ΔCQI^m value, which is defined as the difference between the last two consecutive CQI^m estimates. In other words, ΔCQI^m provides a rough indication of the trend in channel quality evolution. For instance, $\Delta\text{CQI}^m < 0$ implies that the channel quality is temporarily degrading. Since the objective of the MCS selection procedure should be to maximise the link throughput it is a natural choice to define the reward function as the instantaneous link-layer throughput achieved when taking action a (i.e., applying a correction factor to current CQI value taken from the mapping function) when in state s (i.e., given the pair $\{\text{CQI}_t^m, \Delta\text{CQI}_t^m\}$). More precisely, we assume that the reward value of an erroneous downlink transmission is null. On the other hand, the reward for a successful downlink transmission is given by

$$R(s_{t_1}, a_{t_1}) = \frac{TB}{\#TTIs \text{ in } [t_1, t_2]} \,, \tag{5.3}$$

where TB is the MAC transport block size (i.e., the number of useful bits that could be carried in a certain number of RBs with a certain MCS), while the denominator is the time between the time t_1 when that segment of data was first scheduled and the time t_2 when it was successfully received[3]. The core of the Q-learning algorithm is represented by the set A of admissible actions. In our learning model we assume that an action consists of applying a correction factor to the CQI value that is initially estimated by means of

[2]We recall that LTE physical layer relies on the concept of resource blocks. A segment of data or transport block is basically a group of resource blocks with a common MCS that are allocated to a user. Typically, a packet coming from the upper layers of the protocol stack will be transmitted using multiple segments of data.

[3]A segment of data that is discarded after a maximum number of retransmissions has also a null reward.

the internal look-up table. As discussed above, the mapping relationship between SINR values and MCS may be inaccurate and the correction factor allows the agent to identify the best modulation and coding scheme (in the sense of maximising the link throughput) for the given channel conditions. For instance, it may happen that the SINR-to-MCS mapping is too conservative for the current channel conditions and an MCS with an higher data rate can be used without violating the target BLER requirement. In this case the correction factor should be positive. Furthermore, a correction factor is also needed to compensate eventual errors due to CQI feedback delay. More formally, we assume that an action taken by the AMC decision agent at time t is one possible choice of an integer number in the set $(-k, \ldots, -2, -1, 0, 1, 2, \ldots k)$, that we denote as a_t in the following. This index is added to the original CQI^m value to compute the CQI to be sent to the eNB, denoted as CQI^f. The line of reasoning for this adjustment is as follows. Let us assume that the agent state at time t is $\{\mathrm{CQI}_t^m, \Delta\mathrm{CQI}_t\}$. We argue that if $\Delta\mathrm{CQI}_t < 0$ we should prefer conservative MCS selections (and thus use values of a_t lower than 0) because the channel trend is negative, while if $\Delta\mathrm{CQI}_t \geq 0$ we can try to use MCSs offering higher data rates (and thus positive values for a_t). Recalling that the CQI is an integer between 0 and 15 [66], this can be expressed by writing that the CQI feedback, say CQI_t^f, that should be sent to the eNB by the UE to guide the selection of the MCS index for downlink transmissions at next epoch $t+1$ should be

$$\mathrm{CQI}_t^f = \max\left[0, \min\left[\mathrm{CQI}_t^m + a_t, 15\right]\right] , \tag{5.4}$$

where $a \in [0, 1, 2, \ldots k]$ if $\Delta\mathrm{CQI}_t \geq 0$ and $a \in [-k, \ldots, -2, -1, 0]$ otherwise. Thus, the set of admissible actions is different whether the channel-quality trend is negative or non-negative. Before proceeding it is useful to point out that the choice of the k value determines how aggressively we want to explore the problem state space. In general, the selection of the k value could take into account the CQI difference statistics, i.e., to what extent a current CQI may be different from the reported CQI after a feedback delay [10]. In Section 5.5.3 we will discuss this aspect more in detail. A very important learning procedure is the action selection rule, i.e., the policy used to decide which specific action to select in the set of admissible actions. As discussed in Section 5.3 there is a tradeoff between exploitation (i.e., to select the action with the highest Q-value for the current channel state) and exploration (i.e., to select an action randomly). The simplest approach (called ϵ-greedy [74]) would be to use a fixed probability ϵ to decide

whether to exploit or explore. A more flexible policy (called *softmax* action-selection rule [74]) is to assign a probability to each action, basing on the current Q-value for that action. The most common softmax function used in reinforcement learning to convert Q-values into action probabilities $\pi(s,a)$ is the following [74]:

$$\pi(s,a) = \frac{e^{Q(s,a)/\tau}}{\sum_{a' \in \Omega_t} e^{Q(s,a')/\tau}} , \tag{5.5}$$

where Ω_t is the set of admissible actions at time t. Note that for high τ values the actions tend to be all (nearly) equiprobable. On the other hand, if $\tau \to 0$ the softmax policy becomes the same as a merely greedy action selection. In our experiments we have chosen $\tau = 0.5$.

5.5 Performance Evaluation

In this section, we assess the performance of our proposed RL-AMC scheme in two different scenarios. In the first one a fixed CQI is fed back to the eNB by each UE. Without the use of reinforcement learning AMC necessarily selects a fixed MCS independently of the current channel conditions. Then, we demonstrate that our RL-based AMC is able to converge towards the best MCS even if the initial CQI estimate are totally wrong. In the second scenario we compare RL-AMC against the solution described in [76], which exploits spectral efficiency estimates to select MCS. Specifically, the spectral efficiency of user i is approximated by $\log_2(1+\gamma_i/\Gamma)$, where γ_i is the effective SINR of user i and Γ is a scaling factor. Then, the mapping defined in the LTE standard [77] is used to convert spectral efficiency into MCS indexes and, then, into CQI feedbacks. In this case, we show that our reinforcement learning algorithm is able to improve the accuracy of the CQI mapping at run time.

5.5.1 Simulation setup

All the following experiments have been carried out using the ns3 packet-level simulator, which includes a detailed implementation of the LTE radio protocol stack. As propagation environment, we assume an *Urban Macro* scenario, where path loss and shadowing are modelled according to the COST231-Hata model [64], which is widely

TABLE 5.1: Simulation parameters.

Parameter	Value
Carrier frequency	2GHz
Bandwidth for downlink	5 MHz
eNB power transmission	43 dBm
Subcarrier for RB	12
SubFrame length	1 ms
Subcarrier spacing	15 KHz
Symbols for TTI	14
PDCCH & PCFICH (control ch.)	3 symbols
PDSCH (data ch.)	11 symbols
CQI reporting	periodic wide-band
CQI processing time	2 TTIs
CQI transmission delay	4 TTIs

accepted in the 3GPP community. The fast fading model is implemented using the Jakes model for Rayleigh fading [78]. To limit the computation complexity of the simulator pre-calculated fading traces are included in the LTE model that are based on the standard multipath delay profiles defined in [79]. In the following tests we have used the *Extended Typical Urban* fading propagation model with pedestrian (3 km/h) and vehicular (30 km/h) users' speeds. The main LTE physical parameters are summarised in Table 5.1. Regarding the network topology, the considered scenario is composed by a single cell and a number of users, chosen in the range $[10, 100]$, which move according a Random Waypoint Model (RWM) [80] within the cell, if not otherwise stated. A downlink flow, modelled with an infinite buffer source, is assumed to be active for each UE. Finally, the eNode B adopts the resource allocation type 0, thus only allocating resource block groups (RBGs) to scheduled UEs. Given the downlink system bandwidth (see Table 5.1) a RBG comprises two RBs [66]. RBGs are assigned to UEs following a Round Robin (RR) scheduler that divides equally the available RBGs to active flows. Then, all the RBs in the allocated RBGs used the MCS index that is signalled in the last received CQI feedback. Furthermore, the implemented version of RR algorithm is not adaptive, which implies that it maintains the same RBGs and MCS index when allocating retransmission attempts. All results presented in the following graphs are averaged over five simulation runs with different network topologies. Confidence intervals are very tight and are not shown in the figures. Each simulation run lasts 150 seconds.

5.5.2 Results for fixed CQI

In this first set of simulations we assume that ten UEs are randomly deployed in the cell and they are static. Then an additional tagged user is moving with pedestrian speed

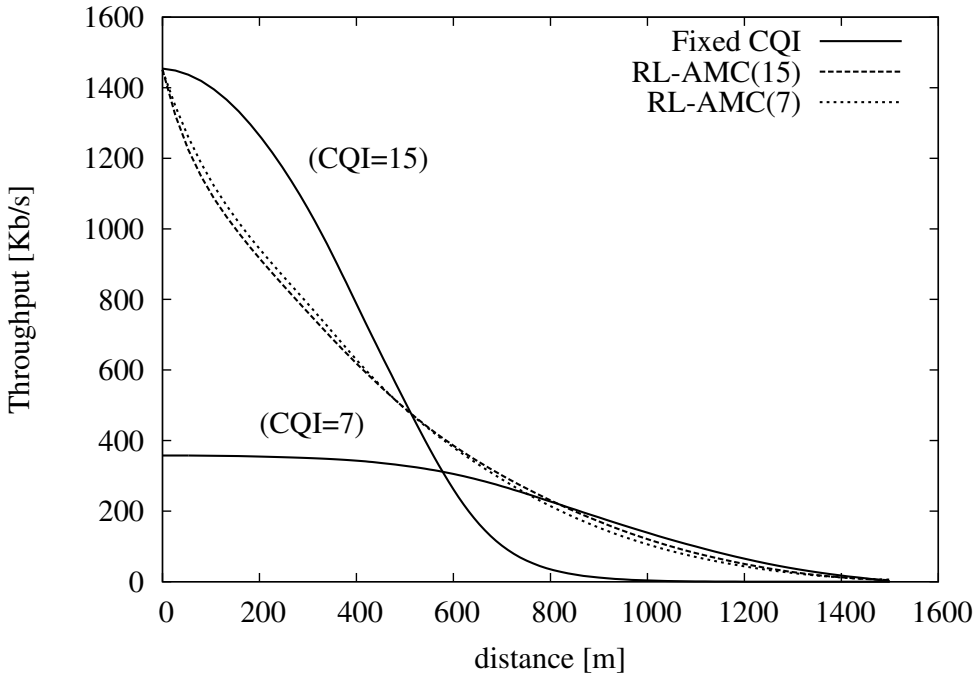

FIGURE 5.2: Average throughput as a function of the distance of the tagged user from the eNB in a pedestrian scenario.

from the center of the cell to its boundaries. However, independently of the UE position the CQI feedback is constant. Then, Figure 5.3 shows a comparison of the throughput achieved by the tagged user with and without reinforcement learning. This is obviously a limiting case which is analysed to assess the robustness of our RL-AMC scheme even when CQI provides a very poor prediction of channel performance. As expected with fixed MCS the user throughput is constant when the MCS is over provisioned, while it rapidly goes to zero after a critical distance. On the contrary, our RL-AMC is able to discover the correction factor that should be applied to the initial CQI to force the selection of a more efficient MCS. In addition, the performance of RL-AMC are almost independent of the initial CQI value. Note that in this case RL-AMC must explore the full range of CQI values and we set k in (5.4) equal to 15.

5.5.3 Results with adaptive CQI

In the following experiments we assume that each UE implements the SINR to CQI mapping described in [76]. First of all we consider the same network scenario as in Figure 5.2, i.e., ten static UEs randomly deployed and one tagged UE moving at pedestrian speed. Then, Figure 5.3 shows a comparison of the throughput achieved by the tagged user with both SE-AMC and RL-AMC schemes at different distances of the tagged UE

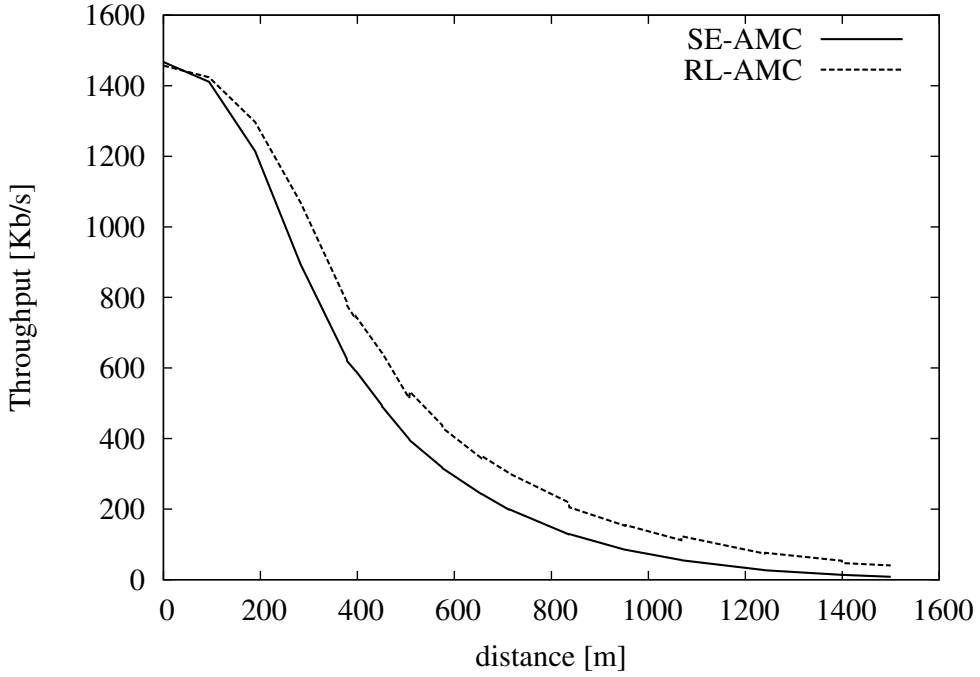

FIGURE 5.3: Average throughput as a function of the distance of the tagged user from the eNB in a pedestrian scenario.

from the eNB. We can observe that the MCS selection in SE-AMC is too conservative and this results in a throughput loss. On the contrary, RL-AMC method is able to discover the MCS configuration that can ensure a more efficient use of the available channel resources. This is more evident at intermediate distances from the eNB when short-term fading may lead to use more frequently low-rate MCSs. As shown in the figure, the throughput improvement varies between 20% and 55% in the range of distances between 200 meters and 800 meters. In the second set of simulations we consider a more dynamic environment in which there is an increasing number of UEs in the cell, and all the UEs are moving according to RWM with speed 30 km/h and pause time equal to 5 seconds. Figure 5.4 shows a comparison of the aggregate cell throughput with both SE-AMC and RL-AMC schemes as a function of the network congestion (i.e., number of UEs). The results clearly indicate that the throughput improvement provided by RL-AMC is almost independent of the number of UEs and it is about 10%. We can also observe the the cell capacity initially increases when going from 10 to 20 UEs. This is due to two main reasons. First, RR is able to allocate RBs in a more efficient way when the number of UEs is higher. Second, the higher the number of UEs and the higher the probability that one of the UEs is close to the eNB and it can use high data-rate MCSs. To investigate more in depth the behaviour of the considered AMC schemes, in Figure 5.5 we show the probability mass function of the number of retransmissions that

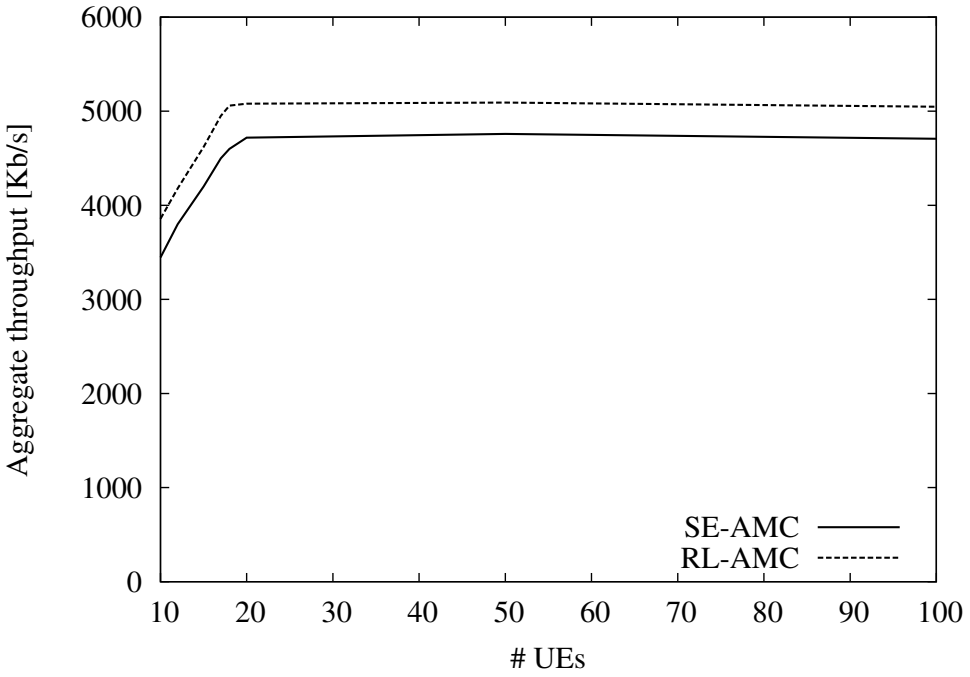

FIGURE 5.4: Average cell throughput as a function of the number of UEs in an urban vehicular scenario.

are needed to successfully transmit a segment of data in a cell with 50 UEs moving as described above. We remind that the same MCS is used for both the first transmission attempt and the eventual subsequent retransmissions. We can observe that with RL-AMC the probability to successfully transmit a segment of data at the first transmission attempt is slightly lower than with SE-AMC. However, the probability of successfully transmiting a segment of data after one or two retransmissions is higher with RL-AMC than with SE-AMC. This confirms our previous observation that the initial MCS selection of SE-MAC is more conservative. On the contrary, RL-AMC is able to also explore MCS with higher data rates when the channel conditions are more favourable and this is beneficial for the throughput performance. Note that this is achieved without violating the BLER requirements imposed by the LTE standard.

5.6 Summary

In this Chapter,we have presented a new AMC method for LTE networks that is based on reinforcement learning techniques, We have discussed how inaccurate feedbacks on channel qualities and the complexity of modelling link performance under realistic channel models may easily lead to inaccurate MCS selections. By exploiting reinforcement

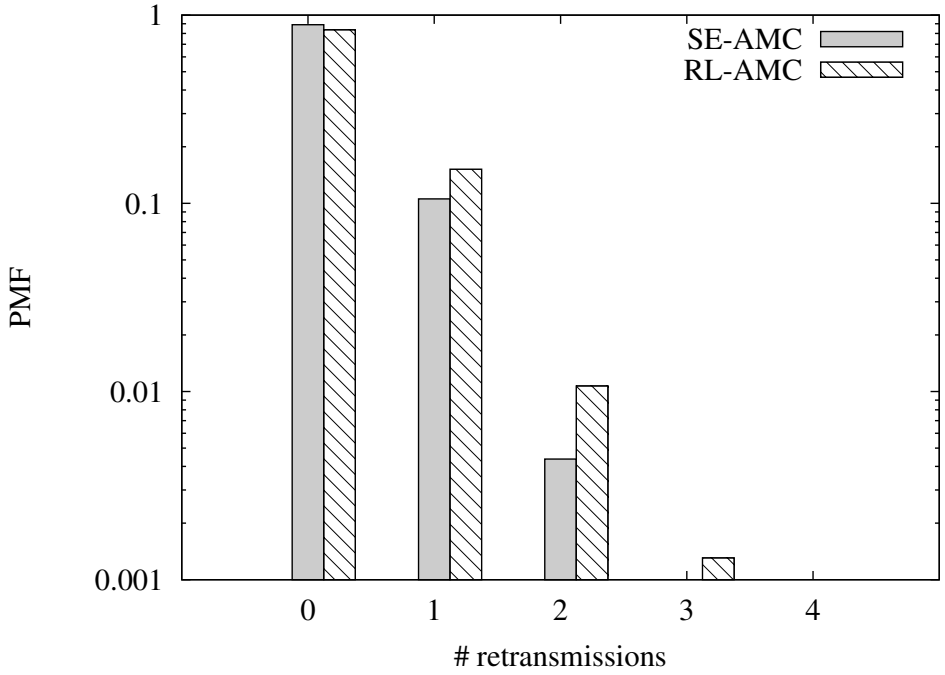

FIGURE 5.5: Probability mass function of the number of retransmissions in an urban vehicular scenario with 50 UEs.

learning, we can significantly reduce the impact of channel prediction errors on the performance of link adaptation. As side effect has been show as this scheme can improve the system bandwidth in terms of downlink throughput.

Chapter 6

Offloading through Opportunistic Networks in LTE environment

6.1 Introduction

Offloading is gaining momentum as a technique to overcome the cellular capacity crunch due to the surge of mobile data traffic demand. Multiple offloading techniques are currently under investigation, from modifications inside the cellular network architecture, to integration of multiple wireless broadband infrastructures, to exploiting direct communications between mobile devices. In this Chapter we focus on the latter type of offloading, and specifically on offloading through opportunistic networks. As opposed to most of the literature looking at this type of offloading, we have considered the case where requests for content are *non-synchronised*, i.e. users request content at random points in time. We support this scenario through a very simple offloading scheme, whereby no epidemic dissemination occurs in the opportunistic network. Thus our scheme is minimally invasive for users' mobile devices, as it uses only minimally their resources. Then, we provide an analysis on the efficiency of our offloading mechanism (in terms of percentage of offloaded traffic) in representative vehicular settings, where content needs to be delivered to (subsets of the) users in specific geographical areas. Depending on various parameters, we show that a simple and resource-savvy offloading scheme can nevertheless offload a very large fraction of the traffic (up to more than 90%, and always more than 20%). We also highlight configurations where such a technique is less effective, and therefore a

more aggressive use of mobile nodes resources would be needed. We focus our attention both in vehicular scenarios and indoor scenarios. We deliberately use a very simple offloading scheme, described in Section 6.2, whereby resources provided by mobile nodes are minimally used. Nodes interested in a content store it for a limited amount of time after receiving it. New requests from other users are satisfied either when the requesting user encounters another user storing a copy of the content, or through the cellular network upon expiration of the delivery deadline. As opposed to most of the literature looking at offloading through opportunistic networks, in our scheme we do not use any epidemic dissemination mechanism. On the one hand, this allows us to test a minimally invasive offloading scheme from the mobile users' perspective. As additional resources spent by mobile devices are sometimes considered a possible roadblock for offloading, our results show the offloading efficiency when this additional burden is extremely low. On the other hand, this simple scheme allows us to stress the efficiency of offloading in a particularly unfavourable configuration, thus providing a worst-case analysis, all other conditions being equal. As regards the vehicular case, we focus on two complementary scenarios. In the first one, users move in a given physical area, and *all* request a piece of content, though at different points in time. This scenario is representative of users moving inside a limited area, and accessing very popular content, though not particularly time critical (i.e., content that does not generate a surge of requests immediately when it is generated). In the second scenario, users enter and exit (after a short amount of time) a given geographical area, and request content after a random amount of time after they entered the area. This complementary scenario is thus representative of users traversing a geographical area, as opposed to roaming there. Finally, in this scenario we also consider the case where content is requested only with a certain probability, i.e., when content has different levels of popularity. We have also analyzed two case of indoor scenario. In both scenario users move inside a buildings, thus their mobility is constrained by the buildings layout. This type of layout, even if more siple, is rappresentative of a museum use case in which visitors can download additional multimedia as they get close to the different artworks in each room or roam through the halls of the museum. However each room contains contents that are not present in other rooms. For this reason a content item can be disseminated only in the room where it is relevant. then , when a user changes room, the content items that are stores in its lo0cal cache are not disseminated anymore. We have analyzed several configuration of this scenario in terms of content's popularity and requesting rate. In particular we have started from

the basic case when in each room the contents have the same popularity. Then we have done a more realistic investigation by diving the contents in three class o popularity. In particular, a coording to a zipf distribution [81], we have introduced contents with high popularity, intermediate popularity and low popularity. Finally we have observed the behaviour of the opportunistic network when the requesting rate increase. We analyse the offloading efficiency in these scenarios, defined as the fraction of nodes receiving content through the opportunistic network. We characterise efficiency as a function of key parameters such as the number of users, the deadline of content requests, the time after which users drop the content after having received it, the popularity of the content. As we show in Section 6.3, even with an unfavourable opportunistic dissemination scheme, we find that offloading can be very efficient, as it is possible to offload up to more than 90% of the traffic. In other configurations, we find that the considered offloading scheme is less efficient, resulting in an offloading of only about 20%. In such cases, however, there is ample room for improvement, by further leveraging opportunistic networking resources, e.g., through more aggressive content replication schemes

6.2 Offloading Mechanisms

As anticipated in Section 6.1 we deliberately consider a simple scheme that uses very little resources of mobile nodes to support the offloading process. In general, we support scenarios where content is requested by users at random points in time. Similarly to [20], we assume the existence of a Central Dissemination Manager (CDM), that can communicate with all nodes through the cellular network and keeps track of the dissemination process. Without loss of generality[1], in the following we focus on the dissemination of a single piece of content to the set of interested users. The offloading mechanism is defined by the actions taken by requesting nodes and by the CDM, as described by Algorithms 1 and 2, respectively.

Let us focus first on the actions taken by requesting nodes (Algorithm 1). When a request is generated at a node, the node sends it to the CDM via the cellular network (line 3). The node is guaranteed to receive the content within a given *content timeout*. During the timeout, the node tries to get the content from encountered nodes (lines

[1]Strictly, this is the case when congestion on the opportunistic network is low, and therefore the effect of multiple contents offloaded at the same time can be neglected. This is typically assumed in the literature on offloading through opportunistic networks.

5-12). If the timeout expires, it receives it directly from the CDM (lines 13-16). Upon receiving the content, the node sends an ACK to the CDM (line 9 and, implicitly, line 14). In addition, it keeps the content for a *sharing timeout*, during which it can share the content with other encountered nodes (lines 18-20). After the expiration of the *sharing timeout* the content is deleted from the local cache. Note that requests and ACKs are supposed to be much shorter than the content size, and thus do not significantly load the cellular network.

Algorithm 1 Actions taken by requesting nodes

```
                                                    ▷ Run by a tagged node k
 1: Upon request for content C
 2: content_received = false
 3: Send content_request to CDM
 4: if C not received immediately from CDM then
                                                    ▷ try with opportunistic contacts
 5:     while content_timeout is not over do
 6:         request C to encountered nodes
 7:         if content received then
 8:             content_received = true
 9:             Send ACK to CDM
10:             break
11:         end if
12:     end while
13:     if content_received == false then
14:         Receive C from CDM
15:         content_received = true
16:     end if
17: end if
18: while sharing_timeout is not over do
                                                    ▷ available for opportunistic sharing
19:     Send C to encountered nodes upon request
20: end while
21: Cancel content C
```

Let us now focus on the actions taken by the CDM (Algorithm 2). Thanks to requests and ACKs, the CDM is always aware of the status of content availability in the network. Upon receiving a request, it checks whether some other node is already storing a copy of the content or not. In the latter case (lines 4-6) there is no chance that the user can get the content opportunistically through another node, and the CDM sends the content directly through the cellular network. In the former case (lines 7-21), it waits to receive an ACK during the *content timeout* (lines 8-15), indicating that the node has received the content. If this does not happen, it sends the content directly to the node

(lines 16-20). Finally, upon expiration of the *sharing timeout* for a given node the CDM updates the view on the number of nodes with the content (lines 22-23)[2].

Algorithm 2 Actions taken by CDM

```
                                          ▷ Run by the CDM for content C
    Init #nodes_with_C = 0
 1: Upon request from node k
 2: k_served = false
 3: if #nodes_with_C == 0 then
 4:     Send C to k
 5:     #nodes_with_C++
 6:     Set sharing_timeout for node k
 7: else
 8:     while content_timeout is not over do
 9:         if ACK received by k then
10:             #nodes_with_C++
11:             k_served = true
12:             Set sharing_timeout for node k
13:             break
14:         end if
15:     end while
16:     if k_served = false then
17:         Send C to k
18:         #nodes_with_C++
19:         Set sharing_timeout for node k
20:     end if
21: end if

22: Upon sharing_timeout for node k over
23: #nodes_with_C = #nodes_with_C-1
```

With respect to offloading mechanisms proposed for opportunistic networks (e.g., [18, 20]) our algorithms present several differences. First, there is no proactive seeding of the network. This is because requests arrive at the CDM dynamically, and there is no knowledge of which nodes will generate a request, and when. Therefore, we adopted a reactive policy, i.e. we wait for requests without doing any proactive seeding. Second, we want to use minimally mobile node resources in the opportunistic network. This is to make the offloading mechanism less intrusive as possible, as the additional mobile devices' resource usage brought about by offloading is often considered a possible severe

[2]Note that the CDM implementation could be further simplified by allowing the nodes that select a content to send a message over the cellular network to inform the CDM. In this way, the CDM does not need to maintain separate timers for each of the nodes that have received the content. It is also reasonable to assume that such confirmation message would be a negligile overhead for the cellular network.

drawback. Therefore, we do not use epidemic dissemination in the opportunistic network. For the same reasons, we assume that users drop content some time after receiving it. Still, our algorithms guarantee bounded delay, and impose similar overhead on the CDM as in previous proposals [20]. Clearly, Algorithms 1 and 2 can be easily modified to exploit additional resources of mobile devices (e.g., using more aggressive forms of dissemination or doing initial proactive seeding), if needed.

6.3 System Performance

6.3.1 Scenarios and performance indices

We test the performance of the proposed offloading schemes in many different scenarios. In particular we have analyzed two different vehicular scenarios, hereafter denoted as Scenario V_1 and Scenario V_2, and two different Indoor scenarios, hereafter denoted as Scenario I_1 and Scenario I_2.

In V_1 we capture cases where a group of vehicles move inside a geographical area covered by a cell, and roam always inside that cell. Vehicles move on a stretch of road crossing the cell, and come back when arriving at the boundary. The resulting traffic is therefore bidirectional. Nodes move with a speed randomly selected (with uniform distribution) in an interval $[v_{min}, v_{max}]$, and can exchange content directly while being within a maximum transmission range T_{RX} from each other. We consider N nodes in the simulations, wich can all request a set of content items (there are M content items in total). Requests are generated from the beginning of the simulation sequentially, according to a Poisson process with rate λ (i.e. two requests are spaced by an exponentially distributed time interval). Simulations lasts until all nodes have requested the content, and their *sharing timeouts* are all expired. In other words, we start from a condition where no nodes have any copy of the content, and we analyse the behaviour of the system until no copy of the content is available after all nodes have received it. While assuming vehicles go back and forth on a given road segment is a simplification, the scenario is still representative of movement patterns confined in a geographical area served by a cellular network, where a given content is very popular and thus requested by all users (though at different points in time). More in general, the scenario is representative of movement

patterns whereby vehicles roam in such a geographical area, can move in opposite directions and can communicate with each other when being close enough, irrespective whether such movements occur on the same street or on different, nearby streets. In V_2 we capture cases where nodes are not necessarily staying in the same area, but there is a constant flux of vehicles entering and exiting the area. Again, we assume that vehicles move on a road and we focus on a road segment covered by a cell (we select speeds as in V_1). Traffic is again bidirectional, and we keep the number of nodes constant, and assume that a new vehicle enters the area when another one has left. When entering the area, vehicles become interested in the content with a given probability p. If they are interested, they generate a request after a time interval uniformly distributed between the time when they enter and the time when they reach the centre of the cell. Taking the same terminology of [20], we define a panic zone as the area of the cell Δ meters before the boundary. The *content timeout* is set so that the CDM sends the content directly when vehicles enter the panic zone. Finally, vehicles keep the content while being inside the cell. At the beginning of simulations, nodes are distributed randomly (with a uniform distribution) in the cell, are interested in content with probability p, and generate a request at a point in time uniformly distributed between the simulation start time and when they are midway towards the border of the cell. Simulations stop after 100 requests have been generated (50 in the case of low popularity content, without noticeable loss of statistical significance of the results), and the corresponding users have been all served. With this scenario we explore different cases with respect to V_1. After an initial transient phase, we are able to show a steady-state behaviour of offloading, in cases where vehicles enter and exit an area with a given flux and density. In other words, we can show how much offloading is efficient in making a given content "survive" in a geographical area, by only exploiting replicas available on vehicles of interested users passing through that area. This is an application of the basic floating content idea [82] to the case of vehicular networking environment in presence of offloading. In addition, only a fraction of the nodes can be interested into the content, i.e. the content can have different levels of popularity. In Scenario I_1 we consider an indoor environment in wich the mobility of users is constrained by the building layout (rooms, corridors, stairs etc.). This scenario is used to exemplify a museum use case in wich visitors can download additional multimedia content as they roam through the halls of the museum and get close to the different artworks in each room. The visitors can get this content not only through the cellular network but also by nearby visitors that have that content item in

the local caches of the portable devices (e.g., smartphones) using an opportunistic offloading technique. The main target of these simulation is to validate the effectiveness of the proposed offloading system also for constrained mobility patterns indoor conditions. In this set of simulations, we consider a grid layout that consists of four squared rooms with a side length of 20 meters. Then the users moves between rooms and within each room using a Constrained Randiom Waypoint Mobility (CRWM) model. Specifically, in a CRWM a user picks a random destination inside the room with a probability P_{stay}, or a destination point in one of the other rooms with probability $(1 - P_{stay})$. Then the user proceeds to this desination point following a straight-line trajectory with constant speed v, and pauses for an exponetially distributed time interval with mean T_{pause}. We assume that there is a global set of M content items, but each content item is assigned to a room with an equal probability. Users request content items according to a Poisson process with rate λ. It is important to point out that the users can request only content items that are relevant for the room they are visiting. Thus, there is not content dissemination between rooms. Simulation lasts until all nodes have requestd all the content items and their sharing timeouts are all expired. In other words, this means that all the nodes have visited all the rooms. The Scenario I_2 has the same enviroments settings of the Scenario I_1. The substantial difference between those scenarios consists on how the set of the content items are distributed in each room. In this scenario we have considered a set of M content items equally suddivided into 3 different class of content popularity. In particular we have considered a class within High popularity contents (C_H), a class within Intermediate popularity contents (C_I) and finally a class within Low popularity contents (C_L). Each class is represented by its interest probability, i.e. P_{C_i}, which means that a user results interested in a generic content of class C_i with probability P_{C_i} and in others kind of contents with probability $1 - P_{C_i}$. The contents popularity are chosen in order to follows a Zipf-like distribution Zipf(x;M) [81]. The distribution is given by $P_{C_i} = c/i^{1-x}$ for each i, where $c = \frac{1}{\sum 1/i^{1-x}}$ is a normalizzation constant, and respect the following constraints:

$$\begin{cases} \sum P_{C_i} = 1; \\ P_{C_L} < P_{C_I} < P_{C_H} \end{cases} \tag{6.1}$$

Setting $x = 0$ corresponds to a pure Zipf distribution, which is highly skewed. On the other hand, setting $x = 1$ corresponds to a uniform distribution with no skew. In our tests we have used a pure Zipf distribution. Previous work have dimostrated that

some contents request follows a Zipf-like distribution [83]. However, in other works the Zipf distribution was used for modelling some content requests. For example in [84] the Zipf distribution is used to perform a theoretical analysis of the cost of distributing multimedia files over content distribution networks. After the classification, the global set of content items has been uniformly distributed among each room. This make us able to create a generic case in wich each room not necerssary has contents of each class, but are possible the cases in which one room has contents of only two class or even only one kind of contents. Due this aspect we performed at least 5 simulation runs for each set of parameters. Also in this case simulation lasts until all nodes have requestd all the content items and their sharing timeouts are all expired.

We ran simulations, using the NS3 with the LENA module for LTE[3], for various sets of parameters, as indicated in Table 6.1 and Table 6.2. Specifically, we varied the number of nodes in all Scenarios, the request rate in V_1, the *content timeout* and the *sharing timeout* in Senarios V_1, I_1 and I_2, and the contents popularity in Scenarios V_2, I_1 and I_2. We performed at least 5 simulation runs for each set of parameters, using the independent replication method [85]. The main performance figure we consider is the offloading efficiency, defined as the fraction of content messages that reach the users through opportunisitc communications. For this index we computed the confidence intervals (with 95% confidence level) over the replications. To get a more precise idea on the dynamics of the offloading process over time, we also computed, on each 5s time window, the average (across simulation replicas) number of copies of content stored on mobile nodes, and the average number of new content deliveries through the cellular and the opportunistic network, respectively.

TABLE 6.1: Simulation parameters Scenarios V_1,V_2

	Scenario V_1	Scenario V_2
speed (Km/h)	[80,120]	[80,120]
cell diameter (Km)	4	1
N (nodes)	20, 40	20, 40
T_{RX} (m)	200	50
p	1	0.5, 0.75, 1
λ (req/s)	1, 0.5, 0.2	–
content timeout (s)	60, 90, 120	–
sharing timeout (s)	5,10,20,30,60,120	–
Δ (m)	–	50

[3]http://networks.cttc.es/mobile-networks/software-tools/lena/

TABLE 6.2: Simulation parameters Scenarios I_1,I_2

	Scenario I_1	Scenario I_2
speed (Km/h)	6	6
cell diameter (Km)	–	–
N (nodes)	20	20
T_{RX} (m)	28	28
p	1	1
λ (req/s)	–	–
content timeout (s)	10, 20,30	10, 20,30
sharing timeout (s)	20, 30, 60	20, 30, 60
Δ (m)	–	–

6.3.2 Analysis of scenario V_1

The analisys of this scenario was divided in two steps. In the first step we have investigated the performance of the offloading system when only one content item was requested by all the nodes. In the second step we have extended the analysis by observing the behaviour of the offloading mechanism in the case when all the nodes do a request from a set of M content items.

We start by analysing the system performance in V_1 in the case of only one content item. To this end, Figure 6.1 shows the offloading efficiency obtained in a wide set of different network configurations, in which we vary the node density, the content request rate, as well as the *content timeouts* and the *sharing timeouts*. Several general observations can be drawn from the shown results. First, the offloading efficiency increases with the node density. The main reason is that the higher the node density, the higher the contact rate between the mobile devices. Thus, there are more opportunities for opportunistic dissemination between interested users. As far as the impact of the request rate (λ) we observe two regimes. When the *sharing timeout* is low, higher request rates result in higher offloading. This is intuitive, because higher request rates results in requests being more concentrated in time. When nodes share the content only for very short amounts of time (see for example the case of 5s), concentrating the requests in time increases the probability of encountering other nodes sharing the content. Less intuitive is the behaviour for large sharing timeouts, where higher request rates results in *lower* offloading efficiency. The reason of this will be more clear when analysing the evolution of dissemination over time (Figure 6.3). Intuitively, when requests are more concentrated in time, *content timeouts* for nodes that do not get the content via the opportunistic network are also more concentrated. As we will discuss later, when a

timeout expires and content is delivered via the cellular network, this kicks off a fast increase in the dissemination of content via the opportunistic network in the region of the node whose *content timeout* has expired. When expirations are less concentrated in time (i.e., when request rates are lower), the opportunistic diffusion process has more time to spread content, and therefore the offloading efficiency increases A second in-

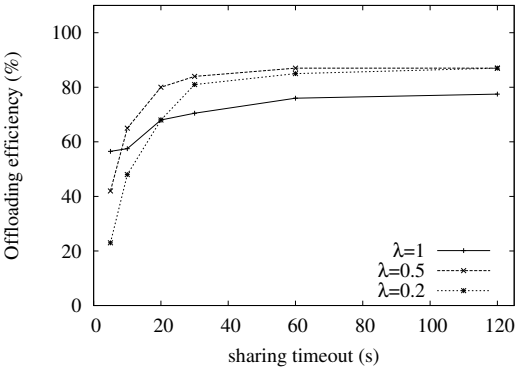

(a) $N = 20, content\ timeout = 60$s,

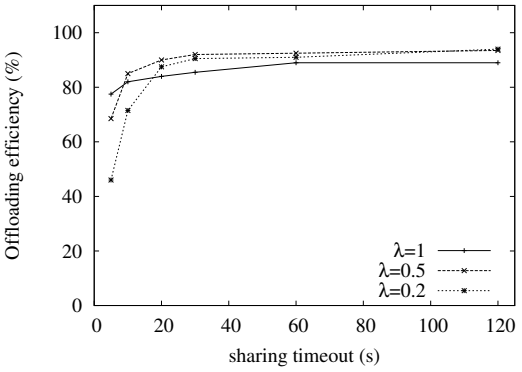

(b) $N = 40, content\ timeout = 60$s

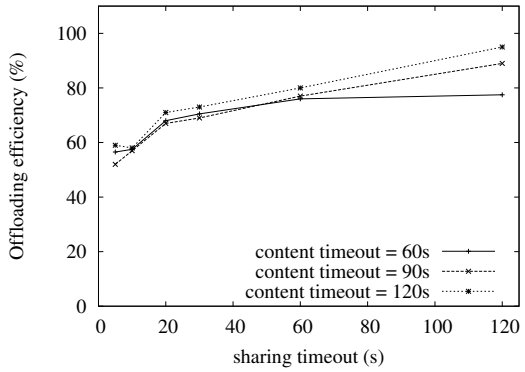

(c) $N = 20, \lambda = 1$,

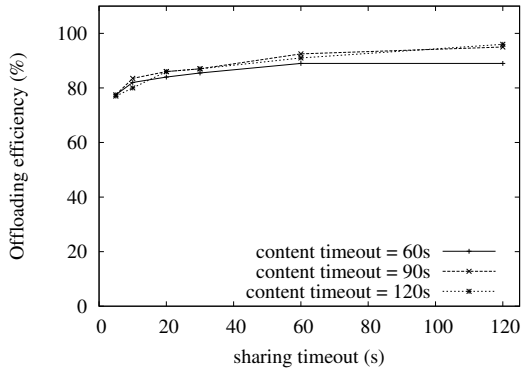

(d) $N = 40, \lambda = 1s$

FIGURE 6.1: V_1: offloading efficiency for varying request rates, *content timeouts* and the *sharing timeouts*.

teresting observation is related to the impact of the *sharing timeout* on the offloading efficiency. Our results indicate that if the content is sufficiently persistent in the network (e.g., *sharing timeout* $\geq$ *content timeout*) then the impact of the *sharing timeout* on the offloading efficiency is negligible. On the other hand, if the content is volatile, i.e., it is cached in the local memory of interested users only for few seconds, then the number of copies of that content in the environment may be too small to allow an efficient opportunistic dissemination. For instance, with 20 mobile devices and a content request rate of 0.2 req/s the offloading efficiency can be as low as 20% (this degradation of the offloading efficiency is less remarkable in denser networks). Interestingly, if the content

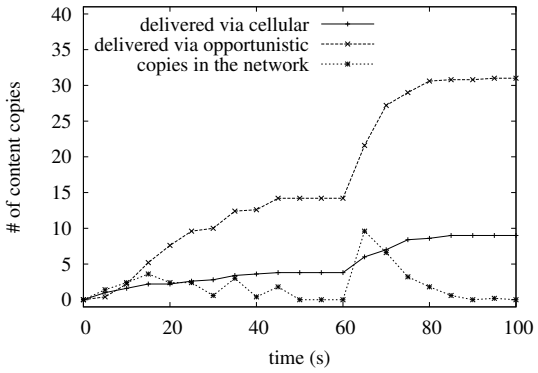

(a) $N = 40, \lambda = 1$ req/s, *sharing timeout* = 5s,

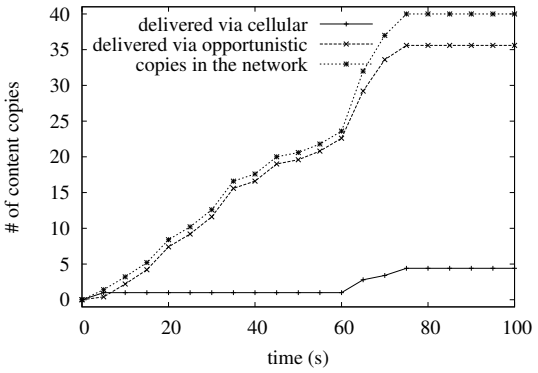

(b) $N = 40, \lambda = 1$ req/s, *sharing timeout* = 120s

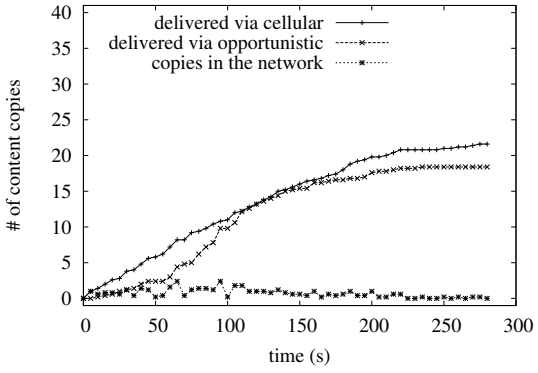

(c) $N = 40, \lambda = 0.2$ req/s, *sharing timeout* = 5s,

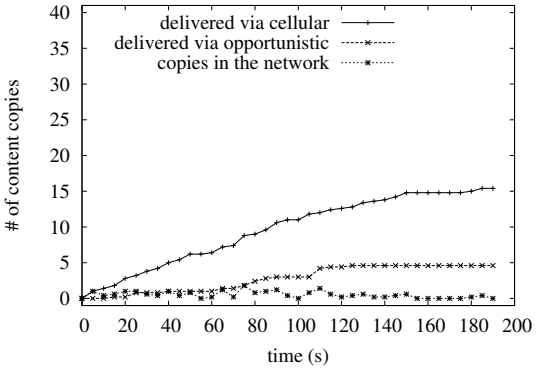

(d) $N = 20, \lambda = 0.2$ req/s, *sharing timeout* = 5s

FIGURE 6.2: V_1: temporal evolution of the number of content copies and served content requests in different network scenarios.

request rate is high (i.e., $\lambda = 1$ req/s) then even a *sharing timeout* = 5s can still provide an offloading efficiency up to 60% in a cell with 20 mobile devices. A last observation is related to the effect of the *content timeout*. As shown in Figure 6.1(c) and Figure 6.1(d) an increase in the *content timeout* results into an increase of the offloading efficiency. This is more noticeable for large *sharing timeouts*, i.e. when content stays available on nodes for opportunistic dissemination longer. This is basically a joint effect of the fact that (i) content is available longer in the opportunistic networks (longer *sharing timeouts*) and (ii) interested nodes wait longer for requesting it via the cellular network (longer *content timeouts*). To get a deeper understanding of the offloading dynamics, plots in Figure 6.3 show the temporal evolution of (i) the total number of mobile devices that have received the content via the cellular and the opportunistic network, respectively, and (ii) the number of copies of the content available in the network (i.e., the number of nodes that are storing and sharing a copy of the content at that time). Note that plots are typically shown until just after the time when the last requesting node has

received the content. The system evolution after that time is not particularly interesting: nodes progressively drop the content when their *sharing timeouts* expire. We show plots for extreme values of the considered parameters. Specifically, in Figures 6.3(a) and 6.3(b) we focus on two extreme values of the *sharing timeout* parameter, for the case of 40 nodes and 1 req/s (*content timeout* is always 60s). As expected, the main difference is the number of copies of the content available in the network, which is much higher in Figure 6.3(b), resulting in a higher offloading efficiency. It is very interesting to observe the behaviour of the system after 60s, i.e. when the *content timeouts* for the first nodes generating requests expire. For larger *sharing timeouts* (larger than the *content timeout*), before that time, only 1 node (the first one requesting the content) can receive the content via the cellular network, as it is clear from Figure 6.3(b). This is due to the behaviour of the CDM explained in Section 6.2, that sends immediately a content to the first requesting node (as no other node stores the content yet), and then waits the *content timeouts* (i.e. 60s) for the next requests before taking any action. In other words, it is impossible to have more than one delivery via the cellular network in the first 60s, due to the CDM algorithm. When the *sharing timeout* is short, more copies of the content can be sent via the cellular network also before the first *content timeout* expires. This happens whenever a new request is generated and all nodes that have previously received the content have already dropped it (due to expiration of the *sharing timeout*). In both cases, after 60s from the start of the simulation, *content timeouts* start expiring, and new copies of the content are sent via the cellular network. This generates a burst of dissemination in the opportunistic network, that is noticed by the steep increase of the curve related to opportunistic deliveries around that time. Note, in particular, that after 60s in both cases the rate of increase of the delivery via the opportunistic network is higher than the rate of increase of cellular deliveries. This means that each delivery via the cellular network is significantly amplified by deliveries in the opportunistic network. Figures 6.3(c) and 6.3(d) show the evolution over time in the least favourable conditions for offloading, i.e. for low request rates ($\lambda = 0.2$) and very short *sharing timeout* (5s). Curves confirm the behaviour described before. In particular at low densities ($N = 20$) the *sharing timeout* is not long enough to sustain significant dissemination over the opportunistic network. The situation improves for denser networks ($N = 40$), but still the *sharing timeout* makes nodes drop content too fast with respect to the rate of arriving requests (anyway, the offloading efficiency is still between 20% and 40% even in these cases).

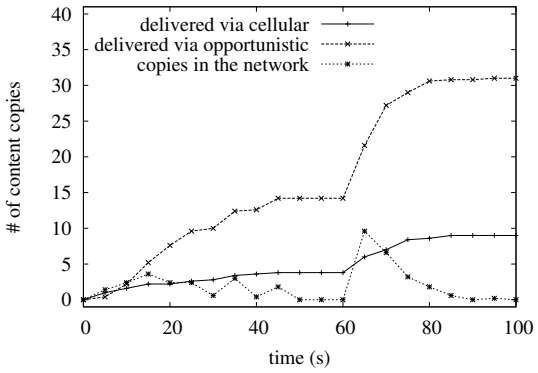

(a) $N = 40, \lambda = 1$ req/s, *sharing timeout* = 5s,

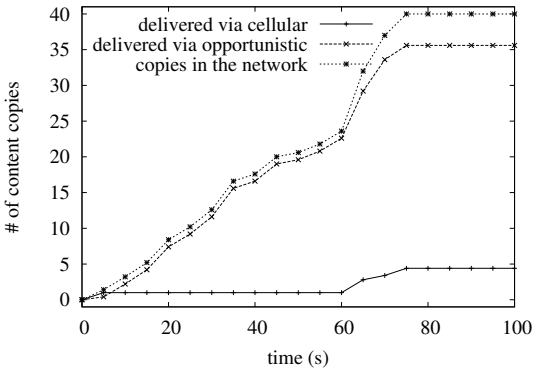

(b) $N = 40, \lambda = 1$ req/s, *sharing timeout* = 120s

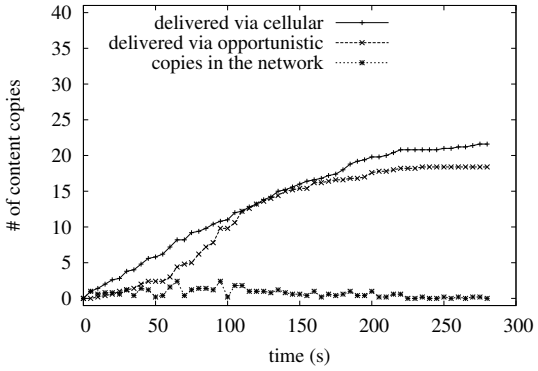

(c) $N = 40, \lambda = 0.2$ req/s, *sharing timeout* = 5s,

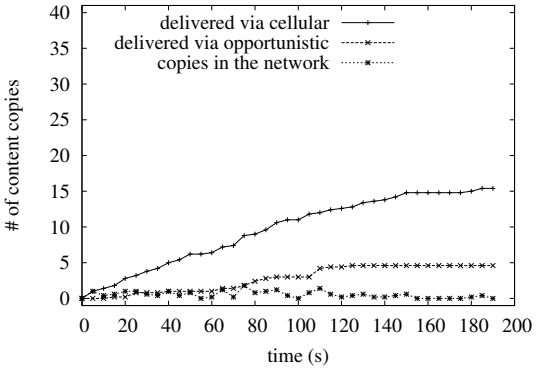

(d) $N = 20, \lambda = 0.2$ req/s, *sharing timeout* = 5s

FIGURE 6.3: V_1: temporal evolution of the number of content copies and served content requests in different network scenarios.

After this preliminary study, as mentioned above, we have evaluated the performance of the offloading mechanism in the case when a set of M available contents is present in the network. In Figure 6.4 we can see how the offloading efficiency vary by incrementing the number of the available content items. The main effect that is possible to capture, is that the offloading efficiency decrease while the number of content items increase. This result is enough easy to understand. In fact, when the number of the content items increas, the probability that a generic encountered node has a desidered content is his local cache became smaller. Due to this lower probability, the offloading efficiency decrease. However this scenario maintains some characterisitcs of the scenario where a single piece of content is present, such as the dipendence of the system from the *content timeout* and the *sharing timeout*. Both these effects can be observed in Figure 6.5. In fact, for a fixed *content timeout* value, we have observed an increment of the offloading efficiency by increasing the *sharing timeout*, because as previously explained, the persistence of a content in the network depends from this parameter. On the other side, an increment

of the *content timeout* corresponds also to an increment of the offloading efficiency, because interested nodes wait longer for requesting the content via the cellular network. Finally, in order to do a complete comparison with the single content scenario, also

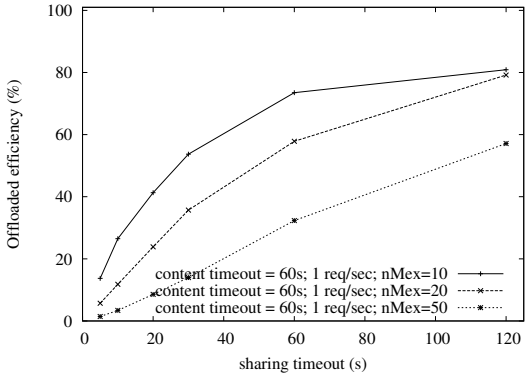

(a) $N = 20, \lambda = 1, content\ timeout = 60$ s,

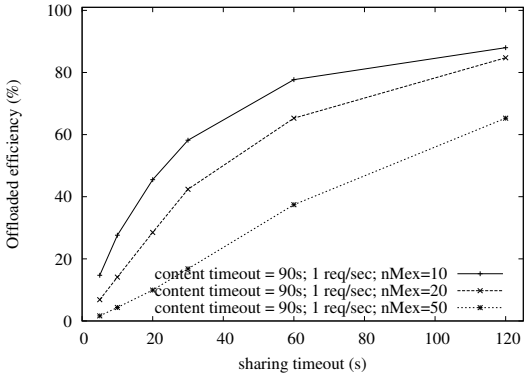

(b) $N = 20, \lambda = 1, content\ timeout = 90$ s

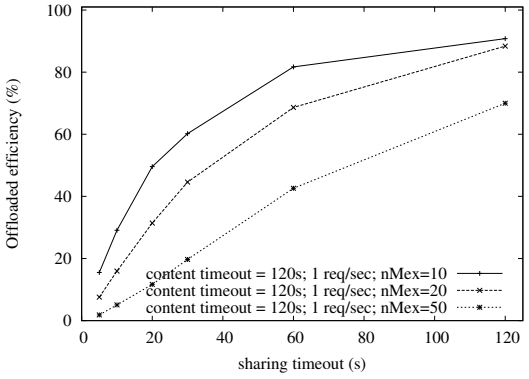

(c) $N = 20, \lambda = 1, content\ timeout = 120$ s

FIGURE 6.4: Scenario V_1: offloading efficiency for varying number of content items and the *sharing timeouts*.

in this case we have performed a temporal analysis of the offloading system. Without loss of generality, in this case Figure 6.6 shows the temporal evolutionof the average number of content items that each node has received via the cellular network, the average number of content items that each node has received via the opportunistic network and the average number of content items that persists in the network. In particular we have reported to limit case of *sharing timeout*. In the case of long *sharing timeout* (Figure 6.6(b)), the first node that requests some content, receive it through the cellular network. Then, nothing happen until th first *content timeout* elapsed, i.e. around 120s. After that point in time, a few *content timeout* expired, and content items are served via the cellular network (the corresponding curves increase). As the previous case, this boost the opportunistic dissemination process, wich results in a marked increase of the

number of nodes receiving content items via the opportunisitc network. On the other hand, for short *sharing timeouts* (Figure 6.6(a)) nodes receive content through the cellular network more uniformly over time. This is because content items stay available in the opportunistic network for short amounts of time. Even during the first 120s, while *content timeouts* have not expired the CDM knows that some content requestes can only be satisfied via the cellular network, because no nodes are storing those items anymore. All this behaviour has been consistently observed also for the other se of parameters.

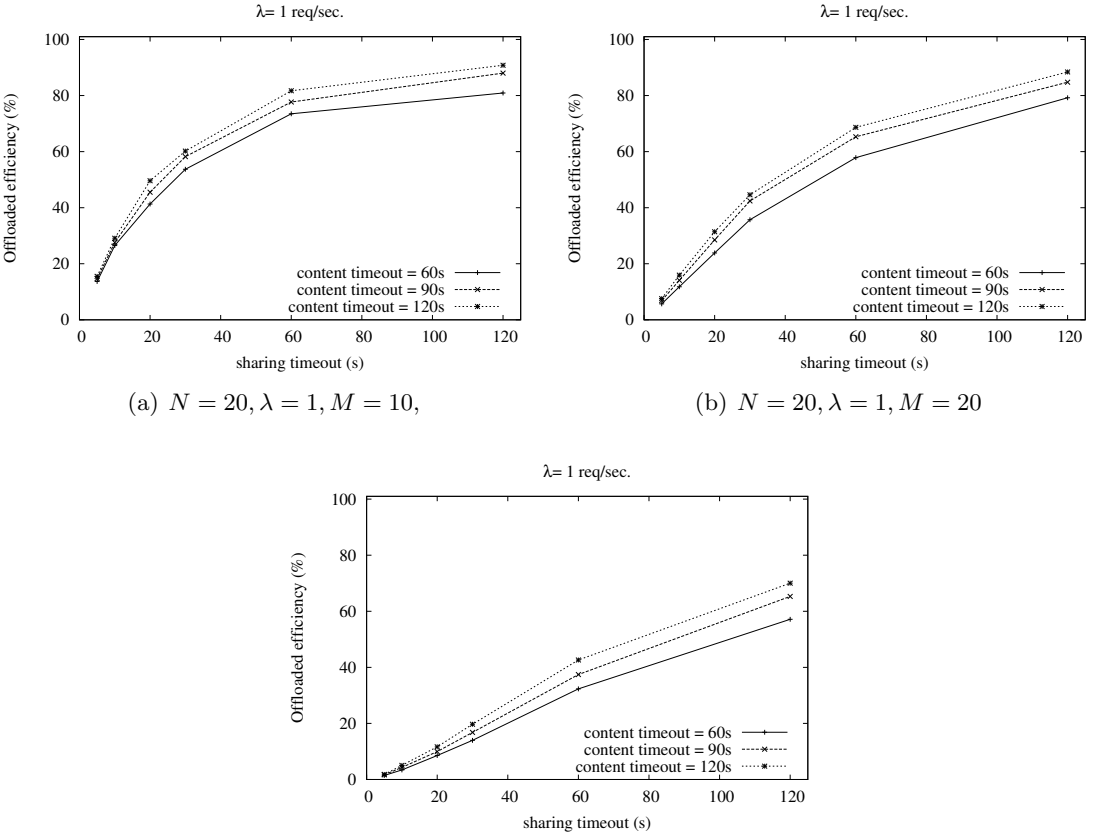

(a) $N = 20, \lambda = 1, M = 10,$

(b) $N = 20, \lambda = 1, M = 20$

(c) $N = 20, \lambda = 1, M = 50$

FIGURE 6.5: Scenario V_1: offloading efficiency for varying number of content items, *content timeouts* and the *sharing timeouts*.

6.3.3 Analysis of scenario V_2

Figure 6.7 shows the offloading efficiency in V_2 for the two considered densities of nodes and the different content popularities (p). Results basically confirm previous observations. This is nevertheless important, as V_2 is more representative of a "steady state" behaviour of the offloading system, as nodes constantly enter and exit the cell at a

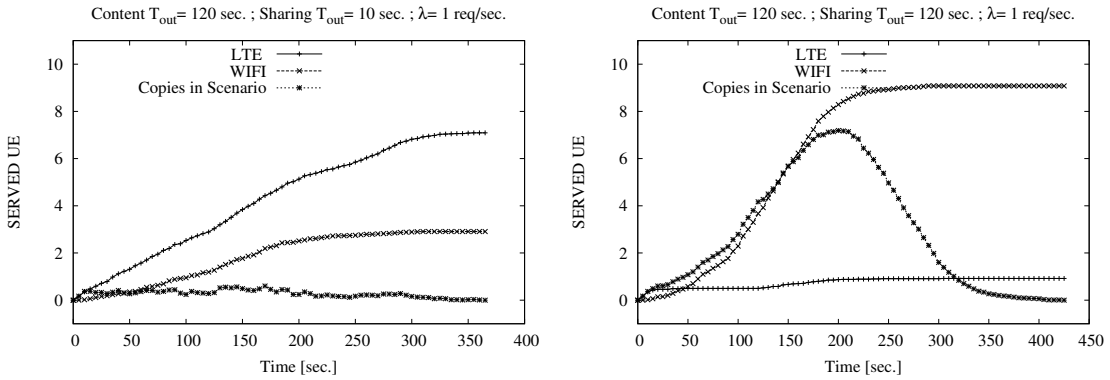

(a) λ=1, M=10, *sharing timeout*=10 s (b) λ=1, M=10, *sharing timeout*=120 s

FIGURE 6.6: V_1: Temporal Evolution for short and long *sharing timeout* and *content timeout*=120 s.

given rate, and continuously generate requests (with a given probability). Again, denser networks ($N = 40$) achieve higher offloading efficiency. The effect of the popularity parameter is similar to that of the request rate in V_1: the higher the popularity, the higher the number of nodes sharing content, the higher the offloading efficiency. It is interesting to note, however, that, due to the mobility of the nodes, they stay within the cell only for about 30s in total, and, on average, stay in the cell for about 22s after having generated a request. This is the "useful time window" during which they can receive content via opportunistic dissemination. Even though this time window is rather short, offloading is very efficient, even at quite low popularities ($p = 0.2$). Finally, Figures 6.8(a) and 6.8(b) show the evolution over time for $N = 40$ nodes at the extreme popularity values. Besides confirming the general behaviour observed also in V_1, it is interesting to note that at high popularity the opportunistic dissemination alone is sufficient to keep enough copies of the content in the cell so that requesting nodes can find at least one before exiting. This is shown by the fact that the curve of delivery via the

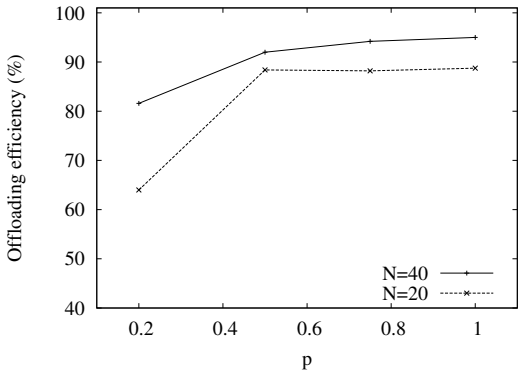

FIGURE 6.7: V_2: offloading efficiency for different content popularities.

cellular network flattens out after an initial "seeding" interval. Instead, in case of less popular contents, there are cases where nodes do not encounter other nodes sharing a copy of the content before getting out of the cell, and therefore the CDM needs to serve them through the cellular network. Fluctuations in the number of copies stored in the network are mainly due to statistical fluctuations in the contacts and requests events. In addition, the curves drop towards the end of the simulation when only few requests need to be satisfied and no new requests are generated (remember that simulations stop when a maximum number of requests is reached).

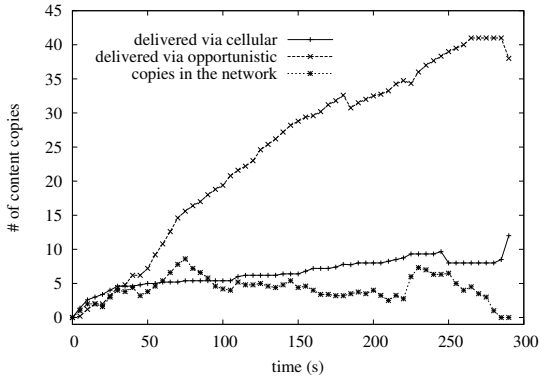

(a) low popularity ($p = 0.2$)

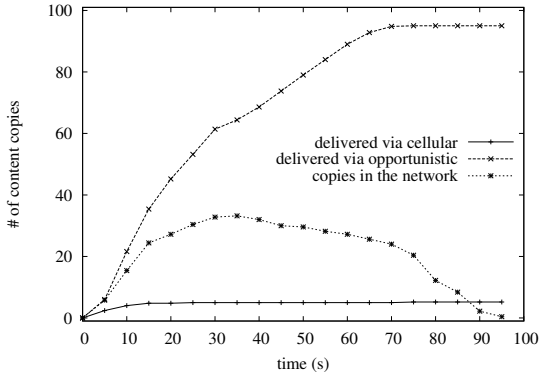

(b) high popularity ($p = 1$)

FIGURE 6.8: V_2: temporal evolution of the number of content copies and served content requests in a network with $N = 40$ users.

6.3.4 Analysis of scenario I_1

After the illustaration of the vehicular scenarios, now we illustrate the system performance related to the indoor sceranios. We start from scenario I_1, which differs from the scenario I_2 for the popularity of the content. In particular, in this case, there are different

contents per each room, but all the content in each room have the same popularity. To this end Figure 6.9(a) shows the offloading efficiency for different *content timeouts*. It is interesting to observe how the offloading efficiency, is not affected by the *content timeout*. This is a side effect of the environment configurations. In fact all users in a room can directly communicate with each other. In this condition, the opportunistic dissemination is tipically fast in distributing the content item to the interested users, and the capacity of the opportunistic communications is mainly limited by the channel contention. Thus, increasing the *content timeouts* does not improve the offloading efficiency because local copies of the content items are rapidly disseminated to interested users. In this scenario we have also analyzed the offloading efficiency when the content items that a user can requests increas. By observing Figure 6.9(b) is possible to observe that, as in Scenario V_1, the more content items there are, the lower is the the offloading efficiency. This can be explained by observing that a user can randomly request any of the content items that are assigned to the room where he/she is. Thus, the more the content items and the lower the probability that two users request the same content (although not at the same time). Clearly, the opportunistic offloading technique is effective only when there are multiple requestes of the same content. It is also worth pointing out that a content item can be disseminated only in the room where it is relevant. In fact, when a user changes room, the content items that are stored in his/her local cache are not disseminated anbymore, because in the new room there are not users interested in that content. thus, the cached content items are simply deleted as the *sharing timeouts* elapsed. Finally, in Figure 6.10 we show the temporal evolution of content diffusion for short

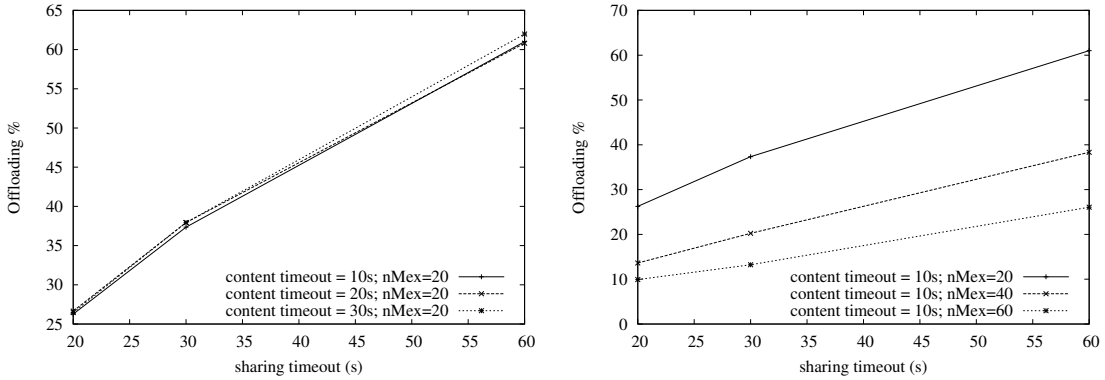

(a) λ=1, M=20 (b) λ=1, *content timeout*=10 s

FIGURE 6.9: I_1: Comparison for different number of content items and different content timeout.

and long *sharing timeout* and different number of content items. From this Figures, is important to note that for short *sharing timeouts* the content items stay available in the opportunistic network for short amount of time. Thus, the combined effect of short *sharing* and *content* timeouts caused *content timeouts* to frequently elapse before the opportunistic diffusion is able to distribute the cached content item to other interested users. On the other hand, when the *sharing timeout* increases there are more copies of the content item in the opportunistic network and this boost the dissemination process. Specifically, as show in Figure 6.10(b) the number of nodes receiving content items via the opportunistic network rapidly increases at the beginning of the simulation and more nodes are served by the opportunistic network than by cellular network. However, when nodes start changing rooms (after 180 seconds, on average), the effivciency of the dissemination process decreases and more content items are sent through LTE.

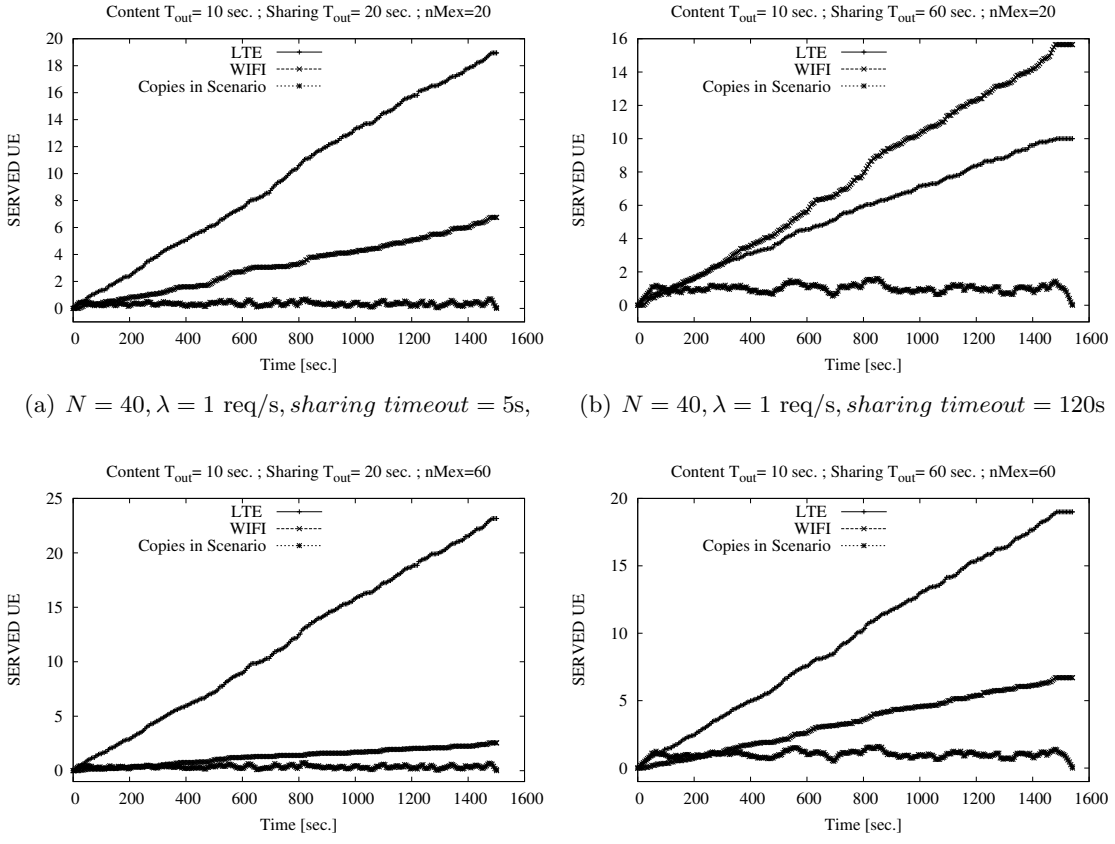

(a) $N = 40, \lambda = 1$ req/s, *sharing timeout* = 5s, (b) $N = 40, \lambda = 1$ req/s, *sharing timeout* = 120s

(c) $N = 40, \lambda = 0.2$ req/s, *sharing timeout* = 5s, (d) $N = 20, \lambda = 0.2$ req/s, *sharing timeout* = 5s

FIGURE 6.10: I_1: temporal evolution of the number of content copies and served content requests in different configuration of Scenario I_1.

6.3.5 Analysis of scenario I_2

As mentioned in Section 6.3.1, this scenario has the same environments configurations of the Scenario I_1. The substantial difference is rappressented by the suddivision of the content items in three class of popularity. As initial step we have evaluated the global offloading efficiency, thus we have evaluated the fraction of content messages that have reached the users through the opportunistic communication, without taking into account the classification of the contents. From this, we have observed the same characterisitcs shown in Figure 6.9(a), thus the independecy from the *content timeouts*. This was an expected result because, due to the enviromnet configurations, also in this case the opportunistic dissemination is tipically fast in distributing the content item to the interested users. After this preliminary evaluation, then we have evaluated the offloading efficiency for each class of popularity. From this analysis, as first result, we observed that the independece from *content timeout* persist also in each type of traffic (Figure 6.11(a)). Another observation that we can do about this analysis, is about the percentage of offloaded traffic for each type of content. By evaluating the efficiency class by class, as illustrated in Figure 6.11(b), we can observe that to an high popularity content correspond an high offloading efficiency. This result is of simple comprension, because higher is the popularity higher will be the requests for a content of this class, thus an higher disponibility of this kind of content which result in an high support of the offloading reception than the content with a decrescent popularity. This results was been consistently observed also for the other sets of parameter. However this results was obtained in the case when a generic user do a single request.

However, all the results until now exposed, are referred to the case when the generic node do a single request. In order to complete the analysis of the offloading mechanism, we tried to stress the opportunistic network, by incrementing the requesting rate from 1 req/sec. up to M req/sec. In order to increment the requesting rate, intuitively an increment of the content items per room was necessary. As first step we observed the offloading efficiency by fixing the requesting rate and incrementing the number of content items. In this case the results have basically confirmed previous obervation. In fact in figure 6.12(a), by fixing the requesting rate, is possible to seen that the offloading efficiency decreae while the number of content items increase. On the other hand, in Figure 6.12(b), is possible to see the opposite case. In fact, by fixing the

number of content items, to an higher requesting rate corresponds an higher offloading efficiency.this is simple to understand, because ifall the nodes requests more contents at the same time. the probability to receive these contents through the cellular network increase. Even if we have illustrated the case of the global offloading, all these features was consistently observed for each class of content.

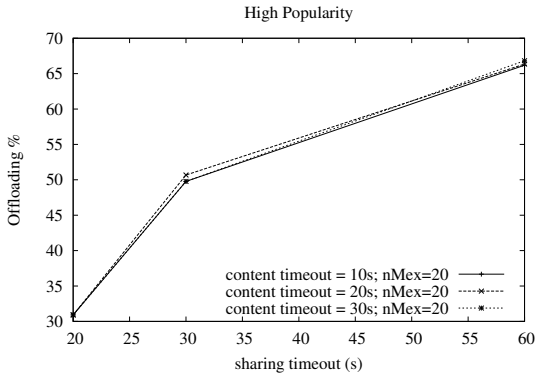

(a) High Popularity, *content timeout*=10 s

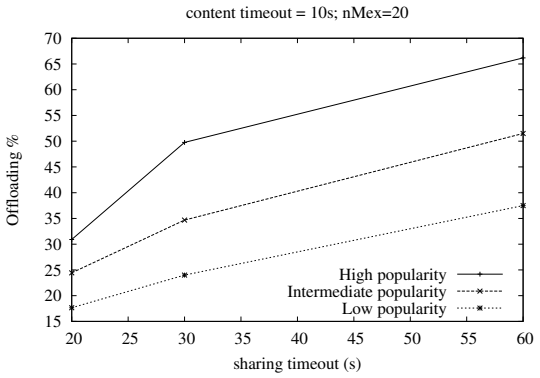

(b) Offloading efficiency per class, *content timeout*=10 s

FIGURE 6.11: I_1: Evaluation of offloading efficiency in the case of *content timeout*=10 s.

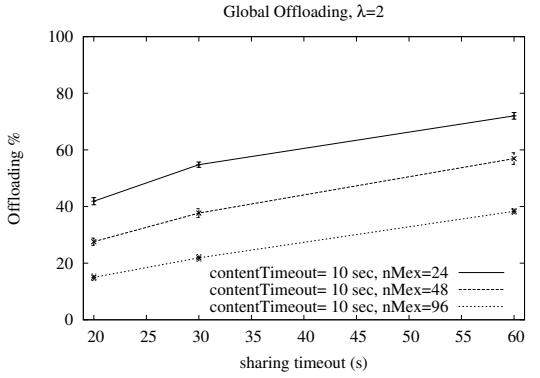

(a) High Popularity, *content timeout*=10 s

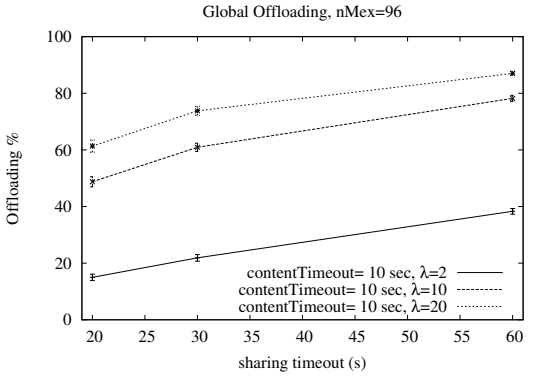

(b) Offloading efficiency per class, *content timeout*=10 s

FIGURE 6.12: I_1: Evaluation of offloading efficiency in the case of *content timeout*=10 s.

6.4 Summary

In this chapter we have studied the performance of offloading through opportunistic networks, in cases where content request are generated dynamically, and are not all

synchronised at the moment when content becomes available. This general scenario is still to be satisfactorily addressed in the literature, and represents a large number of more specific scenarios. Interestingly, in such cases no support from cellular multicast mechanisms can be used, therefore offloading is even more critical. We have defined offloading mechanisms that guarantee bounded delays in content delivery, but, differently from existing literature, use as little as possible resources of mobile users' devices. This is also a critical point, as additional consumption of mobile devices' resources (storage, battery, etc.) is a drawback of offloading with opportunistic networks, that could limit its practical applicability. By considering minimal use of mobile devices' resources, we show that offloading can still be able to drastically reduce the traffic over the cellular network, also in a configuration that is unfavourable for its efficiency. Specifically, we tested the performance of our offloading schemes in vehicular environments, considering different densities of nodes, different popularity of content, and different parameters of the offloading protocols. Our results show that offloading can be very efficient also when using very limited resources of mobile devices, achieving offloading ratios up to more than 90%. Moreover, our results also highlight configurations of the protocols and parameters of the investigated scenarios where offloading is less efficient, and therefore would benefit from more aggressive policies, using additional resources of mobile devices. Then we have also tested the offloading schemes in indoor environments. Through these scenarios was possible to seen new feature, as the independence of the percentage of offloaded traffic from the *content timeouts* or the system behaviour when contents with different popularity are present in the same scenario. In fact we have illustrated that efficiency linearly increase with the popularity of the contents. Another pointed out feature, was related to the dipendence from the number of contemporany requestes that the generc user do and the number of content items. In this case has been observed that, by fixing the Requesting rate to an higher number of content items corresponds a lower offloading wfficiency. On the other side for a fixed number of content items, to an higher requesting rate correspond an higher offfloading efficiency. It is worth noticing, however, that offloading efficiency never drops below 20% in the considered cases, even though they may be quite challenging for the considered offloading mechanisms.

Chapter 7

Conclusions

During my PhD studies, I have dealt with several aspects of optimisation of the performance of 4G networks. In particular, my studies were organized in order to follow two main branches , i.e., analisys and evaluation of the user's perceived throughput in the LTE network and design and evaluation of opportunistic traffic offloading protocols. With respect to the evaluation of the performance in terms of perceived throughput by the generic user in LTE network, through the analysis of a wide set of possible scenarios, we have been able to point out the limits of the network service, more precisely at MAC/PHY level. At this point, I have proposed a modification of the algorithm for the Adapative Modulation and Coding scheme used at PHY level [70]. This scheme, based on Reinforcement Learning, is able to improve the system performance, in particular to increse the throughput received by the users and the the global throughput into the cell up to 22%.

Furthemore, this analysis step contributes to the development of an analytical model to estimate the user perceived throughput [55]. The main feature of this mathematical model is the cross-layer approach. In other words this model takes into account both the Physical layer behaviour, such as Block Error Rate and link rate adaptation, and the MAC operations such as Hybrid-ARQ and user scheduling. Through this modellization process we have been able to understand the dependence between the PHY and MAC layer mechanisms and how these intaractions impact on the throughput perceived at the Application level.

With respect to the other branch of study, I focused my attention on how the usage of Device-to-Device techniques can improve the performance of the LTE networks. In

particular the main activity has been the development of offloading protocols when the requests from a group of user, of a particular contents, are not synchronized and then it is impossible to use a multicast communications to reduce the network congestion. The main performance index considered was the offloading efficiency, defined as the fraction of content messages that reach the users through opportunisitc communications. During this study both the pedestrian and vehicular scenarios were analyzed through a wide set of possible cases obtained by varyng the main system parameters such as the *content timeuot*, the *sharing timeout*, the requesting rate (λ), the content popularity (p) and the set of available contents in the network (M).

I used a very simple offloading scheme, whereby no epidemic dissemination occurs in the opportunistic network. Thus this scheme is minimally invasive for users' mobile devices, as it uses only minimally their resources. Through the results obtained from the simulation of all these scenarios, it has been possible to prove the efficiency of the offloading tecnique in reducing the network congestion, by achieving offloading ratios up to more than 90% [4].

Appendix A

Proofs of Chapter 4

A.1 Proof of Theorem 2

By definition, the CDF of the spectral efficiency in equation (4.1) is computed as

$$\begin{aligned} F_\eta(x;i,k) &= Pr\{\eta_{i,k} \leq x\} \\ &= Pr\left\{\log_2\left(1+\frac{\gamma_{i,k}}{\Gamma}\right) \leq x\right\} \\ &= Pr\left\{1+\frac{\gamma_{i,k}}{\Gamma} \leq 2^x\right\} \\ &= Pr\left\{\gamma_{i,k} \leq \Gamma(2^x-1)\right\} \ . \end{aligned} \tag{A.1}$$

Given that $\gamma_{i,k} \sim Exp(\lambda_k)$ it follows that

$$F_\eta(x;i,k) = \int_0^{\Gamma(2^x-1)} \lambda_k e^{-\lambda_k y} dy \ . \tag{A.2}$$

Solving the integral in (A.2) provides the formula in (4.6).

A.2 Proof of Claim 1

Following the procedure described in [58] to derive the CQI index from the corresponding spectral efficiency we can write that

$$\begin{aligned} g_{i,k}[j] &= Pr\{C_{i,k}=j\} \\ &= Pr\{S_j \leq \eta_{i,k} \leq S_{j+1}\} \\ &= Pr\{\eta_{i,k} \leq S_{j+1}\} - Pr\{\eta_{i,k} \leq S_j\} \ . \end{aligned} \tag{A.3}$$

By substituting (4.6) in (A.3) we obtain (4.7), and this concludes the proof.

A.3 Proof of Claim 2

The wideband CQI for the k^{th} UE is defined as follows

$$\widehat{C}_k = \left\lfloor \frac{1}{q} \sum_{i=1}^{q} C_k \right\rfloor \ . \tag{A.4}$$

Let us denote with Z_k the sum of the CQI values for each RB, i.e. $Z_k = \sum_{i=1}^{q} C_{i,k}$. Note that Z_k is a discrete random variable and $Z_k \in [0, qL]$ since $C_{i,k} \in [0, L]$. Let $z_k[j]$ be the PMF of Z_k. it is a well-known results that the pdf of the sum of i.i.d. RVs is the convolution of the pdf of the constituent RVs. Thus, it follows that $z_k[j] = g_k^{(q)}[j]$, i.e. the q-fold convolution of $g_{i,k}[j]$. Now we can write that

$$\begin{aligned} g_k[j] &= Pr\{\widehat{C}_k = j\} \\ &= Pr\left\{ \left\lfloor \frac{1}{q} Z_k \right\rfloor = j \right\} \\ &= Pr\{qj \leq Z_k < q(j+1) - 1\} \\ &= \sum_{l=qj}^{q(j+1)-1} Pr\{Z_k = l\} \ . \end{aligned} \tag{A.5}$$

By substituting $g_k^{(q)}[l]$ in (A.5) we obtain (4.8), and this concludes the proof.

A.4 Proof of Claim 3

By definition $H_{i,m,k} = \mu_m[v]$ is $Q_{m,v} \leq \gamma_{i,k} \leq Q_{m,v+1}$. The probability $h_{i,m,k}[v]$ that $H_{i,m,k}$ is equal to $\mu_m[v]$ is thus

$$\begin{aligned} h_{i,m,k}[v] &= Pr\{Q_{m,v} \leq \gamma_{i,k} \leq Q_{m,v+1}\} \\ &= \int_{Q_{v,m}}^{Q_{(v+1),m}} f_\gamma(x; i, k)dx \ . \end{aligned} \tag{A.6}$$

Solving the integral in (A.6) provides the formula in (4.12).

A.5 Proof of Claim 4

Let us denote with $Z_{m,k} = \sum_{i \in \Omega(k)} H_{i,m,k}$. Thus, $Z_{m,k}$ is a discrete random variable which takes on any value equal to the sum of all possible $\omega(k)$-combinations of the V elements in the set $\mathcal{V}_m$. Then, it holds that

$$\widehat{H}_{m,k} = \frac{Z_{m,k}}{\omega(k)} \ . \tag{A.7}$$

However, the analysis is complicated by the fact that the MMIB-to-BLER mapping is defined only over the discrete set $\mathcal{V}_m$. Thus, approximations are needed to map $Z_{m,k}/\omega(k)$ onto one of the $\mu_m[v]$ values. First of all, we observe that the PMF of $Z_{m,k}$ is the convolution of the PMFs of the individual constituents because $H_{i,m,k}$ RVs are independent. Now, let us define with Φ_v the set of all attainable values for $Z_{m,k}$ that are between $\omega(k)\mu_m[v]$ and $\omega(k)\mu_m[v+1]$. Then, we approximate the probability $h_{m,k}[v]$ that $H_{i,m,k}$ is equal to $\mu_m[v]$ as

$$\begin{aligned} h_{m,k}[v] &= Pr\{\widehat{H}_{m,k} = \mu_m\} \\ &\approx Pr\{\mu_m[v] \leq \frac{Z_{m,k}}{\omega(k)} \leq \mu_m[v+1]\} \\ &= \sum_{l \in \Phi_v} h_{i,m,k}^{(\omega k)}[l] \ . \end{aligned} \tag{A.8}$$

In other words, in formula (A.8) the discrete MMIB value is associated to a range of values for the variable $Z_{m,k}$.

A.6 Proof of Theorem 1

By exploiting the law of total probability we can write that

$$\begin{aligned} E[TB|Succ]_k = & \sum_{j=0}^{L} E[TB|Succ, MCS=m(j)] \\ & Pr\{Succ|MCS=m(j)\}Pr\{\widehat{C}_k=j\} \\ = & \sum_{j=0}^{L} TBS(m(j),b)\left[1-P_d(m,k)\right]g_k[j] \ , \end{aligned} \tag{A.9}$$

where $\widehat{C}_k$ is the CQI value reported by the k^{th} UE. Similarly, by considering the HARQ protocol behaviours

$$\begin{aligned} & E[T_{ARQ}]_k = \\ & = \sum_{j=0}^{L} E[T_{ARQ}|MCS=m(j)\}]_k Pr\{\widehat{C}_k=j\} \\ & = \sum_{j=0}^{L} \left[\sum_{r=0}^{r_{max}} E[T_{ARQ}|MCS=m(j), n_{rtx}=r\}]_k \right. \\ & \qquad \left. Pr\{n_{rtx}=r|MCS=m(j),\}\right] Pr\{\widehat{C}_k=j\} \ . \end{aligned} \tag{A.10}$$

By considering the HARQ timing as illustrated in Figure 4.2 it immediately follows that

$$E[T_{ARQ}|MCS=m(j), n_{rtx}=r\}]_k = (1+r)(1+\tau_{ARQ}) \ . \tag{A.11}$$

Finally, by substituting (A.11) in (A.10) we obtain (4.5b).

Bibliography

[1] Cisco, "Cisco visual networking index: Global mobile data traffic forecast, update, 2013–2018," Cisco, Tech. Rep., http://www.cisco.com/c/en/us/solutions/collateral/service-provider/visual-networking-index-vni/white_paper_c11-520862.html, 2013.

[2] J. Wortham, "Customers Angered as iPhones Overload AT&T," *NY Times*, 2009, http://www.nytimes.com/2009/09/03/technology/companies/03att.html?_r=0.

[3] "Growing data demands are trouble for verizon, lte capacity nearing limits." [Online]. Available: http://www.talkandroid.com/97125-growing-data-demands-are-trouble-for-verizon-lte-capacity-nearing-limits/

[4] R. Bruno, A. Masaracchia, and A. Passarella, "Offloading through opportunistic networks with dynamic content requests," in *Mobile Ad Hoc and Sensor Systems (MASS), 2014 IEEE 11th International Conference on*. IEEE, 2014, pp. 586–593.

[5] M. Rinne and O. Tirkkonen, "LTE, the radio technology path towards 4G," *Computer Communications*, vol. 33, pp. 1894–1906, 2010.

[6] M. Sharif and B. Hassibi, "On the capacity of MIMO broadcast channels with partial side information," *IEEE Transactions on Information Theory*, vol. 51, no. 2, pp. 506–522, February 2005.

[7] K. Brueninghaus, D. Astely, T. Salzer, S. Visuri, A. Alexiou, S. Karger, and G.-A. Seraji, "Link performance models for system level simulations of broadband radio access systems," in *Proc. of IEEE PIMRC'05*, 2005.

[8] Z. He and F. Zhao, "Performance of HARQ With AMC Schemes In LTE Downlink," in *Proc. of IEEE CMC'10*, 2010, pp. 250–254.

[9] Y. Blankenship, P. Sartori, B. Classon, V. Desai, and K. Baum, "Link error prediction methods for multicarrier systems," in *Proc. of IEE VTC-Fall'04*, vol. 6, 2004, pp. 4175–4179.

[10] M. Ni, X. Xu, and R. Mathar, "A channel feedback model with robust SINR prediction for LTE systems," in *Proc. of EuCAP'13*, 2013, pp. 1866–1870.

[11] J. Francis and N. Mehta, "EESM-Based Link Adaptation in Point-to-Point and Multi-Cell OFDM Systems: Modeling and Analysis," *IEEE Transactions on Wireless Communications*, vol. 13, no. 1, pp. 407–417, January 2014.

[12] J. Ikuno, S. Pendl, M. Simko, and M. Rupp, "Accurate SINR estimation model for system level simulation of LTE networks," in *Proc. of IEEE ICC'12*, 2012, pp. 1471–1475.

[13] A. Kuhne and A. Klein, "Throughput analysis of multi-user ofdma-systems using imperfect cqi feedback and diversity techniques," *IEEE Journal on Selected Areas in Communications*, vol. 26, no. 8, pp. 1440–1450, October 2008.

[14] R. Akl, S. Valentin, G. Wunder, and S. Stanczak, "Compensating for CQI Aging By Channel Prediction: The LTE Downlink," in *Proc. of IEEE GLOBECOM'12*, 2012, pp. 4821–4827.

[15] S. Dimatteo, P. Hui, B. Han, and V. O. Li, "Cellular traffic offloading through wifi networks," in *Mobile Adhoc and Sensor Systems (MASS), 2011 IEEE 8th International Conference on*. IEEE, 2011, pp. 192–201.

[16] "Data offload-connecting intelligently." White Paper, Juniper Research,, 2013.

[17] L. Pelusi, A. Passarella, and M. Conti, "Opportunistic networking: data forwarding in disconnected mobile ad hoc networks," *Communications Magazine, IEEE*, vol. 44, no. 11, pp. 134–141, November 2006.

[18] M. V. Barbera, A. C. Viana, M. D. de Amorim, and J. Stefa, "Data offloading in social mobile networks through {VIP} delegation," *Ad Hoc Net.*, vol. 19, no. 0, pp. 92 – 110, 2014.

[19] A. Vahdat and D. Becker, "Epidemic routing for partially connected ad hoc networks," Duke University, Tech. Rep. CS-200006, 2006.

[20] J. Whitbeck, Y. Lopez, J. Leguay, V. Conan, and M. D. de Amorim, "Push-and-track: Saving infrastructure bandwidth through opportunistic forwarding," *Pervasive and Mob. Comp.*, vol. 8, no. 5, pp. 682 – 697, 2012.

[21] L. Valerio, R. Bruno, and A. Passarella, "Adaptive data offloading in opportunistic networks through an actor-critic learning method," in *ACM CHANTS*, 2014.

[22] M.-X. Chang and Y.-T. Su, "Performance analysis of equalized OFDM systems in Rayleigh fading," *IEEE Transactions on Communications*, vol. 1, no. 4, pp. 721–732, October 2002.

[23] P. Tan and N. Beaulieu, "Effect of channel estimation error on bit error probability in ofdm systems over rayleigh and ricean fading channels," *IEEE Transactions on Communications*, vol. 56, no. 4, pp. 675–685, April 2008.

[24] P. Banelli, "Theoretical analysis and performance of ofdm signals in nonlinear fading channels," *IEEE Transactions on Wireless Communications*, vol. 2, no. 2, pp. 284–293, March 2003.

[25] H. Bolcskei, D. Gesbert, and A. Paulraj, "On the capacity of OFDM-based spatial multiplexing systems," *IEEE Transactions on Communications*, vol. 50, no. 2, pp. 225–234, February 2002.

[26] E. Lo, P. Chan, V. Lau, R. Cheng, K. Letaief, R. Murch, and W. Mow, "Adaptive Resource Allocation and Capacity Comparison of Downlink Multiuser MIMO-MC-CDMA and MIMO-OFDMA," *IEEE Transactions on Wireless Communications*, vol. 6, no. 3, pp. 1083–1093, March 2007.

[27] H. Li, G. Ru, Y. Kim, and L. H., "Ofdma capacity analysis in mimo channels," *IEEE Transactions on Information Theory*, vol. 56, no. 9, pp. 4438–4446, September 2010.

[28] N. Varanese, J. Vicario, and U. Spagnolini, "On the Asymptotic Throughput of OFDMA Systems with Best-M CQI Feedback," *IEEE Wireless Communications Letters*, vol. 1, no. 3, pp. 145–148, June 2012.

[29] S. Donthi and N. Mehta, "An Accurate Model for EESM and its Application to Analysis of CQI Feedback Schemes and Scheduling in LTE," *IEEE Transactions on Wireless Communications*, vol. 10, no. 10, pp. 3436–3448, October 2011.

[30] ——, "Joint Performance Analysis of Channel Quality Indicator Feedback Schemes and Frequency-Domain Scheduling for LTE," *IEEE Transactions on Vehicular Technology*, vol. 60, no. 7, pp. 3096–3109, September 2011.

[31] J. Leinonen, J. Hamalainen, and M. Juntti, "Capacity Analysis of Downlink MIMO-OFDMA Resource Allocation with Limited Feedback," *IEEE Transactions on Communications*, vol. 61, no. 1, pp. 120–130, January 2013.

[32] G. Xu and Y. Lu, "Channel and Modulation Selection Based on Support Vector Machines for Cognitive Radio," in *Proc. of WiCOM'06*, 2006, pp. 1–4.

[33] R. Daniels, C. Caramanis, and R. Heath, "Adaptation in Convolutionally Coded MIMO-OFDM Wireless Systems Through Supervised Learning and SNR Ordering," *IEEE Transactions on Vehicular Technology*, vol. 59, no. 1, pp. 114–126, January 2010.

[34] R. Daniels and R. Heath, "Online adaptive modulation and coding with support vector machines," in *Proc. of EW'10*, 2010, pp. 718–724.

[35] J. Leite, P. H. De Carvalho, and R. Vieira, "A flexible framework based on reinforcement learning for adaptive modulation and coding in OFDM wireless systems," in *Proc. of IEEE WCNC'2012*, 2012, pp. 809–814.

[36] K. Samdanis, T. Taleb, and S. Schmid, "Traffic offload enhancements for eutran," *Comm. Surveys Tutorials, IEEE*, vol. 14, no. 3, pp. 884–896, Third 2012.

[37] S. Singh and J. G. Andrews, "Joint resource partitioning and offloading in heterogeneous cellular networks," *IEEE TWC*, vol. 13, no. 2, pp. 888–901, February 2014.

[38] F. Mehmeti and T. Spyropoulos, "Performance analysis of on-the-spot mobile data offloading," in *IEEE GLOBECOM*, Dec 2013.

[39] K. Lee, J. Lee, Y. Yi, I. Rhee, and S. Chong, "Mobile data offloading: How much can wifi deliver?" *IEEE/ACM Trans. Netw.*, vol. 21, no. 2, pp. 536–550, Apr. 2013.

[40] F. Malandrino, C. E. Casetti, C. F. Chiasserini, and Z. Limani, "Fast resource scheduling in hetnets with d2d support," in *IEEE INFOCOM 2014*.

[41] F. Rebecchi, M. D. de Amorim, and V. Conan, "Flooding data in a cell: Is cellular multicast better than device-to-device communications?" in *ACM CHANTS*, 2014.

[42] X. Wang, M. Chen, Z. Han, D. Wu, and T. Kwon, "Toss: Traffic offloading by social network service-based opportunistic sharing in mobile social networks," in *IEEE INFOCOM*, 2014.

[43] F. Malandrino, C. Casetti, C. Chiasserini, and M. Fiore, "Content download in vehicular networks in presence of noisy mobility prediction," *IEEE TMC*, vol. 13, no. 5, pp. 1007–1021, May 2014.

[44] R. Stanica, M. Fiore, and F. Malandrino, "Offloading floating car data," in *IEEE WoWMoM*, June 2013, pp. 1–9.

[45] 3GPP, "Requirements for evolved utra and evolved utran (release7), 3gpp tr 25.913 version 8.0.0," 2005-06.

[46] ——, "Physical layer aspects for evolved universal terrestrial radio access (release 7), 3gpp tr 25.814 version 7.1.0," 2006-09.

[47] E. Dahlman, S. Parkvall, J. Skold, and P. Beming, *3G evolution: HSPA and LTE for mobile broadband*. Academic press, 2010.

[48] H. Holma and A. Toskala, *LTE for UMTS-OFDMA and SC-FDMA based radio access*. John Wiley & Sons, 2009.

[49] P. Lescuyer and T. Lucidarme, *Front Matter*. Wiley Online Library, 2008.

[50] M. Rinne *et al.*, "Convergence of packet communications over the evolved mobile networks; signal processing and protocol performance," 2010.

[51] F. Capozzi, G. Piro, L. Grieco, G. Boggia, and P. Camarda, "Downlink Packet Scheduling in LTE Cellular Networks: Key Design Issues and a Survey," *IEEE Communications Surveys & Tutorials*, vol. 15, no. 2, pp. 678–700, 2013.

[52] "Key Performance Indicators (KPI) for Evolved Universal Terrestrial Radio Access Network (E UTRAN): Definitions," TS 32.450, Version 9.1.0 Release 9, June 2010.

[53] A. Elnashar and M. El-Saidny, "Looking at LTE in Practice: A Performance Analysis of the LTE System Based on Field Test Results," *IEEE Vehicular Technology Magazine*, vol. 8, no. 3, pp. 81–92, September 2013.

[54] V. Buenestado, J. Ruiz-Aviles, M. Toril, S. Luna-Ramirez, and A. Mendo, "Analysis of Throughput Performance Statistics for Benchmarking LTE Networks," *IEEE Communications Letters*, vol. 18, no. 9, pp. 1607–1610, September 2014.

[55] A. Masaracchia, R. Bruno, A. Passarella, and S. Mangione, "Analysis of mac-level throughput in lte systems with link rate adaptation and harq protocols," in *World of Wireless, Mobile and Multimedia Networks (WoWMoM), 2015 IEEE 16th International Symposium on a.* IEEE, 2015, pp. 1–9.

[56] Z. Lin, P. Xiao, and B. Vucetic, "SINR distribution for LTE downlink multiuser MIMO systems," in *Proc. of IEEE ICASSP'09*, April 2009, pp. 2833–2836.

[57] H. Song, R. Kwan, and J. Zhang, "General results on SNR statistics involving EESM-based frequency selective feedbacks," *IEEE Transactions on Wireless Communications*, vol. 9, no. 5, pp. 1790–1798, May 2010.

[58] 3GPP, "Conveying MCS and TB size via PDCCH," R1-081483, September 2010.

[59] H. Seo and B. Lee, "Proportional-fair power allocation with CDF-based scheduling for fair and efficient multiuser OFDM systems," *IEEE Transactions on Wireless Communications*, vol. 5, no. 5, pp. 978–983, May 2006.

[60] 3GPP, "Evolved Universal Terrestrial Radio Access (E-UTRA): Physical layer procedures (Release 9)," TS 36.213 V9.3.0, September 2010.

[61] IEEE 802.16 Broadband Wireless Access Working Group, "Evaluation Methodology for P802.16m-Advanced Air Interface," IEEE 802.16m-08/004r2, 2008.

[62] M. Mezzavilla, M. Miozzo, M. Rossi, N. Baldo, and M. Zorzi, "A Lightweight and Accurate Link Abstraction Model for the Simulation of LTE Networks in Ns-3," in *Proc. of ACM MSWiM '12*, 2012, pp. 55–60.

[63] WiMAX Forum, "WiMAX System Evaluation Methodology," V2.1, July 2008.

[64] COST Action 231, "Digital mobile radio future generation systems," Final Report - EUR 18957, 1999.

[65] R. Fantacci, D. Marabissi, D. Tarchi, and I. Habib, "Adaptive modulation and coding techniques for OFDMA systems," *IEEE Transactions on Wireless Communications*, vol. 8, no. 9, pp. 4876–4883, Semptember 2009.

[66] 3GPP: Technical Specification Group Radio Access Network, "Evolved Universal Terrestrial Radio Access (E-UTRA); Physical layer procedures (Release 11)," 3GPP TS 36.213 V11.3.0, June 2013.

[67] J. Fan, Q. Yin, G. Li, B. Peng, and X. Zhu, "MCS Selection for Throughput Improvement in Downlink LTE Systems," in *PRoc. of IEEE ICCCN'11*, 2011, pp. 1–5.

[68] S. Tsai and A. Soong, "Effective-SNR mapping for modeling frame error rates in multiple-state channels," 3GPP, Tech. Rep. 3GPP2-C30-20030429-010, 2003.

[69] J. Olmos, S. Ruiz, M. García-Lozano, and D. Martín-Sacristán, "Link Abstraction Models Based on Mutual Information for LTE Downlink," COST 2100, Tech. Rep. 11052, June 2010.

[70] R. Bruno, A. Masaracchia, and A. Passarella, "Robust adaptive modulation and coding (amc) selection in lte systems using reinforcement learning," in *Vehicular Technology Conference (VTC Fall), 2014 IEEE 80th.* IEEE, 2014, pp. 1–6.

[71] P. Tan, Y. Wu, and S. Sun, "Link adaptation based on adaptive modulation and coding for multiple-antenna ofdm system," *IEEE Journal on Selected Areas in Communications*, vol. 26, no. 8, pp. 1599–1606, October 2008.

[72] T. Jensen, S. Kant, J. Wehinger, and B. Fleury, "Fast link adaptation for mimo ofdm," *IEEE Transactions on Vehicular Technology*, vol. 59, no. 8, pp. 3766–3778, October 2010.

[73] T. Tao and A. Czylwik, "Combined fast link adaptation algorithm in LTE systems," in *Proc. of ICST CHINACOM'11*, 2011, pp. 415–420.

[74] R. Sutton and A. Barto, *Reinforcement Learning: An Introduction.* The MIT Press, March 1998.

[75] C. Watkins and P. Dayan, "Q-Learning," *Machine Learning*, vol. 8, pp. 279–292, 1992.

[76] N. Baldo, M. Miozzo, M. Requena-Esteso, and J. Nin-Guerrero, "An Open Source Product-oriented LTE Network Simulator Based on Ns-3," in *Proc. of ACM MSWiM'11*, 2011, pp. 293–298.

[77] 3GPP: Technical Specification Group Radio Access Network, "Conveying MCS and TB size via PDCCH," TSG-RAN WG1 R1-081483, March 2008.

[78] W. Jakes, *Microwave Mobile Communications.* John Wiley & Sons Inc., 1975.

[79] 3GPP: Technical Specification Group Radio Access Network, "Evolved Universal Terrestrial Radio Access (E-UTRA); Base Station (BS) radio transmission and reception," 3GPP TS 36.104 V11.7.0, January 2014.

[80] D. Karamshuk, C. boldrini, M. Conti, and A. Passarella, "Human mobility models for opportunistic networks," *IEEE Communications Magazine*, vol. 49, no. 12, pp. 157–165, 2011.

[81] G. K. Zipf, "Human behavior and the principle of least effort." 1949.

[82] J. Ott, E. Hyytiä, P. Lassila, J. Kangasharju, and S. Santra, "Floating content for probabilistic information sharing," *Pervasive and Mobile Computing*, vol. 7, no. 6, pp. 671 – 689, 2011.

[83] L. Breslau, P. Cao, L. Fan, G. Phillips, and S. Shenker, "Web caching and zipf-like distributions: Evidence and implications," in *INFOCOM'99. Eighteenth Annual Joint Conference of the IEEE Computer and Communications Societies. Proceedings. IEEE*, vol. 1. IEEE, 1999, pp. 126–134.

[84] M. Yang and Z. Fei, "A model for replica placement in content distribution networks for multimedia applications," in *Communications, 2003. ICC '03. IEEE International Conference on*, vol. 1, May 2003, pp. 557–561 vol.1.

[85] A. M. Law and W. D. Kelton, *Simulation Modeling and Analysis.* McGraw-Hill, 2000.